arXiv:1504.05465v2 [astro-ph.GA] 8 Jan 2016

Galaxy alignments: Observations and impact on cosmology

Donnacha Kirk[1], Michael L. Brown[2], Henk Hoekstra[3], Benjamin Joachimi[1], Thomas D. Kitching[4], Rachel Mandelbaum[5], Cristóbal Sifón[3], Marcello Cacciato[3], Ami Choi[6], Alina Kiessling[7], Adrienne Leonard[1], Anais Rassat[8], Björn Malte Schäfer[9]

drgk@star.ucl.ac.uk

ABSTRACT

Galaxy shapes are not randomly oriented, rather they are statistically aligned in a way that can depend on formation environment, history and galaxy type. Studying the alignment of galaxies can therefore deliver important information about the physics of galaxy formation and evolution as well as the growth of structure in the Universe. In this review paper we summarise key measurements of galaxy alignments, divided by galaxy type, scale and environment. We also cover the statistics and formalism necessary to understand the observations in the literature. With the emergence of weak gravitational lensing as a precision probe of cosmology, galaxy alignments have taken on an added importance because they can mimic cosmic shear, the effect of gravitational lensing by large-scale structure on observed galaxy shapes. This makes galaxy alignments, commonly referred to as intrinsic alignments, an important systematic effect in weak lensing studies. We quantify the impact of intrinsic alignments on cosmic shear surveys and finish by reviewing practical mitigation techniques which attempt to remove contamination by intrinsic alignments.

Subject headings: galaxies: evolution; galaxies: haloes; galaxies: interactions; large-scale structure of Universe; gravitational lensing: weak

Contents

1 Introduction 2

2 Quantifying orientations and shapes 6

2.1 Using orientations . . . 6

2.2 Spin alignments . . . 7

2.3 Measuring shapes . . . 8

2.3.1 Shape measurement systematics . . . 10

2.3.2 Intrinsic alignment measurements and cosmic shear . . . 10

[1]Department of Physics & Astronomy, University College London, Gower Street, London, WC1E 6BT, UK

[2]Jodrell Bank Centre for Astrophysics, School of Physics and Astronomy, University of Manchester, Oxford Road, Manchester M13 9PL, UK

[3]Leiden Observatory, Leiden University, PO Box 9513, NL-2300 RA Leiden, Netherlands

[4]Mullard Space Science Laboratory, University College London, Holmbury St Mary, Dorking, Surrey RH5 6NT, UK

[5]McWilliams Center for Cosmology, Department of Physics, Carnegie Mellon University, Pittsburgh, PA 15213, USA

[6]Scottish Universities Physics Alliance, Institute for Astronomy, University of Edinburgh, Royal Observatory, Blackford Hill, Edinburgh EH9 3HJ, UK

[7]Jet Propulsion Laboratory, California Institute of Technology, 4800 Oak Grove Drive, Pasadena, CA 91109, USA

[8]Laboratoire d'astrophysique (LASTRO), Ecole Polytechnique Fdrale de Lausanne (EPFL), Observatoire de Sauverny, CH-1290 Versoix, Switzerland

[9]Astronomisches Recheninstitut, Zentrum für Astronomie der Universität Heidelberg, Philosophenweg 12, 69120 Heidelberg, Germany

3 Shape correlations **11**
3.1 Two-point correlation functions . . . 11
3.2 Estimators of the two-point correlation functions . . . 13
3.3 Projected correlation functions . . . 14
3.4 Using correlation functions to test intrinsic alignment models . . . 15
3.5 Tests for systematics . . . 17

4 Observations of alignment in large galaxy samples **17**
4.1 Late-type galaxies . . . 18
4.2 Early-type Galaxies . . . 21
4.3 Other Large-Scale Measurements . . . 26

5 Environmentally dependent alignments **28**
5.1 Galaxy position alignments in the field and the Local Group . . . 29
5.2 Galaxy alignments within galaxy groups and clusters . . . 29
5.3 Galaxy alignments with voids . . . 31
5.4 Galaxy alignments with filaments and sheets . . . 34
5.5 Alignments between galaxy groups and clusters . . . 35

6 Impact on cosmology & Mitigation **37**
6.1 Quantifying Impact . . . 38
6.2 Exploiting redshift dependence . . . 42
6.3 Parameterisation and marginalisation . . . 43
6.4 Self-calibration . . . 44
6.5 Higher-order cosmic shear statistics . . . 47
6.6 Probes of the unlensed galaxy shape . . . 47
6.6.1 Radio polarisation as a tracer of intrinsic orientation . . . 47
6.6.2 Rotational velocities as a tracer of intrinsic orientation . . . 49

7 Summary & Outlook **49**

1. Introduction

Galaxies show a wide variation in morphological appearance, due to the complex processes of galaxy formation and evolution. Both initial conditions and interactions between galaxies can play an important role. For instance, most elliptical galaxies are believed to be the result of major mergers of galaxies (Toomre & Toomre 1972; Schweizer 1986; Barnes & Hernquist 1992). Consequently the morphology of galaxies is connected to the local environment, as is evidenced by the well-established morphology-density relation (e.g. Dressler 1980). The connection between morphology and galaxy formation and evolution was made early-on, most notably by Hubble (1926) who believed that elliptical galaxies would eventually transform into grand-design spiral galaxies. Although this picture has been reversed in recent years, the importance of morphology has remained and galaxy shape is one of the most important observables that can be used to describe a galaxy.

As it was realised that galaxies may influence each other, other questions become relevant for our understanding of galaxy formation and evolution, such as "Why are galaxies spinning?" and "Are the orientations of galaxies correlated?" These questions have been the main motivator for observational studies of galaxy alignments during the 20th century (a detailed historical overview of the subject can be found in our companion paper Joachimi et al. 2015). However, no consensus was reached on the existence of of alignments between galaxy shapes or spins. For instance,

some studies have claimed that cluster galaxies are preferentially oriented towards the bright central galaxy, whereas others found no evidence for this. Much of this controversy can be attributed to the quality of the data, but differences in observational techniques can play a role as well. Weak gravitational lensing as a cosmological tool provided new impetus for the study of galaxy shapes and alignments in the 21st century. Weak lensing measures coherent distortions to the images of background sources that can be mimicked or hidden by galaxy shape alignments.

Galaxy shapes and orientations can be measured using different approaches. For instance, one can consider the region of a galaxy above a given surface brightness and determine its ellipticity and position angle. In particular, early studies, based on photographic plates, tend to fall into this category because the measurement involved determining the semi-major and semi-minor axis above some surface brightness limit. Even though the resulting ellipticity might be biased, due to the particular choice of surface brightness, the estimate of the position angle from these early studies is expected to be robust, provided the galaxy is much larger than the size of the point spread function (PSF). The adopted surface brightness limit, which may itself be determined by the depth of the observations, can affect the result because low surface brightness features, such as discs or even tidal tails, only show up if the data are sufficiently deep. Figure 1 highlights this problem: we show an example of a well resolved galaxy observed by the Hubble Space Telescope (HST) as part of the COSMic evOlution Survey (COSMOS, Scoville et al. 2007). The different isophotes that are indicated show how the morphology of real galaxies varies dramatically as a function of surface brightness level. For reference the green ellipse in Figure 1 corresponds to the best fit single Sérsic model (Sersic 1968) to the galaxy image.

That this change in morphology with surface brightness can lead to wildly varying conclusions about the level of galaxy shape alignments can be understood by considering a very simple case: imagine a scenario where all galaxies are made up of a central bulge component and a broad disc. Now let the bulges of galaxies be strongly aligned but discs be oriented randomly. If one were to measure the orientation of some faint isophote, i.e. probing the discs, no alignment would be measured. On the other hand, shallower data would probe the brighter bulges, leading to strong alignments. Remember that this is not a particularly physical example as interactions between bulge and disc components could introduce alignments.

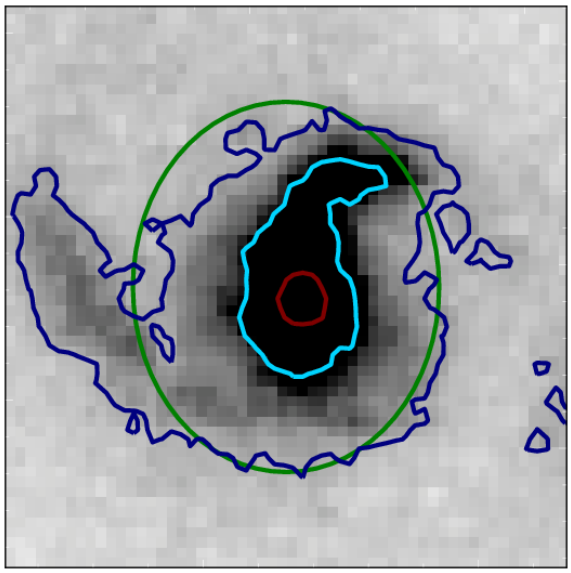


Fig. 1.— An example of a well-resolved galaxy observed as part of the COSMOS survey. The dark blue, light blue and red contours mark isophotes that match 5%, 20% and 50% of the peak flux level, respectively. The morphology clearly varies with surface brightness and the measured shape will be a strong function of the isophotal limit that is adopted. For comparison the green ellipse indicates the ellipticity of the best fit single Sérsic model.

Similarly, as we discuss in more detail below, weak lensing studies usually measure galaxy shapes using algorithms that give more weight to the brighter, central regions of galaxies, although the precise radial weighting differs between methods. Biased measurements may lead to incorrect conclusions: light from bright cluster galaxies may affect the shape measurements of fainter satellites, resulting in spurious alignments. Similarly, if the PSF is anisotropic, it will lead to apparent alignments, especially if the galaxies are poorly resolved. A comparison of alignment results therefore requires a careful study of the methodology used to perform the measurement.

Early observational studies focused on understanding the physical origin of the alignments of galaxy positions and shapes, but the first detections of the weak lensing signal by large-scale structure (LSS) (Bacon et al. 2000; Kaiser et al. 2000; Van Waerbeke et al. 2000; Wittman et al. 2000) spurred new interest in the topic. Weak gravitational lensing seeks to exploit the alignment in observed galaxy shapes caused by the deflection of light by gravity *en route* from the source galaxy to the observer. What makes weak gravitational lensing particularly interesting is that the observed galaxy alignments can in principle be used to reconstruct the projected mass distribution or to study the statistical properties of the large-scale structure (Takada & Jain 2004; Hoekstra & Jain 2008; Munshi et al. 2008). We will refer to the alignments of galaxy shapes caused by galaxy formation and evolution as *intrinsic alignments* to differentiate them from alignments sourced by gravitational lensing which we will call *cosmic shear*. Weak lensing is a powerful cosmological probe. It is directly sensitive to the dark matter distribution, unlike galaxy redshift surveys which rely on using galaxies as biased tracers of the underlying dark matter field. In addition weak lensing is sensitive to both the growth of structure and the expansion history of the Universe through a geometric term in the lensing kernel. See Bartelmann & Schneider (2001); Hoekstra & Jain (2008); Munshi et al. (2008); Bartelmann (2010) for general reviews of weak lensing.

For the study of cosmic shear we need accurate estimates for both the ellipticity (also referred to as the third flattening) and orientation on the sky of the galaxies, which can be expressed as

$$\begin{pmatrix}\epsilon_1\\ \epsilon_2\end{pmatrix} = \frac{1-q}{1+q}\begin{pmatrix}\cos 2\vartheta_{\rm P}\\ \sin 2\vartheta_{\rm P}\end{pmatrix}, \tag{1}$$

where ϵ_i, with $i = 1, 2$, are the two ellipticity components, $q = b/a$ is the ratio ($0 \leq q \leq 1$) of the estimated semi-minor and semi-major axes, or axial ratio in short, and $\vartheta_{\rm P}$ is the position angle with respect to some reference axis. The factors of $2\vartheta_{\rm P}$ come from the spin-2 nature of ellipticity due to the symmetry of an ellipse under 180° rotation. Alternatively one can use complex notation, such that $\epsilon = \epsilon_1 + {\rm i}\epsilon_2$ or $\epsilon = |\epsilon| e^{2{\rm i}\vartheta_{\rm P}}$. If observed galaxy images are randomly oriented, the ensemble average $\langle\epsilon_i\rangle = 0$.

The differential deflection of light rays by the intervening large-scale structure distorts the images of distant galaxies, resulting in *apparent* alignments of the observed shapes. To leading order, i.e. in the weak lensing limit, the effect is to change $\epsilon^{\rm s}$, the intrinsic (or unlensed) ellipticity of a galaxy, to an observed value (Schneider & Seitz 1995):

$$\epsilon = \frac{\epsilon^{\rm s} + g}{1 + \epsilon^{\rm s} g^*} \approx \epsilon^{\rm s} + \gamma, \tag{2}$$

where the asterisk denotes the complex conjugate and g is the reduced shear, which is related to the weak lensing shear γ and convergence κ through $g = \gamma/(1-\kappa)$. In the weak lensing regime, we assume that $g \approx \gamma$. A brief introduction to the topic is given in Joachimi et al. (2015), which also lists references to more thorough discussions of gravitational lensing. The above approximation, Equation (2), is only true when we take an ensemble average over many galaxies. For individual galaxies there is an additional term of the same order of magnitude. This term is not relevant for the topics covered in the rest of the paper, see Bartelmann & Schneider (2001) for more detail. Note that the above formalism highlights the usefulness of expressing the ellipticity and shear in complex notation.

The measurement of the weak lensing signal involves the correlation, or averaging, of the ellipticity measurements for many galaxies because the typical lensing-induced change in ellipticity is $\sim 1\%$ or less, much smaller than the average intrinsic galaxy ellipticity. This demonstrates the relevance of intrinsic alignments for lensing studies: only if such alignments vanish, $\langle\epsilon^{\rm s}\rangle = 0$, is the observed ensemble-averaged ellipticity an unbiased estimator of the lensing shear. Similarly, the galaxy ellipticity correlation function (see Section 3) comprises types of contributions (where i and j here indicate a pair of galaxies and the average is over all pairs):

$$\underbrace{\left\langle \epsilon^i \epsilon^j \right\rangle}_{\text{observed}} = \underbrace{\left\langle \gamma^i \gamma^j \right\rangle}_{\text{GG}} + \underbrace{\left\langle \epsilon^{s,i} \epsilon^{s,j} \right\rangle}_{\text{II}} + \underbrace{\left\langle \gamma^i \epsilon^{s,j} \right\rangle + \left\langle \epsilon^{s,i} \gamma^j \right\rangle}_{\text{GI}} . \quad (3)$$

We adopt the following common shorthand notation: GG for the cosmic shear correlation, which is the quantity of interest to constrain cosmological parameters, II indicates the correlations between intrinsic ellipticities, and GI denotes correlations between the shear for one galaxy and the intrinsic ellipticity of the other. In principle one of the GI terms should vanish if foreground and background galaxies can be cleanly separated because the lensing of light from galaxies should not correlate with the intrinsic ellipticity of more distant galaxies.

To understand what these correlations mean physically imagine some region of matter overdensity. This overdensity generates a powerful gravitational potential on scales larger than individual galaxies. This large-scale gravitational potential may cause the orientation and shapes of nearby galaxies to align with the overdensity, due to the effect of the gravitational tidal field. Neighbouring galaxies are affected by the same large-scale tidal field so their mutual alignment with the matter overdensity means that the shapes of those galaxies are now correlated - they point in the same direction. This is what we call the intrinsic-intrinsic (II) correlation. It effects physically close galaxies and the induced correlations have the same orientation as those sourced by weak lensing, meaning the II correlation manifests as a spurious extra signal in cosmic shear studies.

The gravitational-intrinsic (GI) correlation is more subtle. As noted by Hirata & Seljak (2004), the II term correlates the shapes of physically close galaxies with some matter overdensity, which in turn is responsible for a lensing effect on background galaxies. The net result is an anti-correlation between the shapes of galaxies in the foreground, whose shape is sourced by the gravitational tidal field from the mass, and those in the background, whose shape is effected by the mass through weak lensing. The GI correlation is a long-range effect and manifests as a negative contribution to measured cosmic shear. The extent to which tidal fields do source alignments, and how this varies between different galaxy populations, is something we explore throughout the rest of this paper.

If the spurious contributions to cosmic shear caused by intrinsic galaxy alignments are significant compared to the statistical errors of the survey then a naive analysis, which ignores the impact of such alignments, will produce biased estimates of cosmological parameters. Although current work indicates that the intrinsic alignment signal is too low to have affected the conclusions of early cosmic shear studies, it is also clear that we can no longer ignore this astrophysical source of bias (Heymans et al. 2013) and that it will be a significant limitation for future projects, unless we can account for intrinsic alignments in the analysis.

Although the existence of intrinsic alignments has now been firmly established for luminous red galaxies (LRGs; Mandelbaum et al. 2006a; Hirata et al. 2007; Okumura et al. 2009; Joachimi et al. 2011; Singh et al. 2015), current observational constraints are not sufficient to correct future cosmic shear surveys (Laszlo et al. 2012; Kirk et al. 2013, 2012). Further progress relies on making observations with sufficient redshift precision and spatial coverage to inform models of intrinsic alignments, or calibration using the cosmic shear survey data themselves (Bernstein 2009; Joachimi & Bridle 2010). Importantly, as we will discuss in more detail below, the intrinsic alignment estimates themselves have to be closely linked to the shear measurements in terms of shape measurement, galaxy populations and observational strategy. A further complication is that the source and strength of galaxy alignment depends on galaxy type for reasons described in detail below and treated extensively in our companion paper Kiessling et al. (2015) and the papers referenced therein. Although one can attempt to restrict the analysis to a particular type of galaxy, the source sample typically comprises a mix of galaxies thus mixing possible alignment mechanisms, complicating the analysis (see Joachimi et al. (2015) and references therein for more detail). We have been fortunate so far that our knowledge of intrinsic alignments, combined with the size of the observed signal, has kept pace with requirements for cosmic shear surveys to remain unbiased (Heymans et al. 2013). As powerful next generation surveys become available, their reduced statistical error will require a new level of accuracy in quantifying systematic effects such as intrinsic alignments. The observation of galaxy alignments will remain an important topic as we demand more precise measurements over a wider range of scales and redshifts for all types of galaxies.

In this review we focus on observations of the intrinsic alignments of galaxies (particularly in Section 4 and Section 5), their impact on cosmic shear measurements and possible mitigation strategies (Section 6). This current paper

is one of three companion papers covering the entire topic of galaxy alignments. Therefore some topics are covered in less detail here or, occasionally, omitted. For a general introduction and historical review of the subject we refer the reader to Joachimi et al. (2015), which summarises the basic concepts and highlights the most important developments in theory, modelling and observations. A detailed discussion of the physical theories used to model alignments on a range of scales is presented in our companion paper Kiessling et al. (2015), which also reviews intrinsic alignment studies conducted through simulations, thus representing the theoretical counterpart of this more observationally-oriented review. Troxel & Ishak (2015) also provide an independent review of galaxy alignments and Schäfer (2009) is a detailed review of angular momentum correlations.

This review is structured as follows: In Section 2 we discuss how galaxy alignments are measured. The main statistics that are used to quantify the galaxy shape alignment signal are reviewed in Section 3. The most important observations of shape alignment on linear and quasi-linear large scales are discussed in Section 4 and details of environmentally-dependent correlations are reviewed in Section 5. In Section 6 we demonstrate the impact that intrinsic alignments can have on attempts to infer cosmological parameters from cosmic shear surveys as well as outlining the most effective ways to mitigate this impact. We summarise in Section 7 and discuss the outlook for future observations of galaxy shape alignments.

2. Quantifying orientations and shapes

According to our current understanding, we can distinguish between two types of alignments. In the case of late-type (disc) galaxies the alignments of the angular momenta are believed to play the most important role, whereas the orientation of early-type (elliptical) galaxies is thought to be largely determined by the build-up of the large-scale dark matter distribution that surrounds them. This is a distinction at the level of the theory of alignment origin but it may also have consequences visible in observations. See Joachimi et al. (2015) for a general overview of these mechanisms and Kiessling et al. (2015) for a detailed discussion.

Although the physical processes at play determine the strength of the alignment as a function of separation, the method used to quantify the alignment signal plays an important role as well. Whether or not this is an issue depends on the scientific question that one wishes to address.

In Section 2.1 we consider the measurement of galaxy orientations, concentrating on observing galaxy spin alignment in Section 2.2. We then cover the measurement of galaxy shapes in Section 2.3, including discussion of some common methods. Prominent systematic effects in shape measurement studies are described in Section 2.3.1 and some specific conclusions on the measurement of galaxy shapes with the aim of mitigating intrinsic alignments in cosmic shear surveys are made in Section 2.3.2.

2.1. Using orientations

Naturally, a critical ingredient in weak lensing studies is the measurement of the alignment of the shapes of galaxies. This measurement is quantified by a galaxy's ellipticity and position angle with respect to some local coordinate system. In this context it is interesting to note that an observation of an alignment of position angles (regardless of ellipticity) will be sufficient to imply that weak lensing measurements are contaminated by galaxy intrinsic alignments. However, an accurate estimate of the *level* of contamination still requires knowledge of the distribution of ellipticities, which itself may vary locally (as the mix of galaxy types depends on environment). Hence, while early studies that focused only on the orientations of galaxies have been useful, a successful correction of the intrinsic alignment signal in weak lensing studies requires more information.

Studies using orientations rather than shapes also suffer a particular ambiguity: what is the orientation of nearly round galaxies? For a fixed total signal-to-noise galaxy detection, the uncertainty on the galaxy orientation is smallest for highly flattened galaxies and largest for those that are nearly round. The way this problem is dealt with in practice varies, with some studies ignoring it entirely (e.g., Pereira & Kuhn 2005; Agustsson & Brainerd 2006; Faltenbacher et al. 2007, 2009; Okumura et al. 2009; Li et al. 2013a). Since ignoring this issue will tend to dilute any alignments by adding random noise, that simple strategy is in fact a valid approach when trying to simply *detect* alignments. However, ignoring the dilution of the orientation correlations due to nearly round galaxies in the sample complicates

both the theoretical interpretation of the results and also the comparison with results from other samples (which may have different intrinsic shape distributions and/or levels of noise).

Another approach is to exclude galaxies with axial ratios $b/a \sim 1.0$ on the grounds that their position angles are meaningless (Niederste-Ostholt et al. 2010). Again, such exclusion does not cause any problem for claiming a detection of intrinsic alignments but this comes at the cost of the interpretation of the measured alignments in terms of a theoretical model being complicated by selection biases. Smargon et al. (2012) give a simple example of a mathematical model for including uncertainties in position angles in real data in a theoretical model for alignments. This is done in the context of cluster alignments, but the same argument is valid for galaxy alignments. Unfortunately, in this model, all galaxies are assumed to have, on average, the same position angle uncertainty; if alignments vary with shape (just as the position angle uncertainties do), then this prescription would no longer be applicable. An alignment estimate based on shape measurements does not suffer from these problems as there is no ambiguity in assigning a small ellipticity to a nearly circular galaxy, though, of course, signal-to-noise may be lower for galaxies with small ellipticities in real, noisy data.

2.2. Spin alignments

Looking beyond position angles, measurements of the alignments between the angular momenta of galaxies may provide unique insights into the formation of disc galaxies, especially on the origin of the observed galactic angular momentum. The ellipticities of disc galaxies are the result of the projection of their orientation with respect to the observer, combined with any intrinsic ellipticity due to not being a perfectly circular disc. If we assume that disc galaxies obtain their angular momentum from tidal torquing, they should spin around their minor axis. Inclination angle, ξ, refers to the angle between the observer's line of sight and the symmetry axis of a disc galaxy. Position angle, $\vartheta_{\rm P}$, refers to the angle between the major axis of the ellipse of a projected galaxy image and the north of some coordinate system. Assuming the circular, infinitely thin-disc approximation and measurements of both of these angles, the components of the unit spin vector are given by

$$\hat{J}_r = \pm \cos\xi, \tag{4}$$

$$\hat{J}_\theta = (1 - \cos^2\xi)^{1/2} \sin\vartheta_{\rm P}, \tag{5}$$

$$\hat{J}_\phi = (1 - \cos^2\xi)^{1/2} \cos\vartheta_{\rm P}, \tag{6}$$

where r, θ and ϕ are spherical polar coordinates with an origin at the galactic centre and r pointing along the line of sight. The spatial correlation of the spin axes can then be written as

$$\eta(r) \equiv \left\langle |\hat{J}(x) \cdot \hat{J}(x+r)|^2 \right\rangle - \frac{1}{3}, \tag{7}$$

where we are averaging over the position, x, of all galaxy pairs separated by a distance r (Lee 2011). The value of $1/3$ is subtracted since it is the value of the ensemble average when there is no correlation.

The direction of the galactic angular momentum (i.e. the spin axis of the galaxy) is expected to be connected to the properties of the underlying dark matter halo. If the correlation between angular momentum and the distribution of dark matter is retained after galaxy formation, then the correlation of the density field, which can be predicted using numerical simulations (Kiessling et al. 2015), should be replicated in correlations of galaxy orientation. Alternatively, a lack of correlation may provide insights into the processes that allow galaxies to form large rotating discs. For instance, van den Bosch et al. (2003) showed how pre-heating of the intergalactic medium unbinds baryons from their dark matter haloes, which may lead to misalignments between the angular momentum of the gas and the dark matter.

For studies that seek to correlate galaxy spins, a fundamental observational problem is the "deprojection" of the observed galaxy shape and the accurate determination of the direction and sign of the spin vector. Using a galaxy's observed axial ratio, q, and position angle, ϑ_P, it is possible to determine the unit spin vector, $\hat{\mathbf{J}}$, up to a two-fold ambiguity in the sign of the spin i.e. clockwise or anti-clockwise (Lee 2011). Early works (Lee & Pen 2000) assumed a thin disc geometry in this calculation. In reality discs have finite thickness which must be accounted for to make an accurate estimate. This involves the assumption of an intrinsic flatness parameter which depends on galaxy

morphological type (Haynes & Giovanelli 1984; Lee & Erdogdu 2007). One simplistic way to avoid deprojection uncertainties would be to use only galaxies which are edge-on or face-on to the observer (Trujillo et al. 2006; Slosar & White 2009), however this greatly reduces the available number density in a given sample.

If the right observations are available, it is possible to lift the degeneracy in the sign of the spin of a galaxy. The presence of dust lanes (Colina & Wada 2000) or the use of kinematic data (Obreschkow et al. 2015) can both be used to determine clockwise or anti-clockwise spin. In the absence of such additional information, authors have adopted a number of strategies. Some assumed the sign of the spin of each galaxy was completely independent (Kashikawa & Okamura 1992), some assumed all galaxies had the same spin direction (Lee & Erdogdu 2007) and some attempted a statistical approach that combined distributions which assumed all spin signs were positive or negative into a single corrected distribution (Varela et al. 2012). Each approach resulted in a serious decrease in the available information. Future mapping of the neutral hydrogen density with 21cm measurements using the Square Kilometre Array (SKA) will be able to deliver unambiguous measurements of the spin sign as well as measurements of angular momentum accurate to $3-5\%$ for millions of disc galaxies (Obreschkow & Glazebrook 2014; Obreschkow et al. 2015).

Reproducing the observed finite thicknesses and sizes of disc galaxies has been a challenge for numerical hydrodynamic simulations, because the results are sensitive to the implementation of the various processes of baryonic physics. Consequently it is not clear whether the predicted shapes can be compared to observations. On the other hand, the prediction for the orientation of the spin axis should be more robust. Measurements of the alignments of the spin axes of disc galaxies may therefore be useful to provide insights to the process that aligns the angular momentum. The usefulness of such observations for weak lensing studies, in particular to *correct* cosmic shear measurements, is limited because this would require a prediction for the galaxy shapes as well. We therefore focus for the remainder of this section on the measurement of galaxy shapes.

2.3. Measuring shapes

The practical measurement of galaxy shapes is fundamental to both weak gravitational lensing studies and much of the intrinsic alignment literature. Galaxy shapes can be quantified using various approaches and a wide range of tools have been used for intrinsic alignment measurements in the past. In the case of cosmic shear, the galaxies for which shapes are measured are typically faint and have sizes that are comparable to that of the PSF. The effect of the PSF is twofold: (i) because it has a finite size, it leads to observed images that are rounder; (ii) the PSF is typically anisotropic, resulting in alignments in the observed images. Measuring accurate shapes for the source galaxies is challenging, and understanding the limitations and improving shape measurement algorithms has been an area of active research (see e.g. results of the Shear TEsting Programme (STEP) and GRavitational lEnsing Accuracy Testing (GREAT) challenges, Heymans et al. 2006; Massey et al. 2007; Bridle et al. 2010; Kitching et al. 2012; Mandelbaum et al. 2015, and references therein). As cosmic shear studies are the main driver for current research on this topic, we focus the discussion on the algorithms used to measure the lensing signal.

One approach, which is gaining popularity thanks to increases in computing power, is to fit a parametric model to the observed surface brightness distribution. In the case of weak lensing studies the initial model is sheared and convolved with the PSF. The model parameters are varied until the resulting image best matches the observations, which yields an estimate for the ellipticity; examples are `lensfit` (Miller et al. 2013) and `im3shape` (Zuntz et al. 2013). However, the choice of suitable models is not straightforward because galaxies can have complex morphologies. If the model is too rigid, the resulting shapes will be biased (Voigt & Bridle 2010; Melchior et al. 2010), but if the model is too flexible, the shape will be biased too, because of noise in the image (Refregier et al. 2012; Kacprzak et al. 2012; Melchior & Viola 2012). Forward modelling requires many calculations and is therefore computationally expensive when many parameters are included. For this reason model-fitting algorithms have not yet been extensively used, although `lensfit` was employed to analyse the Canada France Hawaii Telescope Lensing Survey data (CFHTLenS; Heymans et al. 2012b). An additional advantage of these forward modelling approaches is that various instrumental effects can be incorporated into a Bayesian framework, with priors imposed on the various model parameters. However, accurate priors are needed, particularly for faint galaxies and such information is not always available.

Alternatively, galaxy shapes can be quantified using the moments of the surface brightness distribution of a galaxy.

The quadrupole moments Q_{ij} are defined as

$$Q_{ij} = \frac{1}{F_0} \int \mathrm{d}\mathbf{x}\; x_i x_j W(\boldsymbol{x}) f(\boldsymbol{x}), \tag{8}$$

where $\mathbf{x}$ denotes the two-dimensional position on the sky (with $i, j \in \{1, 2\}$ denoting each dimension), where $f(\boldsymbol{x})$ is the surface brightness of the galaxy image and $W(\boldsymbol{x})$ is a weight function. Note that the centre is chosen such that the weighted dipole moments vanish and we normalise using the weighted monopole moment, F_0 (which corresponds to the flux in the case of unweighted moments). When measuring moments from real data, a weight function is needed to suppress the contribution of noise to the moments. In terms of the signal-to-noise ratio, the optimal choice for the weight function is to match it to the galaxy image. However, other choices can be made to reduce the sensitivity to possible sources of bias, such as the uncertainty in the underlying ellipticity distribution. Similar to the model fitting approach, where models used are often brighter in the center and deviations from the model there affect the fit a lot because of the high signal-to-noise ratio, the effect of the weight function in Equation (8) is to give more weight to the central (brighter) regions of the galaxy.

As we discuss below, moments are not only a useful way to quantify shapes; they can also, as was shown in Massey et al. (2013), give insights into the relative importance of various observational biases, such as those caused by the PSF. The observed surface brightness distribution is the convolution of the true galaxy image and the PSF. For both cosmic shear and intrinsic alignment studies we wish to infer the moments (or shapes) of the former. In the case of unweighted moments the correction for the PSF is straightforward as

$$Q_{ij}^{\mathrm{obs}} = Q_{ij}^{\mathrm{true}} + Q_{ij}^{\mathrm{PSF}}. \tag{9}$$

The galaxy ellipticity, or third flattening, can be expressed in terms of the corrected *unweighted* quadrupole moments (i.e. adopting $W = 1$) through:

$$\begin{pmatrix} \epsilon_1 \\ \epsilon_2 \end{pmatrix} = \frac{1}{Q_{11} + Q_{22} + 2\sqrt{Q_{11}Q_{22} - Q_{12}^2}} \begin{pmatrix} Q_{11} - Q_{22} \\ 2Q_{12} \end{pmatrix}. \tag{10}$$

Noise in real data prevents the use of unweighted moments. However, the need to use weighted moments leads to new complications: the correction for the PSF (and weight function itself) involves knowledge of higher order moments, which themselves are affected by noise. Limiting the expansion in moments is similar to the model bias mentioned above. Although Equation (10) can be used to compute the ellipticity from the best-fit parametric model, moment-based methods tend to make use of the polarisation, also called the third eccentricity or distortion (Bernstein & Jarvis 2002), given by:

$$\begin{pmatrix} e_1 \\ e_2 \end{pmatrix} = \frac{1}{Q_{11} + Q_{22}} \begin{pmatrix} Q_{11} - Q_{22} \\ 2Q_{12} \end{pmatrix}, \tag{11}$$

which avoids the square root of a combination of moments in the denominator. The two definitions are related through $e = 2\epsilon/(1 + |\epsilon|^2)$. A discussion of these quantities, and their probability distributions is presented in Viola et al. (2014), see e.g. Heymans et al. (2006) for a discussion of the various choices made in actual implementations.

Kaiser et al. (1995) considered the first-order change in the polarisation, δe_i, induced by a small constant gravitational shear, for an arbitrary weighting function $W(x)$, and found that this can be expressed as $\delta e_i = P^{\gamma}_{ij}\gamma_j$, where the indices denote the two components of the ellipticity and shear, respectively, and the Einstein summation convention is assumed. The polarisability tensor P^{γ}_{ij} depends in a rather complicated manner on the morphology and surface brightness distribution of the galaxy. However, it can be directly measured for each individual galaxy, and thereby can be used to calibrate the polarisation measurements: the average of e_i/P^{γ}_{ij} in a particular patch of sky will be directly proportional to the gravitational shear γ_j in that region. This can therefore be used to construct an unbiased estimate of the gravitational shear. This is why image simulations are used to not only compare the performance of algorithms (e.g. Heymans et al. 2006; Bridle et al. 2010; Kitching et al. 2012; Mandelbaum et al. 2015), but also to calibrate algorithms (e.g. Miller et al. 2013; Hoekstra et al. 2015). The various definitions for the shapes of galaxies are often used loosely in the literature, which is important to keep in mind when comparing published results.

2.3.1. *Shape measurement systematics*

A bright, isolated galaxy which subtends a large angle on the sky would be an ideal candidate for shape estimation. However, galaxies are clustered on the sky and much of the cosmological signal comes from galaxies near dense regions. Hence, most galaxies are not isolated but "blended" with other sources and the shape measurements are compromised (see Hoekstra et al. 2015; Dawson et al. 2014, for the impact of very faint galaxies in image simulations). This is particularly important if we wish to study intrinsic alignments as a function of environment.

For example, Hao et al. (2011) showed that significant detections of satellite galaxy alignments using some shape measurement methods can be attributed to contamination by neighbouring galaxies. Satellite galaxies are particularly prone to suffer this effect, being usually relatively dim with many bright neighbours. In addition there is an intra-cluster light contribution from stars bound to the cluster after being stripped from member galaxies (Zwicky 1951; Gonzalez et al. 2007; Burke et al. 2012; Guennou et al. 2012; Adami et al. 2013; Presotto et al. 2014). The amount of bias will depend on the shape measurement method (Hao et al. 2011), with isophotal measurements being particularly sensitive, see discussion of Figure 1 above. Indeed, the papers that report detections of satellite alignments have been made using isophotal measurements (Pereira & Kuhn 2005; Agustsson & Brainerd 2006; Yang et al. 2006; Faltenbacher et al. 2007) which weight the outskirts of galaxies more strongly than weak lensing-optimised measurements. The later results, which report no significant alignment (Hao et al. 2011; Hung & Ebeling 2012; Schneider et al. 2013; Chisari et al. 2014; Sifón et al. 2015), are therefore less prone to these effects. A conclusion to the same effect was reached by Schneider et al. (2013).

The correction for smearing by the PSF is critical in any lensing analysis: the finite size of the PSF leads to rounder images and observed ellipticities lower than the true values. This bias is commonly referred to as multiplicative bias as it merely scales the amplitude of the signal. However, due to (inevitable) misalignments of optical elements and atmospheric turbulence, the PSF is never perfectly round but tends to have a preferred direction, which may vary spatially and with time. This leads to an additional signal (therefore referred to as additive bias), which can mimic the cosmological or intrinsic alignment signal. For this reason cosmic shear studies take great care in characterising the PSF and quantifying any residual systematics (see e.g. Heymans et al. 2012b). Similar rigour is required for accurate measurements of intrinsic alignments. Most recent results (see Section 4) are based on weak lensing pipelines, but we note that this is not the case for older studies of intrinsic alignments.

The change in observed shape depends on the size of the galaxy relative to the PSF. How various biases propagate was studied in detail in Massey et al. (2013). If the PSF is sufficiently well understood then it can be used to correct the observed shapes either using the observed moments of the surface brightness distribution or by convolving galaxy models with the PSF model. A complication is that the PSF varies in time, due to turbulence in the atmosphere (e.g. Heymans et al. 2012a) or variations in the thermal and gravitational load on the optical elements. However, if a sufficiently large number of stars are visible in the field-of-view, these can be used to quantify the spatial variation of the PSF (Hoekstra 2004; Jain et al. 2006). The PSF is not the only instrumental source of bias. Imperfections in the detector can also affect the observed shapes. In the case of space-based observations, radiation damage causes charge traps leading to charge-transfer inefficiency during read-out (e.g. Rhodes et al. 2010; Massey et al. 2014). This produces charge trails, which result in alignments of the observed images. This is less relevant for ground-based observations where the brighter sky fills the charge traps but other effects persist, including charge-induced pixel shifts (Gruen et al. 2015), the brighter/fatter effect for individual charge wells (Antilogus et al. 2014) and others.

2.3.2. *Intrinsic alignment measurements and cosmic shear*

We discuss the issue of mitigating the impact of intrinsic alignments on cosmic shear measurements in more detail in Section 6. Note for now that in the typical situation all terms in Equation (3) are relevant, hence the observed signal is a combination of the lensing signal itself and the II and GI contributions. We have discussed how shape measurement can depend on details of the algorithm deployed; accurately accounting or correcting for the contribution of the intrinsic alignment signal in a cosmic shear measurement therefore requires that the same shape measurement algorithm is used for both the weak lensing measurement and the estimate of the alignment signal. This condition may be trivially satisfied if the intrinsic alignment signal is determined from the cosmic shear survey itself, but one can also imagine scenarios where the intrinsic alignment signal is modelled using external data. Attempts to employ

intrinsic alignment measurements acquired using different data or a different shape measurement algorithm should only be undertaken with great care.

For instance, for low redshift galaxies the shear is low and the correlations between galaxy shapes are dominated by the II term. As such galaxies are bright and large compared to the PSF, their shapes can be measured reliably using deep modern observations. A limitation is that the number of sufficiently large and bright galaxies is small, giving rise to a large shot noise. However, a more serious concern is that it is not clear how to relate such measurements to predictions for the intrinsic alignment signal for galaxies at higher redshifts. As shown in Section 1, the estimated galaxy shape depends on the weight function applied to the galaxy light profile, which might differ for a well-resolved low-redshift observation and a poorly-resolved high-redshift observation of two very similar galaxies. A further complication is that, even if a robust shape measurement method can be found, which can measure shapes well regardless of redshift, the mix of galaxy types and properties may evolve and the intrinsic alignments themselves may vary with time.

Therefore direct measurements of the alignments of distant galaxies are needed. In fact, such studies will have to use the actual cosmic shear survey data. This naturally implies that the requirements on the accuracy of the shape measurements are similar, including a careful correction for the PSF. Moreover, to be able to extract the intrinsic alignment contributions with sufficient precision, good photometric redshift information is required. As the lensing kernel is broad in redshift, the required precision of photometric redshifts for the next generation of cosmic shear surveys is actually driven by our desire to model intrinsic alignments (Amara & Réfrégier 2008; Joachimi & Bridle 2010; Laszlo et al. 2012, see Section 3.3 for more details on the importance of redshift precision).

3. Shape correlations

The average shear and intrinsic alignment signal should vanish on very large scales because of statistical isotropy of the Universe. However, both effects cause local coherent variations in observed ellipticity that can be used to measure cosmic shear and intrinsic alignments over a range of scales. In this section we will introduce some of the statistics used to describe these correlations and measure them in data.

Both weak gravitational lensing and intrinsic alignments produce a correlation between galaxy shape and matter density. In addition to observed galaxy ellipticity, it is useful to consider another quantity, the projection of the ellipticity of a galaxy perpendicular to the line connecting the position of that galaxy to some point. This is called the tangential shear, γ_+, and is related to the observed ellipticity parameters through

$$\gamma_+ = -(\epsilon_1 \cos 2\vartheta_\mathrm{P} + \epsilon_2 \sin 2\vartheta_\mathrm{P}) = -\mathrm{Re}\{\epsilon \exp(2\mathrm{i}\vartheta_\mathrm{P})\}, \tag{12}$$

where ϑ_P is the position angle with respect to the centre of the lens. The sign convention in Equation (12) is such that $\gamma_+ < 0$ implies tangential alignments while $\gamma_+ > 0$ implies radial alignments. As an example, tangential shear is important in determining the masses of galaxy clusters (Okabe et al. 2010; Applegate et al. 2014; Hoekstra et al. 2015), where ensemble-averaged tangential shear as a function of cluster-centric radius can be related to the projected mass, or fit by a parametric model for the mass distribution (see Hoekstra et al. 2013, for a recent review).

In this section we will concentrate on the most frequently used statistics in the intrinsic alignment literature: two-point correlations over large scales. These are particularly relevant for the large-scale measurements presented in Section 4 and for understanding the impact of intrinsic alignments on cosmic shear surveys detailed in Section 6. For more detail on environment-dependent measurements see Section 5 and some discussion of higher-order statistics can be found in Section 6.5.

In Section 3.1 we introduce the relevant two-point correlation functions before describing practical estimators for the same correlation functions in Section 3.2. In Section 3.3 we describe the projection of three-dimensional statistics along the line of sight before relating these observables to intrinsic alignment models in Section 3.4. In Section 3.5 we describe some common systematic and null tests used when making measurements of intrinsic alignments.

3.1. Two-point correlation functions

If the density or ellipticity (or shear) field is Gaussian, then all the cosmological information is contained in the correlations between galaxy positions, galaxy shapes, and the (cross-)correlations between positions and shapes, aver-

aged over pairs of galaxies as a function of separation. These are known as two-point correlation statistics. If redshift information is available, the correlations can be computed for galaxies binned in redshift. This allows the calculation of auto- and cross-correlations of redshift bins. This is referred to as a *tomographic* analysis. In the case of non-Gaussian fields, due, for instance, to non-linear structure formation on small scales, higher-order statistics, such as the bispectrum, can be used to extract further information.

The statistical properties of the projected mass distribution are most easily quantified using the correlations between galaxy shapes as a function of their separation, i.e. in configuration space. This approachs allows for the treatment of complicated masks and survey boundaries. The corresponding ellipticity autocorrelation function is defined as the excess probability that any two galaxies are aligned (with respect to some arbitrarily defined coordinate system):

$$\langle \epsilon^i \epsilon^j \rangle(\theta) = \langle \epsilon^i(\boldsymbol{\theta}') \epsilon^j(\boldsymbol{\theta}' + \boldsymbol{\theta}) \rangle, \tag{13}$$

where $i, j \in \{1, 2\}$ denote pairs of galaxies and the angle brackets represent averaging over all pairs separated by angle $\theta = |\boldsymbol{\theta}|$. Because of parity the correlation vanishes if $i \neq j$ and isotropy ensures that the correlation function is a function only of the separation $|\boldsymbol{\theta}|$ for $i = j$.

Equation (13) is defined with reference to (local) coordinate axes which are somewhat arbitrary. Instead it is more convenient to consider the ellipticities with respect to axes oriented tangentially (+; see Equation (12)) or at 45 degrees ($\times$) to a line joining each pair of galaxies. For convenience, it is common to define the ellipticity correlation functions

$$\xi_\pm(\theta) = \langle \epsilon_+ \epsilon_+ \rangle(\theta) \pm \langle \epsilon_\times \epsilon_\times \rangle(\theta). \tag{14}$$

We note that this notation is used in cosmic shear studies, but that it is different from the conventions commonly used in clustering studies, where the symbol ξ indicates the correlation function in 3D, and w is used for projected quantities. We will try to clarify these differences where needed.

When ellipticity correlation functions are estimated from real, noisy data, a weighted combination of observed ellipticities is employed:

$$\hat{\xi}_\pm(\theta) = \frac{\sum_{ij} W^i W^j \left[\epsilon_+(i|j) \epsilon_+(j|i) \pm \epsilon_\times(i|j) \epsilon_\times(j|i) \right]}{\sum_{ij} W^i W^j}, \tag{15}$$

where the weight W_i typically accounts for the measurement uncertainties and we use $\epsilon_+(i|j)$ to mean the + component of the ellipticity of a galaxy i, measured relative to the vector linking it to galaxy j, $\epsilon_\times(i|j)$ is the same for the $\times$ component. In the absence of intrinsic correlations these estimators are unbiased tracers of the weak lensing shear correlation functions, $\langle \epsilon_+(i|j) \epsilon_+(j|i) \pm \epsilon_\times(i|j) \epsilon_\times(j|i) \rangle = \sigma_\epsilon^2 \delta_{ij} + \xi_\pm(|\boldsymbol{\theta}^i - \boldsymbol{\theta}^j|)$, where δ_{ij} is the Kronecker delta, σ_ϵ denotes the total intrinsic ellipticity dispersion, and the angle brackets indicate an ensemble average over the intrinsic ellipticity distribution and over the cosmic shear field, assuming randomly-oriented intrinsic ellipticities (Schneider et al. 2002a). Though of course, due to intrinsic alignments, this is not the case in reality.

The ellipticity correlations between galaxies with similar redshifts can be used to determine the II signal because it is something that affects physically close galaxies. Correlations in the shapes of physically close galaxies due to a shared local tidal field boosts the intrinsic alignment signal, compared to the gravitational lensing contribution. This requires very good redshift information for the sources, and even in this case the observed signal contains a contribution from gravitational lensing itself, unless one restricts the analysis to $z \lesssim 0.1$, where the lensing signal is very small (Heymans & Heavens 2003). Alternatively one can remove such close pairs from the lensing analysis, thus efficiently suppressing the II contribution.

The GI contribution, on the other hand, cannot be easily removed as it results from correlations between the shapes of galaxies that are separated in redshift, as described in Section 1. To estimate the IA signal directly from data, we need to determine the cross-correlation of tangential galaxy ellipiticity with the matter overdensity, $\xi_{\delta+}(r_\mathrm{p}, \Pi, z)$, or its projection, $w_{\delta+}(r_\mathrm{p})$. The subscript $\delta+$ indicates that we are correlating the density δ with the tangential ellipticity ϵ_+ for pairs separated by a transverse separation r_p and a radial distance Π along the line of sight. In general it is not possible to directly estimate the matter overdensity field, δ, because the bulk of the matter in the Universe consists of dark matter. Instead galaxies are used as (biased) tracers of the density field. The cross-correlation of galaxy position with tangential ellipticity is indicated by $\xi_{\mathrm{g}+}(r_\mathrm{p}, \Pi, z)$. A positive $\xi_{\mathrm{g}+}(r_\mathrm{p}, \Pi, z)$ is a signal of coherent radial alignments

of galaxy ellipticity with galaxy density. Assuming galaxy density traces the matter density, this is the correlation which sources intrinsic alignments of galaxy ellipticity, in both the II and GI flavours. Negative $\xi_{g+}(r_p, \Pi, z)$ indicates tangential alignments induced by gravitational lensing. See Equation (18) for a practical estimator of this correlation. The matter-ellipticity correlation is related to the galaxy-ellipticity correlation by the galaxy bias which can, in general, be a function of position and redshift, $\xi_{\delta+}(r_p, \Pi, z) = b_g(r_p, \Pi, z)\xi_{g+}(r_p, \Pi, z)$.

The shear field can be decomposed into a gradient and a curl component. The curl-free component is commonly referred to as the "E"-mode, whereas the pure curl component is called the "B"-mode, analogous to the polarisations of the electric and magnetic field. If weak gravitational lensing was the only source of correlations in the shapes of galaxies, then one would expect to observe $\xi_{BB}(\theta) = 0$. Although this is a good assumption for current surveys, a number of effects can introduce B-modes. For instance, Schneider et al. (2002b) showed that B-modes are introduced if the source galaxies are clustered. However, most of these effects are expected to be small, and the measurement of the B-mode has been used as a measure of residual systematics (as instrumental effects tend to include B-modes). However, intrinsic alignments can also introduce B-modes. Both the linear and quadratic alignment models are believed to source B-modes (Hirata & Seljak 2004), while Crittenden et al. (2001) and Crittenden et al. (2002) showed that spin alignments are not curl-free. Although the level of actually existing B-modes sourced by IAs (rather than instrumental systematics etc.) remains uncertain, it is too small to be detected in current surveys.

3.2. Estimators of the two-point correlation functions

The ellipticity correlation functions are straightforward to compute from observations and are insensitive to the survey geometry. This geometry is usually rather complex because of areas that need to be masked due to the presence of bright stars or other artefacts in the data and must be accounted for when estimating the galaxy correlation function ξ_{gg}. Nonetheless, it is important that the estimator that is employed accounts for the fact that some measurements are noisier than others. Alternatively, one may want to define estimators that minimise certain biases. In practice the correlation functions are computed from entries in a galaxy catalogue, which lists their positions, shapes, etc.

Assume that D is a catalogue of N_D galaxies with positions from which we can compute $P_{DD}(r_p, \Pi)$, the number of pairs as a function of separation. It is convenient to normalise the result by the total number of pairs, given by $N_D(N_D - 1)/2$, and the volume fraction, to define:

$$DD(r_p, \Pi) = \frac{P_{DD}(r_p, \Pi)}{N_D(N_D - 1)V_{bin}/(2V_{survey})}, \tag{16}$$

where V_{survey} is the total volume of the survey and V_{bin} is the volume of some three-dimensional bin in r_p and Π. The volume of the bin is given by $V_{bin} = 2\pi r_p \Delta r_p \Delta\Pi$, in the limit that Δr_p is small. If the galaxies are clustered then DD will be larger than unity on small scales. If we were considering a cross-correlation, rather than an auto-correlation, the equivalent normalisation would be $N_{D1}N_{D2}V_{bin}/V_{survey}$.

However, we have not so far taken into account the survey geometry - the fact that magnitude limits, source density etc vary across the survey field of view due to observational effects. The simplest way to do this is to consider a catalogue of objects with random positions, but to which the mask (which excludes those regions not observed by the survey) has been applied. This random catalogue is indicated by R and should contain many more entries than the data to avoid introducing unnecessary noise. RR denotes a pair of galaxies where both are drawn from the random catalogue. The most commonly used estimator for modern studies is the Landy-Szalay estimator (Landy & Szalay 1993). For the galaxy position auto-correlation this takes the form:

$$\hat{\xi}_{gg}(r_p, \Pi) = \frac{DD - 2DR + RR}{RR}, \tag{17}$$

where DR means a pair of galaxies with one drawn from the data and one from the random catalogue.

A version of this estimator can be adopted for the GI cross-correlation function. In this form it is referred to as the modified Landy-Szalay estimator (Mandelbaum et al. 2011):

$$\hat{\xi}_{g+}(r_p, \Pi) = \frac{S_+(D - R)}{R_S R} = \frac{S_+D - S_+R}{R_S R}. \tag{18}$$

Here we have assumed that, as well as the galaxy population, D, we have some other set of galaxies, S, with good shape measurements (note these could be the same population, or S could be some sub-set of D). R and R_S are now sets of random positions corresponding to the position sample and shape sample respectively. S_+D is the sum of the + component of the ellipticity over all pairs of galaxies with separations r_p and Π, where one galaxy is in the good shape sample and one is in the position sample,

$$S_+D = \sum_{i\neq j|r_\mathrm{p},\Pi} \epsilon_+(j|i), \tag{19}$$

for a pair of galaxies i and j. Similarly we can define the estimators for the tangential and cross ellipticity autocorrelations,

$$\hat{\xi}_{++}(r_\mathrm{p},\Pi) = \frac{S_+S_+}{R_SR_S}, \tag{20}$$

$$\hat{\xi}_{\times\times}(r_\mathrm{p},\Pi) = \frac{S_\times S_\times}{R_SR_S}, \tag{21}$$

where

$$S_+S_+ = \sum_{i\neq j|r_\mathrm{p},\Pi} \epsilon_+(j|i)\epsilon_+(i|j), \tag{22}$$

$$S_\times S_\times = \sum_{i\neq j|r_\mathrm{p},\Pi} \epsilon_\times(j|i)\epsilon_\times(i|j). \tag{23}$$

Alternatively one can define correlation functions of spin or position angles but, as mentioned earlier, a direct relation to the ellipticity correlation function then requires knowledge of the underlying ellipticity distribution. Hence, to be useful to mitigate the impact of intrinsic alignments in weak lensing studies, shapes need to be measured regardless.

3.3. Projected correlation functions

Although three-dimensional correlation functions are conveniently computed from theory, the observations are most commonly presented as projected quantities. Here we describe the projection of a general correlation function but it applies specifically to each of the correlations described above.

Consider a three-dimensional correlation function, $\xi_\mathrm{ab}(r_\mathrm{p},\Pi,z)$, where the separation of our pair, ab, under consideration has been split into components parallel, Π, and perpendicular, r_p to the line of sight. The presence of z is because the correlation function itself may depend on redshift. The corresponding projected correlation function, $w_{ab}(r_\mathrm{p})$, for objects in a particular redshift bin, separated by a distance r_p, transverse to the line of sight, is obtained by integrating the equivalent 3D correlation function $\xi_\mathrm{ab}(r_\mathrm{p},\Pi,z)$ along the line-of-sight:

$$w_\mathrm{ab}(r_\mathrm{p}) = \int dz\, W(z) \int d\Pi\, \xi_\mathrm{ab}(r_\mathrm{p},\Pi,z), \tag{24}$$

where Π is the distance along the line of sight coordinate, and $W(z)$ is the redshift weighting (Mandelbaum et al. 2011),

$$W(z) = \frac{p^2(z)}{\chi^2(z)\chi'(z)}\left[\int \mathrm{d}z \frac{p^2(z)}{\chi^2(z)\chi'(z)}\right]^{-1}, \tag{25}$$

where $p(z)$ is the unconditional probability distribution of galaxy redshifts. a, b represent any combination of observables, $\mathrm{a},\mathrm{b} \in \{\delta,\mathrm{g},\epsilon,+,\times\}$, where δ is the matter overdensity, g is galaxy position, ϵ is galaxy ellipticity and $+,\times$ are the components of ellipticity parallel/perpendicular or at 45° to the vector connecting the pair of positions. If redshift information is available, it is convenient and straightforward to express the measurements as a function of r_p in physical coordinates. Alternatively one can show results as a function of angular separation, although this only applied to early results in practice.

The most precise results are obtained if spectroscopic redshifts (Appenzeller 2013) are available. However, this requires relatively large investments of observing time on large telescopes, especially for the faint galaxies typically used in weak lensing studies. Alternatively we can use photometric observations in multiple filters which probe features in the spectral energy distribution, which in turn can be used to estimate a photometric redshift (see e.g. Hildebrandt et al. 2012, for their application to the CFHTLenS dataset). Compared to spectroscopy, photometry is less precise but faster and therefore cheaper. Most of the observations discussed here use spectroscopic redshifts but the larger number density available from photometric surveys makes their use desirable, even at the cost of lower redshift accuracy.

Unsurprisingly the photometric redshift scatter tends to smear the intrinsic alignment signal along the line-of-sight direction, Π (Joachimi et al. 2011). When calculating projected two dimensional correlation functions, the full intrinsic alignment signal can be retained by extending the range of Π considered in a measurement. This does however reduce the measured signal-to-noise ratio, because the signal has become more spread out, and increases the contamination by gravitational shear. In practice the line-of-sight integral gets truncated and some portion of the intrinsic alignment signal is lost. This effect can be seen in Figure 2. In the lower panel, where exact redshift information is assumed, the power of the galaxy position-ellipticity correlation falls off very quickly with line-of-sight separation. In the upper panel, where a Gaussian photometric redshift scatter of width $\sigma_z = 0.02$ is assumed, there is still significant correlation, even at line-of-sight separations of $> 100\mathrm{Mpc}/h$.

Careful modelling of the expected signal is even more important when using photometric redshifts. The large line-of-sight spread means the effect of contributions from the galaxy position-gravitational lensing cross-correlation and lensing magnification cross-correlations is more pronounced, see Section 6.4 for further discussion.

3.4. Using correlation functions to test intrinsic alignment models

A detailed physical understanding of our measurements requires comparison with theoretical alignment models, such as the ones that are detailed in Kiessling et al. (2015). From a theory perspective, it is often more convenient to calculate correlations in Fourier space or in spherical harmonic space. The resulting power spectrum can be directly related to the real space statistics, however the choice of space for the measurement can depend on the survey geometry (e.g. for a wide-field survey a spherical harmonic expansion is natural on the sphere), or related to the strength of the signal (e.g. the presence of bad pixels mean configuration space can be preferred), or on the numerical tools available. In this section we will concentrate on the galaxy-ellipticity correlation but the relations generalise to other observables, see Kiessling et al. (2015) for the full range of expressions.

We can relate the projected galaxy position-ellipticity correlation function, $w_{g+}(r_p)$, directly to the three-dimensional density-intrinsic ellipticity function in Fourier space, $P_{\delta I}(k_\perp, z)$, via

$$w_{g+}(r_p) = -b_g \int \mathrm{d}z W(z) \int_0^\infty \frac{\mathrm{d}k_\perp k_\perp}{2\pi} J_2(k_\perp r_p) P_{\delta I}(k_\perp, z), \tag{26}$$

where b_g is the galaxy bias, $J_2(k_\perp r_p)$ is the second-order Bessel function of the first kind, $k_\perp$ is the wavevector perpendicular to the line-of-sight and $W(z)$ is the weighting over redshifts as derived by Mandelbaum et al. (2011), see Equation (25).

The contribution from intrinsic alignments is encoded in the three-dimensional power spectrum $P_{\delta I}(k_\perp, z)$. One model we will refer to throughout this paper is the linear alignment model (Hirata & Seljak 2004),

$$P_{\delta I}(k_\perp, \chi) = -\frac{C_1 \bar{\rho}(\chi)}{\bar{D}(\chi)} a^2(\chi) P_{\delta\delta}(k_\perp, \chi), \tag{27}$$

where C_1 is a constant setting the amplitude of correlation, $\bar{\rho}(\chi)$ is the mean matter density of the Universe, $\bar{D}(\chi) = D(\chi)(1+z)$, $D(\chi)$ is the linear growth function, normalised to $D(\chi = 0) = 1$, $a(\chi)$ is the scale factor and $P_{\delta\delta}(k_\perp, \chi)$ is the linear matter power spectrum. We refer to Kiessling et al. (2015) for more information on this and other specific models. We can also construct projected angular correlation functions, $C(\ell)$, directly from the three-dimensional power spectra, see Section 6 for more details.

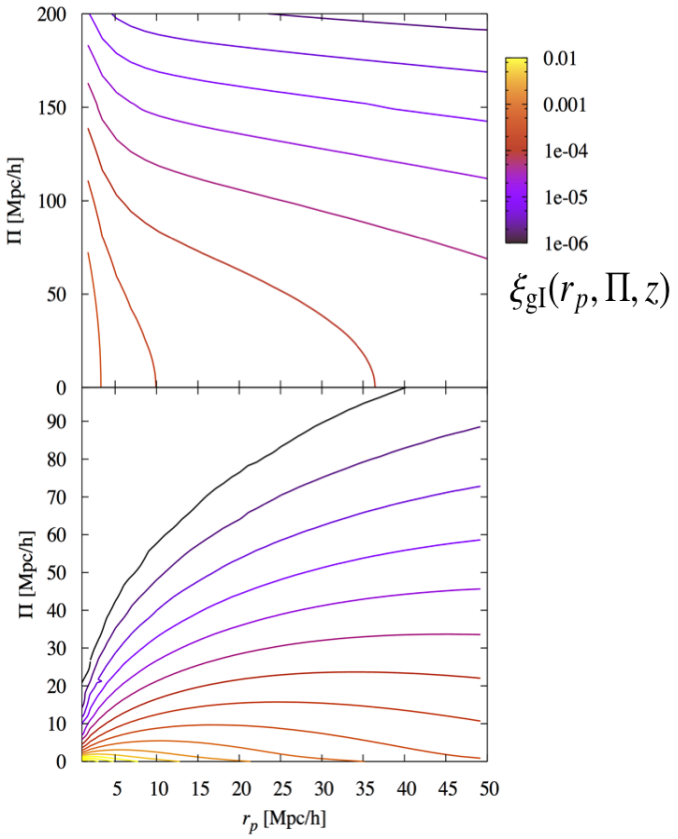


Fig. 2.— Three-dimensional galaxy position-ellipticity correlation function, $\xi_{g+}(r_p, \Pi)$, as a function of comoving line-of-sight separation Π and comoving transverse separation r_p at $z \sim 0.5$. Contours are logarithmically spaced between 10^{-2} (yellow) and 10^{-6} (black) with three lines per decade. **Top panel:** Applying a Gaussian photometric redshift scatter of width 0.02. **Bottom panel:** Assuming exact redshifts. Note the largely different scaling of the ordinate axes. The galaxy bias has been set to unity, and the linear alignment model with SuperCOSMOS normalisation (see Section 4) has been used to model $P_{\delta I}$ in both cases. Redshift-space distortions have not been taken into account. *Reproduced with permission from* Joachimi et al. (2011) © *ESO.*

While several terms in Equation (27) depend on redshift, these dependencies cancel out meaning that, overall, there are no explicit dependencies on redshift or galaxy luminosity in the linear alignment model but it is often thought useful to check for these when fitting to data. This is because the strength of coupling between dark matter and galaxies is unknown. These extra terms help describe the dependence of the coupling. A common approach in the literature is to insert power-law dependences on redshift, z, and the luminosity, L, where the index of the power-law is a free parameter that can be fit to data. Putting these together produces a model of the form

$$P_{\rm gI}^{\rm model}(k, z, L) = A_{\rm I}\, b_{\rm g}\, P_{\delta I}(k, z) \left(\frac{1+z}{1+z_0}\right)^{\eta_{\rm other}} \left(\frac{L}{L_0}\right)^{\beta}, \tag{28}$$

where $P_{\delta I}$ is the power spectrum for the mass density - intrinsic ellipticity correlation, provided by some intrinsic alignment model. $A_{\rm I}$ is a free amplitude term, $b_{\rm g}$ is the (linear, deterministic) galaxy bias, z_0 is a reference pivot redshift, L_0 is a reference pivot luminosity and $\eta_{\rm other}, \beta$ are the free power-law indices for the redshift and luminosity

dependence respectively. The power-law index for redshift has been called $\eta_{\rm other}$ because it attempts to capture redshift evolution due to any "other" physical processes beyond the linear alignment model.

3.5. Tests for systematics

Some of the correlations are expected to be consistent with no signal in the absence of systematics errors. Such *null tests* can be used to test for the presence of systematics in the data, and a significant detection of a signal is a warning that the measurements of real interest may be biased. For instance, we already saw that the ellipticity auto-correlations can be written in terms of curl-free "E" and divergence-free "B" modes. Although the signal caused by spin alignments is not curl-free, the much stronger signal from the linear alignment model as well as weak lensing itself comprise only E-modes to first order. Therefore such a decomposition can be a useful diagnostic in studying the effects of systematics, even though the B-mode signal is not expected to vanish completely.

A common null test in the literature is the measurement of $w_{\rm g\times}$, the correlation of the density sample with the cross-component of the shear from the shape sample, i.e. the ellipticity measured at 45° to the line connecting the pair of galaxies under consideration, one from the shape sample, the other from the density-tracer sample. This statistic is of course very closely related to the measurement of $w_{\rm g+}$, the correlation of the density sample with the ellipticity measured along the connecting vector, and requires no additional data products, random catalogues or statistical tools. Parity symmetry means $w_{\rm g\times}$ is expected to be zero. A non-zero measured value might indicate the presence of a range of systematic effects including residual PSF distortions. The cross-component of the shear is useful generally as a systematic. Another related statistic is $w_{+\times}$, which is expected to be consistent with zero in the absence of systematics because intrinsic alignments only induce alignments in the radial/tangential direction.

A different null test is the calculation of $w_{\rm g+}$, the same statistic used to measure shape alignment, but where only certain pair separations are considered. The chosen scales should be such that this correlation function will vanish because the line-of-sight separation is sufficiently large that intrinsic alignments are negligible, being a local effect, but small enough that gravitational lensing shear is still negligible. Spurious galaxy alignment, whether from optical distortion in the telescope, deblending, mistaken sky subtraction or photometric redshift errors could generate a $w_{\rm g+}$ signal at large (apparent) separation.

These various tests were applied to the observational results that are reviewed in more detail in the next few sections. Many of these studies found $w_{\rm g+}$ consistent with zero at large line-of-sight separation, and $w_{\rm g\times}$ consistent with noise at all scales (e.g. Hirata et al. 2007; Mandelbaum et al. 2011; Joachimi et al. 2011; Singh et al. 2015). While as yet undiscovered systematic effects cannot entirely be ruled out, these results give us hope that the intrinsic alignment signal can be reliably determined from current and near-future data.

Multiple shape measurement codes can be applied to the same data. Of course common systematic effects will manifest in both the resulting shape catalogues, but any method-specific systematics can be detected by looking at differences in correlations using the different shape estimates. For example, Sifón et al. (2015) shows results using two different shape measurement pipelines for this reason.

4. Observations of alignment in large galaxy samples

On small scales, intrinsic alignments are expected to be intimately connected to the environment of the galaxy, in terms of the morphology of the local cosmic web. Details of the galaxy's evolution, including feedback processes, mergers etc. may also be expected to play a role. In contrast it is believed that the mechanisms that give rise to alignments which persist in pairwise correlations of galaxies on large scales can be related to the large-scale gravitational tidal field. Examples of such mechanisms are introduced in Joachimi et al. (2015) and discussed in more technical detail in Kiessling et al. (2015), but many open questions about galaxy alignments including their amplitude, dependence on galaxy type and luminosity and their evolution with redshift, have no obvious analytic answer. Precise and accurate observations are therefore critical.

To understand alignments on small scales we need to consider the dependence on the environment of the galaxies under consideration, which we do in the next section. In this section we start by reviewing the observational status of alignments from the linear regime ($> 10{\rm Mpc}/h$) into the quasi-linear regime ($\sim 5-10{\rm Mpc}/h$). On these scales the

matter power spectrum of density fluctuations is fairly well understood from linear theory and largely unaffected by baryonic physics (e.g. Semboloni et al. 2011). Furthermore, the measurements are based on datasets and methods that are similar to those used for cosmic shear studies.

The first large scale study of intrinsic alignments in the cosmic shear era was Brown et al. (2002). This paper used 2×10^6 galaxies from the SuperCOSMOS sky survey (Hambly et al. 2001) with a median redshift of $z \sim 0.1$. An observed excess correlation above that expected from cosmic shear was seen as evidence of intrinsic alignments. The observed amplitude was subsequently used widely to normalise intrinsic alignment models at low redshift to the value $C_1 = 5 \times 10^{-14} (h^2 \mathrm{M}_\odot \mathrm{Mpc}^{-3})^{-1}$ (Bridle & King 2007). C_1 is the normalisation factor setting the amplitude of Equation (27) and Equation (28). The free parameter A allows the amplitude to vary around this constant. The Brown et al. (2002) observations immediately required several popular IA models (Heavens et al. 2000; Croft & Metzler 2000; Catelan et al. 2001) to be revised downwards in amplitude as they had over-predicted the SuperCOSMOS signal. Brown et al. (2002) also offered the first observation-based assessment of the likely impact for cosmic shear measurements, see Section 6 for more discussion.

In the following we split the results by galaxy type because the leading theories predict that different processes dominate for late- and early-types (see Kiessling et al. 2015, for more details). For example, the linear alignment model for dispersion-dominated galaxies (Hirata & Seljak 2004) and tidal torque theory for angular momentum-dominated galaxies (Peebles 1969; Doroshkevich 1970; White 1984) motivate a split into early- and late-type galaxies. We therefore review results for late-type galaxies in Section 4.1 and for early-type galaxies in Section 4.2. Alternatively, the samples are split by rest-frame colour or spectral energy distribution. Although we note that a split into blue and red galaxies is not exactly the same as a morphological selection, we consider this implicitly to be the case when reviewing the different galaxy samples. Finally, in Section 4.3, we review indirect methods of measuring intrinsic alignments for both early- and late-type galaxies.

4.1. Late-type galaxies

The most commonly accepted scenario for the alignments of disc galaxies is the quadratic alignment model, which describes how the angular momentum of dark matter haloes is spun up to produce correlations between the orientations of galaxies (Hirata & Seljak 2004). Disc-galaxies are believed to be nearly circular when viewed face-on, they appear elliptical as a result of projection due to their orientation with respect to the observer. Total observed ellipticity is the sum of this projection effect and any small intrinsic ellipticity the galaxy may have. If the orientation of the disc is determined by the spin vector of the galaxy, and these are correlated between galaxies, then there will be a correlation between the observed intrinsic ellipticities i.e. intrinsic *alignment*. These can be observed by simply measuring the correlations in measured shapes (Hirata et al. 2007; Mandelbaum et al. 2011). Before reviewing these results, we note that this paradigm gives us another avenue to study intrinsic alignments of disc galaxies: we can measure the correlation of galaxy spins. Note that the quadratic alignment model is so-called because the II three-dimensional power spectrum depends on the square of the linear matter power spectrum and therefore the alignment signal is expected to be suppressed compared to the linear alignment model which is believed to apply to early-type galaxies and has a linear dependence on the matter power spectrum.

Slosar et al. (2009) presented an early example of such a measurement using data from the Galaxy Zoo citizen science project[1]. In Galaxy Zoo, spiral galaxies are classified as clockwise, anti-clockwise or edge-on. For each face-on galaxy there is therefore one bit of information corresponding to the sign of the galaxy spin vector projected along the line-of-sight. This information enabled the measurement of the correlation function of spin chirality of face-on spirals. The authors tentatively reported that galaxy spin directions are correlated at very small scales (< 0.5Mpc), albeit with low significance ($2 - 3\sigma$). There is no obvious reason, under the tidal torquing model, why this chiral correlation should exist. If confirmed to high significance in future studies, it might provide useful insight into the sourcing of galaxy angular momentum.

Going beyond correlations in spin chirality (clockwise vs. anticlockwise), Cervantes-Sodi et al. (2010) searched for correlations between the orientations of the spin vectors themselves in pairs of spiral galaxies from the SDSS survey.

[1] http://www.galaxyzoo.org/

They computed correlations in the spin parameter, λ (Peebles 1969):

$$\lambda = \frac{J|E|^{1/2}}{GM^{5/2}}, \tag{29}$$

where G, E, M and J are Newton's constant, the total energy, mass and angular momentum of the configuration, respectively. λ accounts for the magnitude of the spin, while the position angle was used as an estimate of direction.

Cervantes-Sodi et al. (2010) reported a weak (1.5σ) correlation between the spin magnitude of neighbouring galaxies, but, contrary to Slosar et al. (2009), no clear alignment between their orientation. The authors suggested that this is due to some late-time dilution of a primordial correlation laid down at the time of galaxy formation. They suggest that interactions with close neighbours can significantly redistribute angular momentum through clumpy and irregular mass accretion, reducing the value of λ.

Lee (2011) presented another measurement of intrinsic alignments using spin statistics. This paper used large (angular size $\geq$ 7.92 arcsec) late-type spiral galaxies from the SDSS DR7 over $0 \leq z \leq 0.02$. The SDSS observations provide information on the galaxy's axial ratio, q, and position angle, $\vartheta_{\rm P}$, from which the unit spin vector for each galaxy is reconstructed. These spin vectors are combined to form the two-point spatial correlation function for galaxy spin axes. For this sample a positive spatial correlation is detected at 3.4σ (separation $r \lesssim 1$Mpc/h) and 2.4σ (separation $r \lesssim 2$Mpc/h). The correlations are stronger for galaxies located in dense regions, which have more than 10 neighbours within 2 Mpc/h. The measured correlations are consistent with the predictions of the quadratic alignment model that the spin two-point correlation should follow a quadratic scaling with the linear density correlations. We note that the estimation of the spin vector relies on the assumption that galaxies form thin discs. If this is not the case across the galaxy sample, this assumption can introduce a systematic error of order 10% in the measured spin correlation (Lee & Erdogdu 2007; Lee 2011).

Andrae & Jahnke (2011) also used SDSS data to analyse angular momentum correlations of disc galaxies. They found that positive correlations of spiral-arm handedness and angular momentum orientations on distance scales of 1 Mpc/h are plausible but not statistically significant. Furthermore, they suggested that previous studies such as the ones presented by Slosar et al. (2009) and Lee (2011) overestimated the correlation of spins for spiral galaxies because of bias in ellipticity estimates based on second moments due to galactic bulges. This highlights the importance of how orientations are determined.

Thanks to large imaging surveys, pre-eminently the SDSS, much progress has been made over the last decade in the correlation of galaxy ellipticities. The first to take advantage of SDSS, in the context of late-type galaxies, is the study by Hirata et al. (2007) who attempted to measure intrinsic alignments for a low-redshift sample of blue galaxies, selected from the SDSS main spectroscopic redshift sample. This is a flux-limited sample primarily covering the range $0.05 < z < 0.2$. Hirata et al. (2007) split a colour-selected blue subset of this flux-limited sample into four luminosity bins for analysis, but detected no significant signal in any of those bins (Hirata et al. (2007) did make a positive detection for intrinsic alignments in SDSS red galaxies). While this null result for blue galaxies can be interpreted as beneficial for cosmic shear studies, the statistical uncertainties are relatively large due to the small number of blue galaxies in the high luminosity bins. Furthermore, given the low redshift of the sample, applying the results to cosmic shear surveys, which target galaxies at much higher redshifts, requires a large extrapolation. This motivated attempts to repeat a similar measurement at higher redshifts.

Such a sample was provided by the overlap of the SDSS imaging and the WiggleZ redshift survey (Drinkwater et al. 2010), which targeted a population of blue galaxies, whose mean redshift was $z_{\rm mean} \sim 0.6$, with a primary science goal of measuring Baryon Acoustic Oscillations (BAO). Mandelbaum et al. (2011) measured the intrinsic alignments of the subset of galaxies for which ellipticities were determined from the SDSS. The full WiggleZ sample was used to trace the density field, assuming a linear galaxy bias. While previous papers, notably Hirata et al. (2007), had measured intrinsic alignments for blue galaxies at low redshifts, this was the first paper to push the measurements to intermediate redshifts.

Figure 3 shows the resulting measurements from Mandelbaum et al. (2011) for $w_{\rm g+}$ and w_{++} as a function of transverse separation for the WiggleZ dataset, split into two redshift bins. The correlation functions are consistent with zero within the statistical uncertainties, which are relatively large. By combining with the results for some

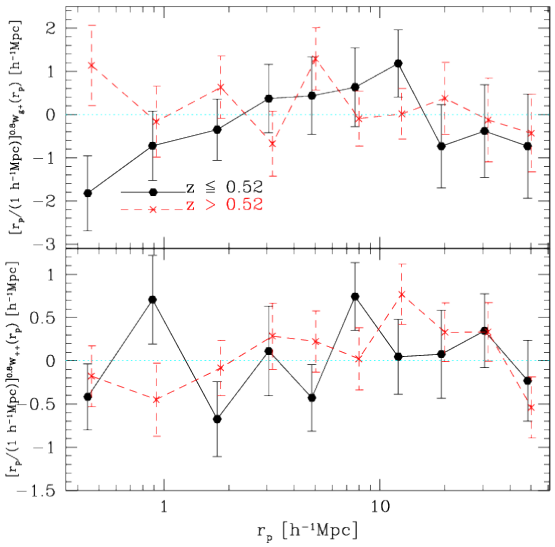


Fig. 3.— **Top panel:** Projected galaxy-tangential ellipticity cross-correlation signal $w_{g+}(r_p)$, multiplied by $r_p^{0.8}$, from the WiggleZ data of Mandelbaum et al. (2011). Results are shown averaged over all WiggleZ regions, for the two redshift subsamples. Points at a given value of r_p are slightly horizontally offset for clarity. **Bottom panel:** Same as the top, but for the ellipticity-ellipticity cross-correlation signal $w_{++}(r_p)$. *Reproduced with permission from* Mandelbaum et al. (2011).

lower-redshift blue galaxy samples from SDSS that were previously presented in Mandelbaum et al. (2006a), the null detection was used to place upper limits on how blue galaxy intrinsic alignments could contaminate weak lensing measurements from a CFHTLenS-like survey, with the result being a bias in the amplitude of the (linear) power spectrum on the scale of 8 Mpc/h, σ_8, of $^{+0.02}_{-0.03}$ at the 95% confidence level. See Section 6 for more details on how intrinsic alignments impact estimates of cosmological parameters from cosmic shear.

Mandelbaum et al. (2011) also placed constraints on the redshift evolution of blue galaxy intrinsic alignments, taking advantage of the broad redshift range of the WiggleZ sample. The full sample was split into two redshift slices containing galaxies below and above $z = 0.52$. Mandelbaum et al. (2011) fit two simple models to their intrinsic alignment measurements: a power-law in transverse separation and the non-linear alignment model with an additional free power-law dependence on redshift (Bridle & King 2007). The non-linear alignment model is simply the linear alignment model of Hirata & Seljak (2004) with the non-linear three-dimensional matter power spectrum substituted in place of the linear matter power spectrum. It is not a truly non-linear formulation of IAs, indeed there is no theoretical justification for this model but, as we shall see, it fits the data better than the linear alignment model (see Section 3.3 of Kiessling et al. 2015 for more details on the non-linear alignment model). The power-law in redshift takes the form given by Equation (28) with the free parameter $\eta_{\rm other}$ and a pivot redshift of $z_p = 0.3$. Constraints on the amplitude of the power law are shown in Figure 4. They are consistent with zero for all samples from both w_{g+} and w_{++}. This tells us that there is no evidence for evolution of the intrinsic alignment signal with redshift.

Note that the most likely sign of contributions of both PSF systematics and intrinsic alignments to w_{++} is positive, so the null detection itself indicates that there are no substantial observational systematics contaminating the measurement. The primary uncertainty in the application of these upper limits to future surveys is that the sample does not correspond to the entire blue cloud (Kauffmann et al. 2003; Wyder et al. 2007), but rather to a specific subset of it that appears to consist of morphologically disturbed starburst galaxies. The signal might therefore be compromised by recent mergers and other environmental effects that apply to the galaxies selected by WiggleZ, but which do not apply

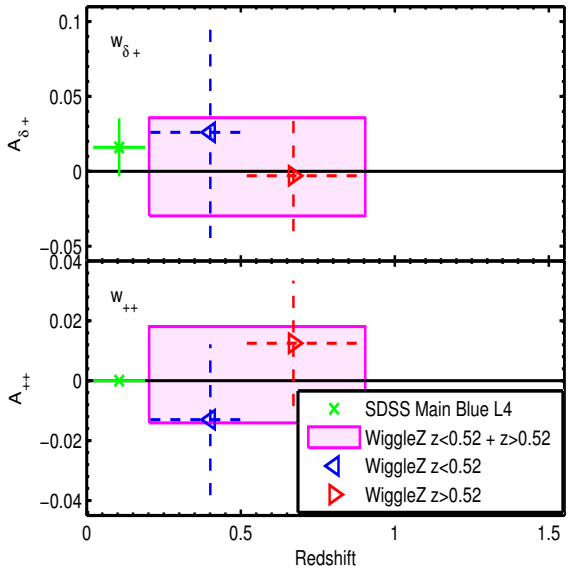


Fig. 4.— Constraints on the power-law amplitude A as a function of redshift from the WiggleZ data of Mandelbaum et al. (2011). This analysis used line-of-sight range, $\Pi_{\rm max} = 60{\rm Mpc}/h$, and fixed the power-law slope at $\alpha = 0.88$. **Upper panel:** Constraints from $w_{\rm g+}$. **Lower panel:** Constraints from w_{++}. From left to right, the points show constraints from SDSS Main Blue L4 (green cross); WiggleZ $z < 0.52$ (blue triangle); and WiggleZ $z > 0.52$ (red triangle). The horizontal lines indicate the redshift range of the observations. The shaded pink rectangle indicates the constraint from the full WiggleZ sample (both redshift ranges). *Reproduced with permission from* Mandelbaum et al. (2011).

to the general population of late-type galaxies.

Much more observational progress is needed before models of intrinsic alignments for late-type galaxies can be confronted with precise observational constraints. Current constraints come from spectroscopic studies, which mostly target the bright early-type galaxies we will discuss next. Unfortunately photometric redshifts are typically the least reliable for late-type galaxies as well, as their 4000Å break is less pronounced. However, the situation may improve thanks to new surveys that aim to cover a significant wavelength range with a large number of narrow-band filters (Martí et al. 2014).

4.2. Early-type Galaxies

Compared to the null-detections for late-type galaxies, the situation is markedly different for early-type galaxies. Luminous Red Galaxies (LRGs) make easier targets for BAO surveys. Thanks to their red colours, indicative of old stellar populations, they are readily identified out to high redshifts. Secondly, they are pressure-supported systems (rather than rotationally-supported), and this lack of angular momentum has led to the view that their alignments are described by the linear alignment model (see Section 3 of Kiessling et al. 2015, for more detail on this model). Therefore the signal is expected to be larger than that of disc galaxies, which is indeed the case, as shown already by Hirata et al. (2007).

Joachimi et al. (2011) studied intrinsic alignments in LRGs from the SDSS MegaZ-LRG dataset. Compared to the other studies discussed in this section, Joachimi et al. (2011) studied galaxies at higher redshifts (closer to the typical redshifts of cosmic shear surveys) and were the first to measure large-scale intrinsic alignments in a dataset with photometric redshifts (see Csabai et al. 2003 for a seminal example of the use of photometry for redshifts). The MegaZ-LRG sample used in Joachimi et al. (2011) contained more than 800,000 LRGs up to $z \sim 0.7$. Compared to

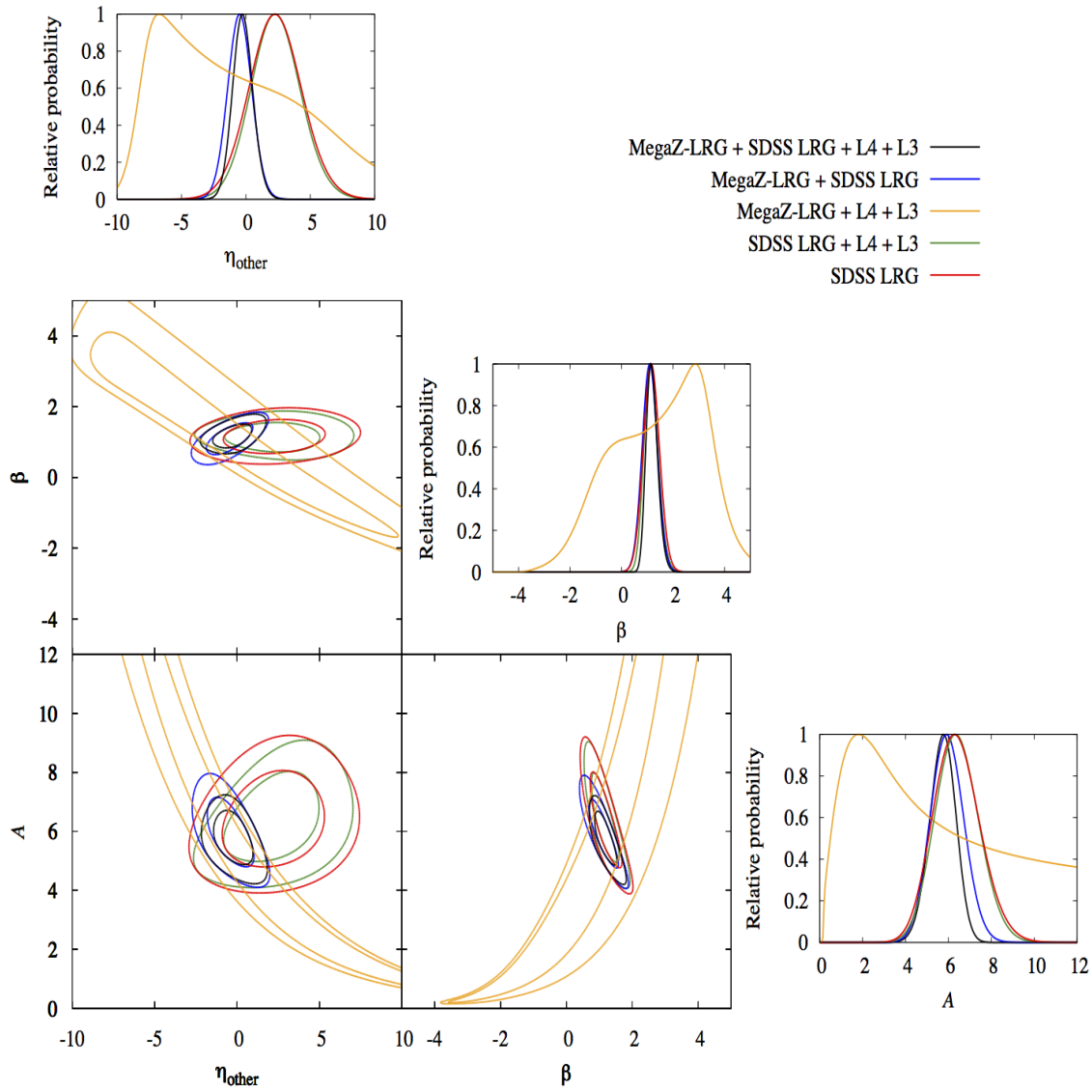


Fig. 5.— Posterior probabilities from the joint fit to the MegaZ-LRG and SDSS spectroscopic samples from Joachimi et al. (2011). Fits are shown for the amplitude A of the intrinsic alignment model (which is the same as the $A_{\rm I}$ we use throughout this paper), the extra redshift dependence with power-law index $\eta_{\rm other}$ and the index β of the luminosity dependence, as in Equation (28). **Lower left triangle of panels:** The two-dimensional 1σ and 2σ confidence contours, marginalised in each case over the parameter not shown with flat priors in the range $A \in [0; 20]$, $\eta_{\rm other} \in [-10 : 10]$, and $\beta \in [-5; 5]$. **Upper right diagonal panels:** Posterior probabilities for A, $\eta_{\rm other}$, and β, each marginalised over the two remaining parameters. The different coloured lines result from using different samples in the fitting process (see legend for details). *Reproduced with permission from* Joachimi et al. (2011) © *ESO.*

spectroscopic redshifts, the advantage of photometric redshifts is that these are cheaper to obtain for large samples, albeit at the expense of redshift precision. Consequently, it is necessary to explicitly model out the gravitational lensing "contamination" due to the intrinsic alignment signal. For more discussion of the use of photometric redshifts, see

Section 3.3.

Joachimi et al. (2011) measured w_{g+} and used the results for $r_p > 6$Mpc/h to place constraints on non-linear alignment model parameters (see Figure 5) by combining this sample with those used by Hirata et al. (2007). Power-laws with an extra free parameter each were introduced to allow for redshift and luminosity dependence, just as in Equation (28). The normalisation of the intrinsic alignment model was found to be $A_I = (0.077 \pm 0.008)\rho_{crit}^{-1}$ (where ρ_{crit} is the critical density) for galaxies at $z = 0.3$ and evolution-corrected r-band absolute magnitude of -22. This result is consistent with the value of $A_I = (0.066 \pm 0.008)\rho_{crit}^{-1}$ found by the more recent study by Singh et al. (2015), which we discuss below. Note that the yellow contour in Figure 5 is for the combination of the MegaZ-LRG and SDSS Main samples (rather than the SDSS LRGs), which yields weak and degenerate constraints because this combination cannot tell redshift from luminosity scaling.

To study deviations from the redshift dependence of the signal predicted by the non-linear alignment model, Joachimi et al. (2011) used several samples at a range of redshifts from $z \sim 0.1$ to $z \sim 0.55$ and found $\eta_{other} = -0.3 \pm 0.8$. Luminosity-dependence was analysed through fits to different luminosity subsamples. The L3 and L4 SDSS samples are defined with absolute magnitude cuts of $-20 \leq M_r + 5\log_{10} h < -19$ and $-21 \leq M_r + 5\log_{10} h < -20$ respectively and colour cuts detailed in Joachimi et al. (2011). L3 contains 66,312 galaxies, with a mean redshift of $\langle z \rangle = 0.07$, L4 contains 118,618 galaxies, with a mean redshift of $\langle z \rangle = 0.11$. The power-law slope of the dependence of the alignment signal with galaxy luminosity was constrained to be $\beta = 1.1^{+0.3}_{-0.2}$, also in agreement with the value of 1.3 ± 0.27 obtained by Singh et al. (2015).

Singh et al. (2015) have presented the most comprehensive study of large-scale intrinsic alignments in early-type galaxies to date. They studied the intrinsic alignments of the low-redshift LRG sample in the Baryon Oscillation Spectroscopic Survey (BOSS) survey, called LOWZ, using data from DR11 (Dawson et al. 2013; Alam et al. 2015). Unlike the original SDSS-I/II LRG sample studied in early works by Hirata et al. (2007) and Joachimi et al. (2011), this sample goes to lower luminosity, with a comoving number density that is three times as high as the earlier sample within the same redshift range ($0.16 < z < 0.36$). The sample used by Singh et al. (2015) to trace the density field contains 173,855 galaxies, of which 159,621 have good shape measurements, and are further divided into subsamples based on colour, luminosity, and environment.

Singh et al. (2015) measured the w_{g+} signal from the cross-correlation of the shape and density samples and modelled the signal using the non-linear alignment model for $r_p > 6$Mpc/h and with a fitting formula for the halo model from Schneider & Bridle (2010) on small scales ($r_p < 1.5$Mpc/h). This provided a set of large-scale and small-scale intrinsic alignment amplitudes that were studied as a function of sample properties.

The measurements of w_{g+} for the full sample agree well with the linear alignment model at scales larger than ~ 10Mpc/h, as shown in Figure 6. Below this scale, the non-linear alignment model provides a good fit to the data above 1 Mpc/h (though there is a notable dip in the measured signal at ~ 2Mpc/h). Note that the non-linear alignment model includes an optional smoothing scale, and the selection of this scale can, in principle, affect the match at small scales. Below ~ 1Mpc/h they apply two versions of the intrinsic alignment halo model. An implementation of the fitting formula and parameter values from Schneider & Bridle (2010) (dotted blue line) does not fit the data well. However, when some of the fitting function parameters are modified to better suit the SDSS LOWZ sample used in this work (dotted purple line), the halo model is shown to fit the data well on the smallest scales, from $0.3 - 1$ Mpc/h. The vertical black line at 0.3 Mpc/h shows the SDSS fibre collision scale, below which the difficulty of placing optical fibres in close proximity makes measuring clustering statistics difficult. Fitting the non-linear alignment model to scales larger than 6 Mpc/h yields an intrinsic alignment amplitude $A_I = 4.6 \pm 0.5$ (with the galaxy clustering suggesting an average linear galaxy bias of $b_g = 1.77 \pm 0.04$). It is interesting to note that the best fit to the data appears to be the non-linear alignment model at large and intermediate scales combined with the halo model at small scales. There is no physical motivation for this combination (compared to the linear alignment+halo model) but it suggests that more modelling and simulations work needs to be done to understand behaviour at intermediate scales, $2 < r_p < 10$Mpc/h. Recent work in this direction has been done by Blazek et al. (2015) which presents all relevant non-linear corrections at one-loop order, under the tidal alignment paradigm.

Singh et al. (2015) also presented results which explore intrinsic alignments as a function of galaxy properties and galaxy environment. As mentioned earlier, the luminosity-dependence of large-scale intrinsic alignments for this sam-

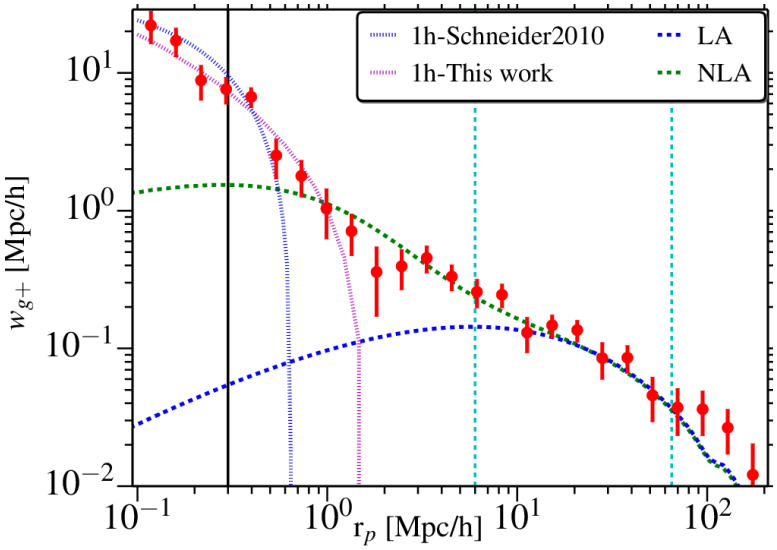


Fig. 6.— The density-shape correlation function, w_{g+} for the SDSS-III BOSS LOWZ sample used in Singh et al. (2015). The data used covers the redshift range $0.16 < z < 0.36$. The red points are the measurements from the data, the dashed green lines are the non-linear alignment model, and the dashed blue lines are the linear alignment model. The non-linear alignment model is fitted only in the range $6\text{Mpc}/h < r_\text{p} < 65$ Mpc/h (shown by dashed vertical lines), while the linear alignment model is shown with the same parameters as the non-linear alignment model. The dotted purple and blue lines show halo model fits to w_{g+} at small scales, see text for more details. The black solid line shows the SDSS fibre collision scale at $z = 0.36$. *Reproduced with permission from* Singh et al. (2015).

ple is consistent with the results from previous work (Joachimi et al. 2011), but with smaller statistical uncertainties. No variation of the intrinsic alignment amplitudes with redshift was found, though given the narrow range of redshift for this sample, the ability to study redshift evolution is quite limited. Importantly, the amplitude of the signal did not depend on the colour of the red-sequence galaxies, which supports the tendency in the literature to predict intrinsic alignments for future surveys using a single estimate for intrinsic alignments for all red-sequence galaxies regardless of their exact colour.

In terms of environmental dependence, using dark matter haloes identified with multiple LRGs and dividing the galaxies into centrals (i.e. Brightest Group Galaxies; BGGs), satellites, and field galaxies, Singh et al. (2015) found that satellite galaxies exhibit no detectable large-scale intrinsic alignments, but the radial alignments of the satellite galaxy semi-major axes towards the centres of their host haloes are detected at high significance. Central galaxies show both small- and large-scale intrinsic alignments, with a higher strength than for field galaxies, consistent with their host halo masses and luminosities being larger. See Kiessling et al. (2015) and attendant references for more discussion on the use of dark matter haloes to model intrinsic alignments and their identification in simulations.

Singh et al. (2015) detail a number of scaling relations for intrinsic alignments with respect to luminosity, dark matter halo mass and galaxy bias, shown in Figure 7. A key finding of Singh et al. (2015) is that dark matter halo mass and galaxy luminosity seem to be equally good (low scatter) predictors of the large-scale intrinsic alignment amplitude (A_I, the non-linear alignment model amplitude) for a given shape sample, whereas the linear bias does not do as well, having a large scatter with respect to intrinsic alignment amplitude. In contrast, the lowest scatter predictor of the *small-scale* intrinsic alignment amplitude (a_h, the halo model amplitude) for a given shape sample, is the linear bias. However, the small-scale amplitude has a non-trivial dependence on the choice of density tracer sample. See Figure 7 for a summary of the results of Singh et al. (2015) in terms of intrinsic alignment amplitudes and galaxy bias as a function of different galaxy properties (of the shape samples). The intrinsic alignment amplitude, A_I, shows a

clear dependence on luminosity, galaxy mass and bias but little change with redshift. Small-scale w_{g+} is fit with a halo model prescription characterised by an amplitude a_h and the bias of the galaxy sample b_s.

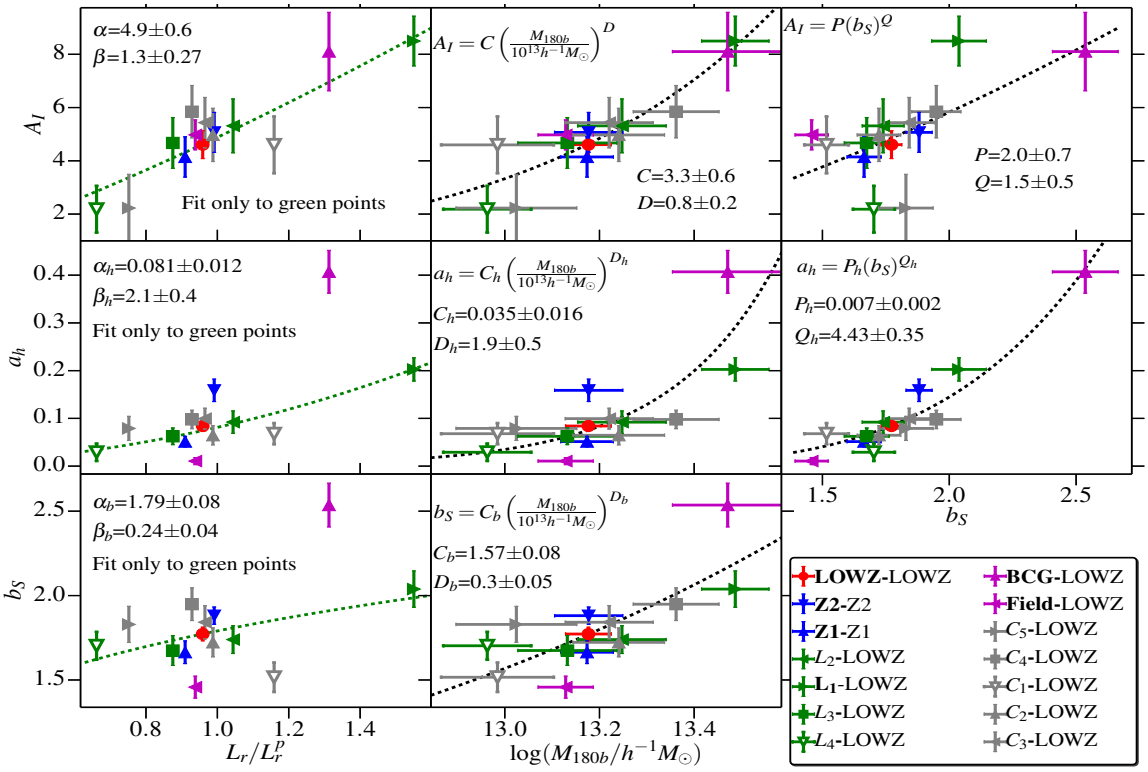


Fig. 7.— Intrinsic alignment amplitudes and bias from the SDSS-III BOSS LOWZ data of Singh et al. (2015). Results are shown for various shape samples, as a function of different galaxy properties of the shape sample. Z1 refers to $0.16 < z < 0.26$ and Z2 to $0.26 < z < 0.36$. Note that the full LOWZ sample was used as the density sample, except in the cases of Z1 and Z2 where these redshift subsets are used instead. L1 contains the brightest 20% of galaxies, L2 the next brightest 20%, L3 the next brightest 20% and L4 the faintest 40%. The bins C1-C5 split the sample by colour. Each C-bin contains 20% of the total sample from bluest (C1) to reddest (C5). The top row shows $A_{\rm I}$ as a function of different properties of shape sample. $A_{\rm I}$ shows clear evolution with luminosity ($L_{\rm r}$) as well as mass, where M_{180b} is the halo mass from weak lensing, and bias, $b_{\rm S}$, with negligible evolution in redshift. The green dotted line in $A_{\rm I}$ vs. $L_{\rm r}$ shows a power-law fit to the luminosity samples (green points). Similarly in $A_{\rm I}$ vs $\log(M_{180b}/h^1 M_\odot)$, the black dotted line is the power-law fit, using all the points. The middle row shows the halo model amplitude, $a_{\rm h}$ as a function of different galaxy properties. For cases where the density sample is fixed to LOWZ, the effects of the non-linear bias of the density sample is the same. The black dotted line in $a_{\rm h}$ vs $M_{\rm r}$ is the power-law fit to the luminosity samples (green points), and the dotted line in $a_{\rm h}$ vs $b_{\rm S}$ is the power-law fit using all the points. Remember that the galaxy properties shown on the x-axis are correlated, for example, more luminous galaxies also have higher bias and live in more massive haloes. *Reproduced with permission from* Singh et al. (2015).

Comparison with other papers on intrinsic alignments in SDSS reveals a possible dependence of the measured intrinsic alignment signal on the way that the galaxy shape is estimated. Okumura et al. (2009) measured large-scale intrinsic alignments of 83,773 LRGs from the SDSS DR6. Interpretation of this data by Blazek et al. (2011) in terms of the non-linear alignment model reveal a systematically higher amplitude compared to measurements for

comparable samples in Hirata et al. (2007) and Joachimi et al. (2011). One key difference is that the measurements of Okumura et al. (2009) use an estimate of the shape based on a low surface brightness isophote, instead of using centrally-weighted PSF-corrected shapes used in Hirata et al. (2007) and Joachimi et al. (2011). Hao et al. (2011) found signatures of systematics in the alignments of galaxies when measured using isophotal shapes which could be the cause of the extra signal for galaxies in clusters. However, it is not implausible that the outer isophotes of galaxies truly are more strongly aligned with large-scale structure, which could mean that the higher alignment amplitude results from a real physical effect. A direct comparison of measurements using the exact same methodology and intrinsic alignment estimator, but different ellipticity estimates, would be necessary to fully understand this discrepancy.

One interesting aspect of the interpretation of the results in Okumura et al. (2009) is that instead of directly comparing the data to an analytic model such as the linear alignment model, they compared with predictions for dark matter halo alignments from N-body simulations, and used the lower signal in the data to infer a typical stochastic misalignment between halo and galaxy position angles of $\sigma_\theta = 35.4^{+4.0}_{-3.3}$ degrees. The authors thus concluded that central LRGs are preferentially but not perfectly aligned with their parent haloes, since perfect alignment would produce an intrinsic correlation signal four times higher than what is measured.

Blazek et al. (2011) used the measurements of Okumura et al. (2009) to calculate the w_{g+} statistic and the intrinsic alignment auto-correlation functions, w_{++}, using LRGs from SDSS DR6 and the New York University value added catalogue (Blanton et al. 2005). The paper is worth noting here because the authors also went beyond the w_{g+}, w_{++} approach by calculating the correlation functions of curl-free E-modes and divergence-free B-modes for intrinsic alignments (see Section 3.1 for a description of these observables). In addition they presented a different statistic, first introduced by Faltenbacher et al. (2009), called the alignment correlation function, $w_{gg}(r_p, \theta_p)$, which describes the dependence of clustering on both projected separation, r_p, and the galaxy orientation angle, θ_p, that is the angle between the major axis of a galaxy and the axis of separation. When comparing their measured statistics w_{g+} and w_{++} with the linear alignment model, they found both fit well at large transverse scales (above 10 Mpc/h). From their fit to w_{g+} they found a best-fit amplitude of $C_1\rho_{crit} \approx 0.13 \pm 0.02$, consistent with the result of Joachimi et al. (2011). They found E-modes largely in agreement with theory and B-modes consistent with zero above 10 Mpc/h. Below this scale other alignment processes are expected to generate B-modes.

At linear order the tidal alignment model predicts that the angular dependence of $w_{gg}(r_p, \theta_p)$ is $w_{gg}(r_p)\cos(2\theta_p)$. Blazek et al. (2011) demonstrated that the alignment correlation function, $w_{gg}(r_p, \theta_p)$, was thus completely described by $w_{gg}(r_p)$ and $w_{g+}(r_p)$. Nevertheless it is useful to measure $w_{gg}(r_p, \theta_p)$ and compare to predictions of the linear alignment model as a check on observations of $w_{g+}(r_p)$. Blazek et al. (2011) found that $w_{gg}(r_p, \theta_p)$ increases with luminosity, in agreement with Joachimi et al. (2011) and Singh et al. (2015). The authors hazarded an explanation for the trend of increased alignment with luminosity, namely that "more luminous objects have formed more recently and have had less time to misalign from the tidal axis along which they formed." More detailed interpretation of these trends can be found in Kiessling et al. (2015).

4.3. Other Large-Scale Measurements

We have so far considered direct measurements of the galaxy-ellipticity correlation of both late- and early-type galaxies at large scales, as well as observations of the correlation of disc galaxy spin vectors and the correlation of major axis with separation vector. Other papers have studied large-scale shape correlations using more indirect methods. Instead of using a dataset to directly measure the alignment of shapes with the galaxy distribution, or with each other, it is possible to learn about intrinsic alignments through the simultaneous modelling of lensing and intrinsic alignments. In these cases the intrinsic alignment signal is sometimes seen as a "contaminant" of the cosmic shear signal. This contamination must be characterised to avoid bias, which can provide information about the intrinsic alignments themselves.

This was done by Blazek et al. (2012) when they presented a formalism for simultaneous modelling of cosmic shear and intrinsic alignments in the context of galaxy-galaxy lensing, where background sources are lensed by specific massive foreground structures associated with galaxies. When using photometric redshifts, as they did in this paper, it is not possible to perfectly separate the foreground and background populations, hence there will be some intrinsic alignment signal sourced by physically close galaxies. The authors exploited this property to measure intrinsic alignments

by removing the galaxy-galaxy lensing contaminant. While this issue was addressed to some extent by Joachimi et al. (2011), who used data with high quality photometric redshifts for which the lensing contamination was present at the $\sim$ 10% level, in Blazek et al. (2012) the formalism was designed to accommodate the case where the photometric redshifts are of more typical quality and therefore the weak lensing contamination is the dominant component of the radial alignment signal, even for sets of galaxies chosen so that they are supposed to be near the lenses in redshift space. Blazek et al. (2012) produced a null detection, interpreted as meaning that the intrinsic alignment contamination of the galaxy-galaxy lensing signal is limited to be $< 10\%$ for $0.1 \leq r_{\rm p} \leq 10$ Mpc/h. Under the assumption that the non-linear alignment model is valid at describing the radial dependence of density-shape alignments of these source galaxies, the constraints become considerably tighter, with the contamination expected to be $<$ 1–2% on those scales.

Chisari et al. (2014) also used this new formalism, extended to allow for full photometric redshift probability distributions, $p(z)$, to place constraints on intrinsic alignments of a deeper sample of source galaxies in the SDSS stripe 82 region (using coadds from Huff et al. 2014 and coadd photometry from Annis et al. 2014). They used galaxy clusters as density tracers and measured the tangential shears of sources around and behind those clusters to compute the lensing contamination to the intrinsic alignments signal. Using the non-linear alignment model to define the scaling of intrinsic alignments with transverse separation, Chisari et al. (2014) constrained the contamination fraction for a galaxy-galaxy lensing measurement to lie between -18% and $+23\%$ (95% confidence level), using this cluster sample and source sample below 1 Mpc/h, more discussion of this paper is given when environment-dependent observations are covered in Section 5.

A more truly "indirect" measurement was made by Heymans et al. (2013). Here the goal was to measure the weak gravitational lensing cosmic shear signal. To this end the expected intrinsic alignment contribution was modelled out before any cosmological inferences were made. In this approach the amplitude of the alignment signal was a free parameter, included as part of the model that was compared to the data. The authors thus marginalised over intrinsic alignment contamination as part of a tomographic cosmic shear analysis using six redshift bins.

Heymans et al. (2013) used the non-linear alignment model with a single free parameter, $A_{\rm I}$, parameterising both the II and GI amplitudes, citing the null result of Mandelbaum et al. (2011) for late-type galaxies as justification for using this relatively inflexible (one free parameter) parameterisation. Note that the same intrinsic alignment model is applied to both early- and late-type galaxies in this analysis. The observable under consideration is the real-space ellipticity two-point correlation function, i.e. the sum of the cosmic shear signal due to weak gravitational lensing *and* both the II and GI signals.

Heymans et al. (2013) split galaxies by the best-fit spectral energy distribution type, as determined by the photometric redshift algorithm into late-type spiral galaxies, which constitute $\sim 80\%$, and early-type galaxies, which make up the remaining $\sim$ 20%. Various combinations were considered: full sample, early-type, late-type and optimised early-type. Optimised early-type uses the same sample as the early-type analysis but includes the full sample (early- and late-type) in the background redshift bins used for tomographic cross-correlations. This optimisation is designed to overcome the noise due to the small sample size of early-type galaxies without changing the intrinsic alignment contribution, which is sourced by the foreground bin population. The intrinsic alignment amplitude, $A_{\rm I}$, is constrained simultaneously with cosmological parameters. Figure 8 shows constraints on $A_{\rm I}$ and Ω_m marginalised over the standard cosmological parameters. Note that these results also include auxiliary cosmological information from outside the CFHTLenS survey.

The results showed a strong dependence on galaxy type. The late-type sample has an alignment signal consistent with zero, as does the full sample, with amplitudes of $A_{\rm I,late} = 0.18^{+0.83}_{-0.82}$ and $A_{\rm I,all} = -0.48^{+0.75}_{-0.87}$, respectively. A tentative signal is detected for the early-type sample, with $A_{\rm I,early} = 5.15^{+1.74}_{-2.32}$, but the null result is inside the 2σ confidence region. The optimised early-type sample is less ambiguous, with a best-fit amplitude of $A_{\rm I} = 4.26^{+1.23}_{-1.39}$. For tomographic surveys like CFHTLenS the linear alignment model has the (negative) GI contribution dominating over the (positive) II signal. A negative value of A_I, as marginally preferred by the full sample, would suggest that the data prefer a more positive intrinsic alignment contribution. It should be noted however that Heymans et al. (2013) applied the linear alignment model to all their galaxy samples, even though intrinsic alignment of late-type galaxies is not expected to be sourced by the same mechanism (see the introduction to thsi section and Kiessling et al. (2015) for more detail). Fitting this simple model to a joint population of late- and early-types, as they do in the full sample

analysis, may not always be appropriate, nor will ignoring luminosity evolution in analyses with larger samples.

Dossett et al. (2015) re-analysed the CFHTLenS data in the context of joint constraints on intrinsic alignments and deviations from general relativity. When they assumed general relativity, their results agreed with those of Heymans et al. (2013). Scale independent modifications to general relativity have no major effect on the intrinsic alignment constraints. However, when the authors allow scale dependent modifications to general relativity, the constraints on $A_{\rm I}$ weaken and the 95% confidence contours of the $A_{\rm I}$ constraint from the optimised early-type sample are consistent with the null result. Effectively the data are not sufficient to simultaneously constrain intrinsic alignments and deviations from general relativity. It should also be noted that Dossett et al. (2015) assumed that modifications to GR did not modify the form of the IA signal, which may not be entirely justified.

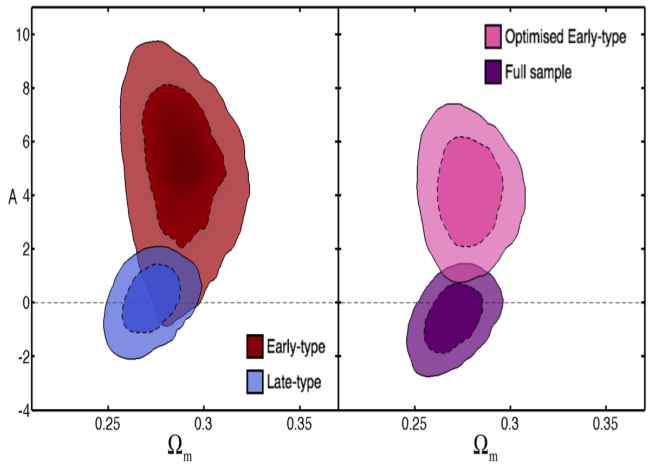


Fig. 8.— Joint parameter constraints on the amplitude of the intrinsic alignment model (A, which is the same as our $A_{\rm I}$) and the matter density parameter, $\Omega_{\rm m}$, from CFHTLenS combined with WMAP7, BOSS and the Riess et al. (2011) supernova sample as presented in Heymans et al. (2013). **Left panel:** Constraints for two galaxy samples split by spectral energy distribution type (early-type in red and late-type in blue). **Right panel:** Constraints from an optimised analysis to enhance the measurement of the intrinsic alignment amplitude of early-type galaxies (pink). The full sample, combining early and late-type galaxies, produces an intrinsic alignment signal that is consistent with zero (shown purple). A flat ΛCDM cosmology is assumed. *Reproduced with permission from* Heymans et al. (2013).

5. Environmentally dependent alignments

In this section, we review measurements of the alignments of galaxies and groups/clusters of galaxies which have considered the specific environment in which such systems reside. At megaparsec scales, the cosmic web can be roughly divided into four different types of environments: voids, sheets, filaments, and knots. In numerical simulations, these environments are defined according to the number of gravitationally collapsed dimensions: 0, 1, 2, and 3, respectively. Voids correspond to the emptiest parts of the sky (in terms of galaxy density): underdense regions with scales of $\gtrsim 10$ Mpc; while knots correspond to massive galaxy groups and clusters (e.g., Hahn et al. 2007).

Alignment measurements that take into account the different environments started in the late 1960s with photographic plates and only in the 21st century did measurements start to be performed with modern CCD cameras and the resulting high accuracy of shape measurements. In the following sections we discuss the most recent results; a full historical review is presented in Joachimi et al. (2015), which also contains extensive referencing of the field.

In this section (particularly in Sections 5.1 and 5.5) we take the distribution of satellite galaxies as an observational proxy for the shape of the host dark matter halo, which is not accessible to observations. This is a reasonable, although not exact, approximation for dark matter haloes with elliptical central galaxies, i.e. mostly groups and clusters (see

Kiessling et al. 2015). It is probably not applicable to spiral (late-type) centrals; for such galaxies a coherent satellite distribution may hint to a common tidal origin of these satellites (e.g. Pawlowski & Kroupa 2013).

For these observations it is of course important that galaxy type and the morphology of the local large-scale structure (groups, filaments, voids, sheets) are determined to high accuracy when attempting to make statements about galaxy shape correlation for a given population. Bailin et al. (2008) assessed different selection criteria for isolated and group galaxies using SDSS and the Millenium simulation (Springel et al. 2005) and showed that most studies correctly identified only $\sim 30-40\%$ of isolated galaxies (and their satellites) in their samples, with the rest typically being incorrectly identified as members of galaxy groups. Improvements in identification are very important for the future of these studies. More discussion of the characterisation of morphology in N-body and hydrodynamical simulations can be found in Kiessling et al. (2015).

Some groups have made interesting attempts to use quasar polarisation as a tracer of alignment (Hutsemékers 1998; Hutsemékers & Lamy 2001; Hutsemékers et al. 2005; Pelgrims & Hutsemékers 2015). The unified picture of Active Galactic Nuclei (AGN), which include quasars, sees them as sourced by the accretion of matter onto a central supermassive black hole. The polarisation is believed to be either parallel or perpendicular to the accretion disc, depending on inclination with respect to the line of sight, based on studies of low redshift AGN (Smith et al. 2004). Hutsemékers et al. (2014) found that quasar polarization in galaxy groups at $z \sim 1.3$ is either parallel or perpendicular to the principal axis defined by group galaxies, as well as being correlated with the polarisation vectors of their neighbouring quasars.

5.1. Galaxy position alignments in the field and the Local Group

Holmberg (1969) originally found that the distribution of galaxies that are satellites around field spirals tend to be located along the minor axis of the central galaxy. He looked at edge-on spiral host galaxies, whose minor axes are easier to identify, and restricted himself to satellites at radii smaller than 50 kpc. Subsequent studies using larger samples of galaxies were not able to confirm this result (e.g. Hawley & Peebles 1975; Sharp et al. 1979). Zaritsky et al. (1997) did find evidence for this "Holmberg effect", but only for satellites at distances between 300 and 500 kpc from their host galaxy. Later studies using SDSS have found that satellites of spiral galaxies are distributed isotropically (e.g. Azzaro et al. 2007; Bailin et al. 2008). In contrast, satellites of early-type centrals are located preferentially along their host's *major* axes, i.e. an anti-Holmberg effect[2] (Brainerd 2005; Azzaro et al. 2007; Sales & Lambas 2009; Nierenberg et al. 2011).

Contrary to the results for field galaxies, there is evidence of a strong Holmberg effect for Milky Way satellites (e.g. Lynden-Bell 1976; Kunkel & Demers 1976; Kroupa et al. 2005; Pawlowski & Kroupa 2013). M31 is probably the only galaxy other than the Milky Way for which the three-dimensional distribution of satellites can be mapped with accuracy because distances can be measured precisely. Koch & Grebel (2006) found that early-type dwarf satellites of M31 are located in a polar plane, only 16 kpc thick, that is only $\sim 6^\circ$ from the pole of M31. Similar findings have been presented by Conn et al. (2013) and Ibata et al. (2013). Pawlowski et al. (2013) have suggested that two similar structures can be found for non-satellite galaxies in the Local Group as a whole, at roughly equal distances to the Milky Way and M31.

As discussed by Bailin et al. (2008) these results need not be contradictory, for two reasons: firstly, the large spirals in the Local Group are not isolated as defined in the above SDSS studies, since M31 and the Milky Way are too close to one another to define either of them as "isolated"; secondly, the satellites of these galaxies are much fainter than the typical satellites of SDSS field galaxies. Indeed, Bailin et al. (2008) found a minor-axis alignment of sufficiently faint satellites around their hosts in hydrodynamical simulations.

5.2. Galaxy alignments within galaxy groups and clusters

Galaxy clusters can host hundreds of galaxies and have therefore attracted considerable attention since the pioneering works of Fritz Zwicky (e.g., Zwicky 1933, 1937). SDSS data have been used to generate catalogues that contain

[2] See Joachimi et al. (2015) for details of the history of these observations and the messy nomenclature that resulted.

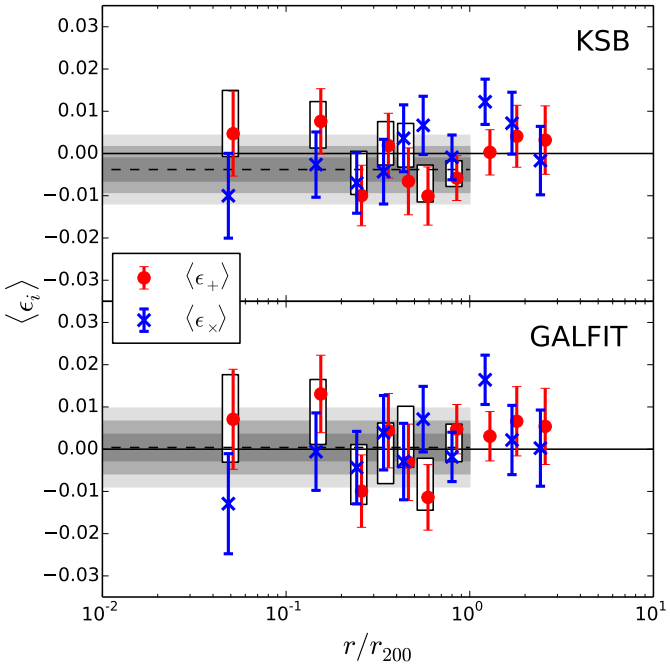


Fig. 9.— The average ellipticities, $\langle \epsilon_i \rangle$ (with i denoting the + or × ellipticity component), of galaxies in galaxy clusters from 14,250 spectroscopically-confirmed cluster members, using two different shape measurement methods on data from the CFHT, as a function of projected distance from the BCG, normalised to the cluster radius, r_{200} (note that r as used here is the same as $r_{\rm p}$ used throughout this paper). KSB measure quadrupole moments of the brightness distribution (Kaiser et al. 1995), Galfit is a model-fitting method (Peng et al. 2002). Positive (negative) red circles represent radial (tangential) alignments, while the blue crosses show the cross component of the ellipticity. Dashed lines and shaded regions show the weighted mean and its 1, 2, and 3σ uncertainty regions for all galaxies within r_{200}, and the white boxes show the results when including photometrically-selected red sequence members. *Reproduced with permission from* Sifón et al. (2015) © *ESO.*

hundreds of thousands of groups and clusters (e.g., Koester et al. 2007; Hao et al. 2010; Wen et al. 2012; Rykoff et al. 2014).

There is consistent evidence that the major axes of centrals in galaxy clusters, typically referred to as brightest cluster galaxies, BCGs, but different from these in some non-negligible fraction of cases (Skibba et al. 2015; Hoshino et al. 2015), seem to produce an inverted Holmberg effect; that is, the major axes of the central galaxy and the satellite distribution (which serves as an observational proxy for the shape of the cluster's dark matter halo) coincide to a good degree. This tendency has been evident since the very first measurements (Sastry 1968; Rood & Sastry 1972; Austin & Peach 1974; Dressler 1978; Carter & Metcalfe 1980; Binggeli 1982; Struble 1987). The most recent measurements have come from analyses of large galaxy group/cluster catalogues from SDSS spectroscopic (Yang et al. 2006; Azzaro et al. 2007; Faltenbacher et al. 2007; Wang et al. 2008, 2010; Siverd et al. 2009) or photometric (Niederste-Ostholt et al. 2010; Hao et al. 2011) data, all of which have confirmed this alignment, which is typically found to be stronger for early-type, or red, central galaxies. The brightest satellite galaxies' shapes are also aligned with the parent halo (Li et al. 2013b; Singh et al. 2015), and there is evidence that BCGs are also aligned with the shape of the X-ray emission from the intracluster medium (Hashimoto et al. 2008). Using a sample of 405 Abell clusters, Struble (1988) showed that pairs of brightest cluster galaxies tend to be aligned parallel to each other and perpendicular to the separation vector. This is at odds with more recents results which show alignment between clusters, discussed in Section 5.5 below.

On the other hand, as reviewed in Joachimi et al. (2015), historically there has not been a strong consensus about the alignments of satellite galaxy shapes within their host haloes (or the lack thereof). However, the latest measurements seem to agree that, on scales from small galaxy groups ($M \sim 10^{13} M_{\odot}$) to massive galaxy clusters ($M \gtrsim 10^{15} M_{\odot}$), the orientations of satellite galaxies are consistent with an isotropic distribution (Sifón et al. 2015; Chisari et al. 2014) (probably with the exception of the brightest satellites, as described in the results above).

The first modern (i.e., using CCD observations), statistical measurements of galaxy alignments in galaxy groups were presented by Pereira & Kuhn (2005), who used SDSS photometric and spectroscopic observations and found anisotropic galaxy orientations at the 4σ level. Some other authors have also found that satellite galaxies are aligned either radially from the position of the central galaxy (Agustsson & Brainerd 2006; Faltenbacher et al. 2007) or aligned with the major axis of the central galaxy (Yang et al. 2006). However, Hao et al. (2011) showed that these detections correspond to systematic effects in the isophotal measurements from SDSS. Since Hao et al. (2011), all measurements have been consistent with no alignments (Hung & Ebeling 2012; Schneider et al. 2013; Chisari et al. 2014; Sifón et al. 2015). Chisari et al. (2014) presented a modelling of intrinsic alignments in photometrically selected groups and clusters, improving upon the method of Blazek et al. (2012) by accounting for photometric redshift errors using the full redshift probability distribution of each galaxy. In a complementary work, Sifón et al. (2015) used a large sample of spectroscopically-confirmed galaxy cluster members to directly measure the average alignment of satellite galaxies.

The work of Chisari et al. (2014) has the advantage of being applicable to photometric data, with great potential for large photometric surveys such as the Large Synoptic Survey Telescope (LSST, LSST Science Collaboration et al. 2009) and Euclid (Laureijs et al. 2011), while that of Sifón et al. (2015) is a cleaner and more direct measurement but depends on large spectroscopic datasets which are less readily available. Both works found no evidence for galaxy alignments in clusters, constraining the average intrinsic ellipticity signal in galaxy groups and clusters to be 0.5% or lower. The measurements of Sifón et al. (2015) are reproduced in Figure 9; they used two different shape measurement methods with different radial weighting schemes (GALFIT, by Peng et al. 2002, and KSB, by Kaiser et al. 1995, see Section 2.3 above for more discussion of the general principles of shape measurement), both of which gave consistent results, suggesting that the non-detection of alignments in clusters is robust to differences in shape measurement. Additionally, thanks to their large, clean sample of cluster members, Sifón et al. (2015) directly measured the alignment *between* cluster satellites, which they also found to be consistent with zero. The fact that the measurement of the cross component, $\langle \epsilon_{\times} \rangle$, was consistent with zero acts as a null test and demonstrates that the analysis of Sifón et al. (2015) is robust to, at least some types of, systematics. Also using spectroscopically-confirmed cluster members but with reduced constraining power due to lower image quality of single-pass SDSS observations (as opposed to deep SDSS Stripe 82 data and deep, better-seeing CFHT/MegaCam images used by Chisari et al. 2014 and Sifón et al. 2015, respectively), Schneider et al. (2013) constrained the average shear signal of satellite galaxies in Galaxy and Mass Assembly (GAMA) survey[3] (Driver et al. 2009) groups to $\lesssim 2\%$. Schneider et al. (2013) note the disagreement between their null detection and results from N-body simulations, suggesting that this is evidence for misalignment between baryonic and dark matter shapes.

As discussed by Singh et al. (2015), the observed radial alignments of the most luminous satellite galaxies by Li et al. (2013b) and Singh et al. (2015) would lead to null detections of fainter satellites as observed by, for example, Chisari et al. (2014) and Sifón et al. (2015). This assumes that the scaling of satellite alignments with luminosity estimated by Singh et al. (2015) for bright red galaxies (specifically LRGs) is extrapolated below the luminosity limit explored by the latter authors, whose sample also incuded blue galaxies which would further dilute any signal. Therefore, to current precision, the latest observations show a consistent picture, in which very luminous (red) satellites align towards the central galaxy and progressively fainter (red and blue) satellites align less and less until the alignment signal of faint satellites is below the current detection limit.

5.3. Galaxy alignments with voids

Voids are an attractive reference against which alignments of galaxies can be measured. They have a higher degree of symmetry than filaments and, in contrast to clusters, tend to become more spherical as they evolve gravitationally

[3] http://www.gama-survey.org/

– the effect of the strongest inward forces acting along the shortest axis in an aspherical overdensity is reversed for underdense voids (Sheth & van de Weygaert 2004). On the downside, large voids are rare objects and are characterised by the absence of luminous structures, so detecting them requires a galaxy survey covering a large, contiguous volume with densely sampled spectroscopic redshifts.

Such a dataset only became available with the advent of SDSS, which additionally supplied imaging of sufficient quality to measure galaxy morphology with high accuracy. Thus it is not surprising that the observational study of void alignments closely follows the development of SDSS, with three publications based on DR3 (Trujillo et al. 2006), DR6 (Slosar & White 2009), and DR7 (Varela et al. 2012). These works shared a lot of their methodology, in particular the algorithm to find and define voids (the HB algorithm described in Patiri et al. 2006 who also give an overview of other methods), but obtained strikingly different results. It is possible that details of the implementation, for example assumed limiting magnitudes, which differed between implementations of the same algorithm are responsible, underlining the sensitivity of void-finding to the method employed.

Trujillo et al. (2006) searched for alignments among galaxies on the surface of voids using data from SDSS DR3 and the Two-Degree Field Galaxy Redshift Survey (2dFGRS). They defined voids as spheres of radius larger than 10 Mpc/h (clearly an idealistic assumption, there will generally be some confusion over void boundaries) within the SDSS survey boundaries that contain no galaxies brighter than $M_{b_J} = -19.32 + 5\log h$. Here, b_J denotes a blue photometric band used for the target photometry of the 2dF Galaxy Redshift Survey (Colless et al. 2001). Disc-dominated galaxies were selected in a shell of 4 Mpc/h thickness on the surface of the voids, using only objects that are nearly face-on or edge-on. The latter step avoids an ambiguity in the inclination of the disc as it is impossible to decide which are the near and far 'edges' of the galaxy if only the axis ratio of the image is known.

In total, Trujillo et al. (2006) used 178 voids and 201 galaxies with estimates of their spin axes. From these they derived the probability distribution of the angle θ between the spin vector of a galaxy and the vector connecting the void centre with the position of the galaxy. Their measurement is inconsistent with random galaxy orientations at the 99.7 % level, preferring an orientation of the spin vector perpendicular to the void radius vector. The signal is well described by a simple model based on tidal torque theory, assuming

$$\left\langle \hat{J}^i \hat{J}^j \right\rangle = \frac{1 + a_\mathrm{T}}{3} \delta_{ij} - a_\mathrm{T} \sum_k \hat{T}^{ik} \hat{T}^{jk} \,, \tag{30}$$

where $\hat{J}^i$ is the normalised spin vector, $\hat{T}^{ij}$ the normalised traceless shear tensor, i, j denote pairs of galaxies, and $a_\mathrm{T} \in [0; 1.0]$ a correlation parameter measuring the alignment of the shear and inertia tensors (Lee & Pen 2000). δ_{ij} is the Kronecker delta. Based on this model for spin correlations, and assuming a Gaussian distribution of the spin vector elements, Lee (2004) derived a general result for the probability distribution of angles of galaxy spin vectors relative to eigenvectors of the tidal shear field which was able to qualitatively recover the observed inclinations of spiral galaxies in the local supercluster. Trujillo et al. (2006) measured $a_\mathrm{T} = 0.7^{+0.1}_{-0.2} (1\sigma)$.

This detection is in marked contrast to that of Slosar & White (2009) who reported a null detection with a constraint $a_\mathrm{T} < 0.13$ at 3σ. Their analysis only differed in that it was updated to the larger and more homogeneous DR6 and used an absolute magnitude limit[4] of $M_r = -20.23 + 5\log h$ as the threshold for void detection. The larger area and higher filling factor for galaxies inside the survey volume resulted in a significantly larger sample of voids. Additionally, their definition of the galaxy sample on which spin measurements were made was slightly different, but even when approximately recovering the selection of Trujillo et al. (2006), no signal was detected.

In the most recent analysis Varela et al. (2012) used galaxies from the SDSS DR7 and included disc galaxies with all inclinations via a fit to a thick-disc model using morphological classifications from Galaxy Zoo. The ambiguity in inclination angle was accounted for statistically. Employing a luminosity threshold of $M_r = -20.17 + 5\log h$, voids with a range of minimum radii between 10 Mpc/h and 18 Mpc/h were identified, with shells for spin measurement between 1 Mpc/h and 10 Mpc/h in thickness. The signals were fitted to the same model as used in the preceding works, but with a different free parameter p which is related to the mean angle and the parameter a_T of Equation (30)

[4] Note the two works use different conventions for the Hubble constant.

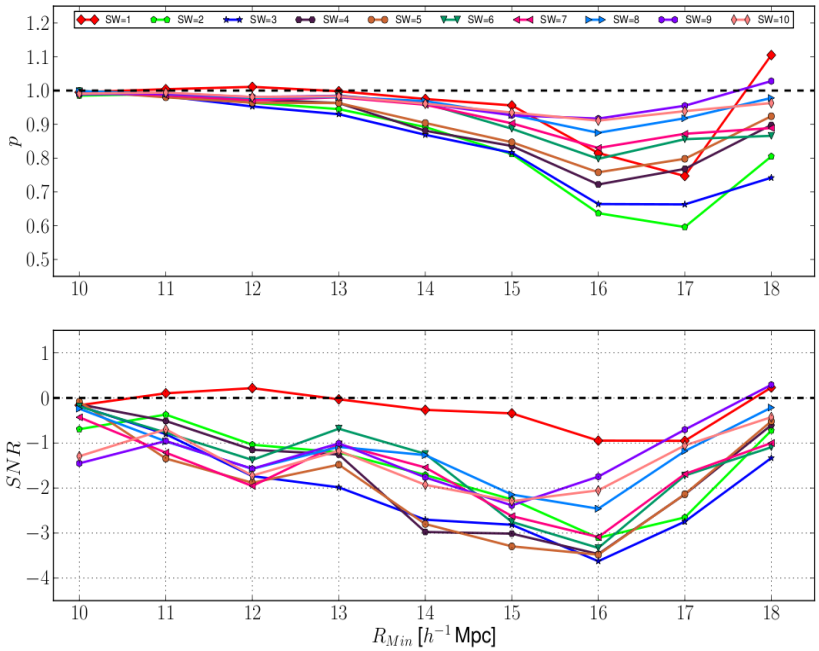


Fig. 10.— **Top:** Alignment parameter, $p = \langle|\cos\theta|\rangle^{-1} - 1$, as a function of minimum void radius $R_{\rm min}$. See Equation (32) for more details of these quantities. The different lines correspond to the width (SW) in Mpc/h of the shell in which galaxy orientations are measured, in the range 1 to 10 Mpc/h as indicated in the legend. **Bottom:** As above but showing signal-to-noise ratio (SNR) of the alignment. Negative SNR and $p < 1$ indicates that the galaxy spin preferentially lies parallel to the line connecting the void centre and the galaxy. © *AAS. Reproduced with permission from* Varela et al. (2012).

as follows:

$$\langle|\cos\theta|\rangle = \frac{1}{1+p}\ ; \tag{31}$$

$$a_{\rm T} = \frac{2(p^2-1)}{2(p^2-1)+3}\ . \tag{32}$$

Hence $p = 1$ implies random orientations of galaxies, while $p > 1$ if galaxy spin is preferentially perpendicular to the vector from void centre to galaxy. Best fits for p and the significance of the alignment signal are shown in Figure 10. For a minimum void radius of 10 Mpc/h and a shell width of 4 Mpc/h, Varela et al. (2012) find no alignment, in agreement with Slosar & White (2009), and corresponding to a constraint $a_{\rm T} = -0.003^{+0.020}_{-0.021}$ (1σ). Using only voids with radii in excess of $\sim$ 15 Mpc/h, alignments with $a_{\rm T} \approx -0.5$ were found around the 3σ level. Note that $a_{\rm T} < 0$ indicates a breakdown of the assumptions underlying the model in Equation (30), which states that the spin vector preferentially aligns with the intermediate axis of the tidal shear tensor. Indeed, Varela et al. (2012) found a tendency for parallel alignment with the radius vector of the void, i.e. the major axis of the tidal shear tensor at the surface of the void. This is exactly the opposite finding from Trujillo et al. (2006).

Hence the observational evidence for galaxy alignments with the surface of voids remains unclear. Varela et al. (2012) stated that the results presented in Trujillo et al. (2006) were selected *a posteriori* as the configuration with the strongest detection, and re-computed the significance to be less than 2σ. Direct comparison with simulations is hindered by observational selection effects and the difficulty of relating galaxy morphology to halo shape and angular momenta. For instance, Cuesta et al. (2008) found, in N-body simulations, for a similar setup as in the observational

studies, $a_T \approx 0.04$ for spin alignment and $a_T \approx -0.17$ for minor axis alignment of haloes. Kiessling et al. (2015) provide a detailed discussion of this and other simulation results.

5.4. Galaxy alignments with filaments and sheets

The notion that galaxies are not randomly distributed on the sky but tend to be concentrated in large, elongated structures predates the demonstration of the extragalactic nature of galaxies (Reynolds 1920). Studies of galaxy position and alignment with respect to the local part of the cosmic web were made from the early 20th century onwards, but results were generally inconclusive and often contradictory. The review by Hu et al. (2006) provides an overview of alignment studies, both early and recent, in the local supercluster.

We first discuss two papers (Lee & Pen 2002; Lee & Erdogdu 2007) which, while they do not discuss filaments or sheets explicitly, do look at the alignment of galaxy spin with the shear field eigenvectors, which in turn are very often used to define filaments, as discussed below. Lee & Pen (2002) claimed the first observational evidence for the alignment of galaxy spin with the tidal shear field at the position of the galaxy. They estimated the matter density field from the Wiener-filtered positions of galaxies from the infrared astronomical satellite (IRAS) all-sky survey[5] (Skrutskie et al. 2006). The tidal shear field was then derived via explicit integration and differentiation of the gravitational potential. Galaxy position angle and axis ratio measurements for about 10^4 spiral galaxies were taken from the photographic plate-based Uppsala General catalogue and its southern counterpart (Nilson 1973). With these data, Lee & Pen (2002) used the thin-disc approximation to calculate galaxy spin. They rejected a random orientation of galaxy spins at 99.98 % confidence and found $a_T = 0.17 \pm 0.04$ (1σ), again using the ansatz in Equation (30).

Lee & Erdogdu (2007) kept the morphology data but included a correction for disc thickness in the calculation of the spin vector and used the 2 Micron All Sky Survey (2MASS) Redshift Survey[6] to determine the tidal field. The 2MASS galaxy positions were expanded on a three-dimensional grid in terms of Fourier-Bessel functions, the tidal field obtained via Fast Fourier Transformation, and then interpolated to the galaxy position. These authors also found a strong detection of spin alignments, obtaining $a_T = 0.08 \pm 0.01$ on average, increasing with increasing overdensity. In the context of tidal torque theory, a correlation with $a_T > 0$ means that galaxy spin is aligned with the intermediate axis of the tidal shear tensor (see the argument in Lee & Pen 2001), i.e. their spin vectors tend to be perpendicular to filaments and lie in the plane of sheets.

Jones et al. (2010) selected edge-on galaxies with axis ratio < 0.2 in SDSS DR5 and constructed the matter density field via Delaunay tessellation, using the eigenstructure of the tidal shear tensor to identify filament candidates. These were then inspected visually to select a clean sample of 67 filaments, containing only 69 galaxies with spin measurements. Nonetheless, the authors claimed that the 14 objects among those 67 filaments which were oriented with spins perpendicular to the filament direction ($\cos\theta < 0.2$, where θ is the angle between the filament axis and the spin axis) constitute a statistically significant detection of this type of alignment.

Based on SDSS DR8, Tempel et al. (2013) fitted three-dimensional bulge+disc models to the light distribution of galaxies at low redshift ($z < 0.2$) to infer the spin vector direction. They approximated the filamentary structure by a network of cylinders, defined by elongated overdensities of galaxies. For their full sample of spiral galaxies, no alignment was found, while for a subsample of spirals with $M_r < -20.7$ the spin axis tended to be parallel to the filament direction. In a sample of flattened early-type galaxies, mostly composed of lenticulars, Tempel et al. (2013) observed a significant alignment of spin perpendicular to the filament axis, which again was stronger for the brightest galaxies. The luminosity dependence could have been due to a physical trend or due to selection effects as, for example, fits to the photometry were more reliable for bright objects. The authors argued that, under the assumption that spiral (S0/elliptical) galaxies mostly live in low-(high-)mass haloes, their findings agree with the established simulation result that massive haloes have their spin aligned orthogonally to filaments, while low-mass haloes show preferentially parallel alignment (e.g. Trowland et al. 2013).

This work was extended by Tempel & Libeskind (2013), who modified the filament-finding algorithm and also included large-scale structure sheets, identified as 'flattened filaments', i.e. a filament whose detection probability

[5] http://irsa.ipac.caltech.edu/Missions/iras.html

[6] http://www.ipac.caltech.edu/2mass/

extends into a plane. The authors found no correlation between the spin axis of early-type galaxies (assumed to be the same as the short axis of the galaxy ellipsoid) and the sheet, whereas the spin of spiral galaxies weakly aligns with filaments and tends to avoid pointing away from the filament into the plane of the sheet. These latter signals vanish inside a 200 kpc/h radius around the filament central axis. It is possible that these results are linked to gas infall along the sheets onto the filaments, where angular momentum is generated with a rotation axis along the filament direction.

Zhang et al. (2013) quantified the alignment of the major axes of galaxy images in SDSS DR7 with sheets and filaments. The analysis was based on a catalogue of close to 5×10^5 'groups' with a minimum estimated halo mass of $10^{12} M_\odot/h$, found using an adaptive halo-based group finder (Yang et al. 2005, 2007). These groups could consist of a single galaxy. Following the method of Wang et al. (2012), the group haloes were used to reconstruct the matter density field via a halo bias model extracted from simulations. Based on this reconstruction, Zhang et al. (2013) identified those groups that resided in a filament or sheet environment via the eigenvalues of the tidal shear tensor at that point (one negative and two positive eigenvalues corresponding to a filament; two negative and one positive eigenvalue corresponding to a sheet), and calculated the angle between the projected major axis of the galaxy and the projected axes of the filament and the sheet normal vector, respectively. Note however, that this study employed the isophotal shapes provided by the SDSS pipeline, which have been flagged as potentially unreliable[7]; see Section 1 for more discussion on isophotes and shape measurement.

Figure 11 shows the probability distribution of alignment angles between galaxy and filament ($\theta_{\rm GF}$) and galaxy and sheet normal ($\theta_{\rm GS}$), for subsamples split into blue/red and central/satellite (centrals are defined as the brightest group galaxies). Generally, galaxies preferentially align with the direction of the filament (small $\theta_{\rm GF}$) and lie within the sheet ($\theta_{\rm GS}$ close to a 90° angle). The signals are weak for blue galaxies and highly significant for central (and bright) red galaxies. These dependencies prevail for the alignments of galaxy major axes with the eigenvectors of the tidal tensor. Here, Zhang et al. (2013) find preferentially orthogonal alignment with the largest eigenvector, parallel alignment with the smallest eigenvector and none with the intermediate eigenvector. These results are in good agreement with N-body simulations for red galaxies. The null detection for blue galaxies is somewhat in tension with N-body studies: for example Wang et al. (2011) found significant correlation between the spin axes of dark matter haloes and the eigenvectors of the tidal field. This tension lessens if there is some mismatch between the spin of the overall dark matter halo and that of the galaxy at the centre, which the subsequent study of Zhang et al. (2015) indicates may be the case.

Zhang et al. (2015) conducted the equivalent study for galaxy spins, reconstructing the three-dimensional direction of the spin vector for galaxies via a simple thick-disc model for galaxies that were classified as spiral by Galaxy Zoo, and as central in their group catalogue. They saw only weak evidence for an alignment with the intermediate axis of the tidal shear tensor (as predicted by tidal torque theory), and therefore for galaxy spins to be preferentially perpendicular to filaments and parallel to the normal of sheets. Comparing their results to N-body simulations, they found better agreement with the observations when calculating the spin only in the inner part of dark matter haloes, i.e. closer to the scales of the bright parts of a galaxy. Since the surfaces of voids and sheets classified via the tidal shear tensor should define similar environments, the results of Zhang et al. (2015) are qualitatively consistent with those of Varela et al. (2012). Note both studies are restricted to low redshifts ($z < 0.2$ and $z < 0.12$ respectively), additional studies will be required to increase this baseline.

5.5. Alignments between galaxy groups and clusters

As with galaxy alignments, the alignments of galaxy groups and galaxy clusters with the large-scale structure have received considerable attention. Binggeli (1982) originally discovered that neighbouring galaxy clusters tend to point towards each other. He found that all pairs of clusters within 30 Mpc of each other (11 out of 30 clusters studied) pointed towards one another, with a misalignment of at most 45°. West (1989) showed that this alignment can also be seen for less massive galaxy groups out to similar scales, and Plionis (1994) found that it decreases with distance and is stronger for clusters residing in the same supercluster.

More recently, Wang et al. (2009) used a large sample of galaxy groups to show that the orientations of groups

[7] https://www.sdss3.org/dr8/algorithms/classify.php#photo_iso

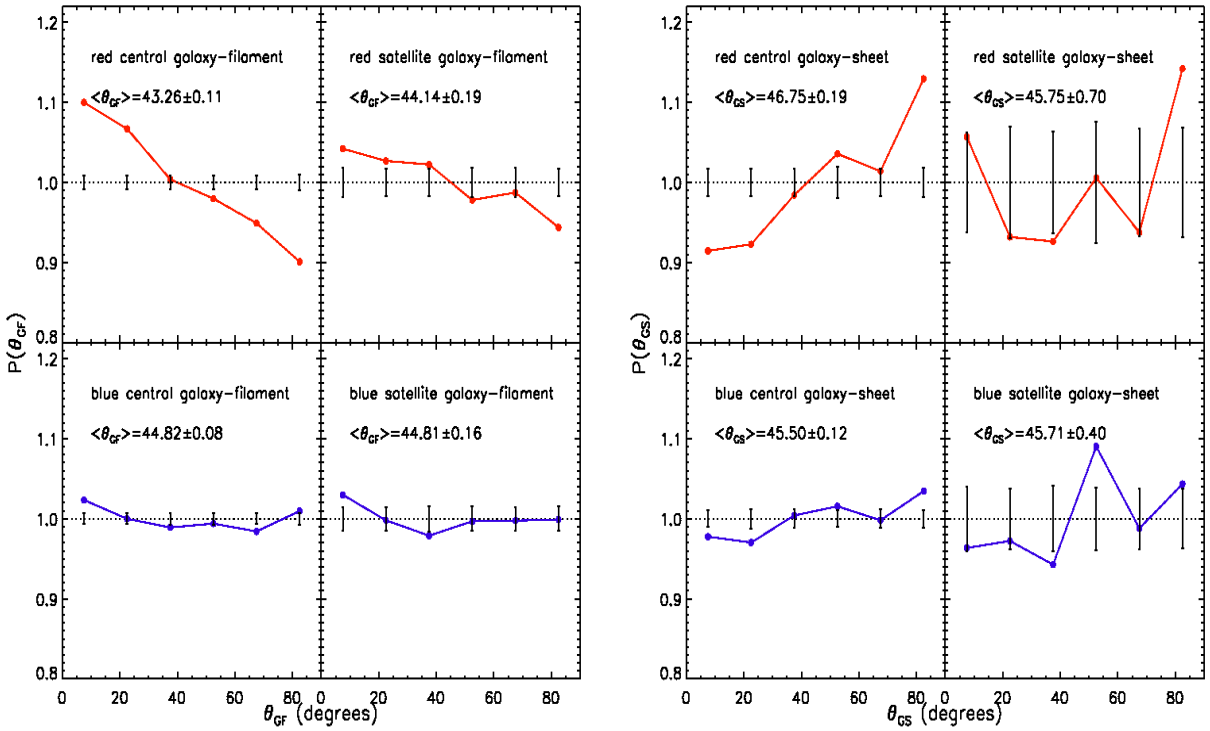


Fig. 11.— **Left:** Renormalised probability distribution of the angle $\theta_{\rm GF}$ between the projected galaxy major axis direction and the filament axis. For random galaxy orientation a constant value of unity is expected, as indicated by the black dotted line. Error bars are obtained from 100 Monte-Carlo realisations of randomised galaxy orientations. Data are shown for red/blue and central/satellite subsamples, as shown in the legends. **Right:** Same as on the left, but for the angle $\theta_{\rm GS}$ between the projected galaxy major axis direction and the sheet normal. © *AAS. Reproduced with permission from* Zhang et al. (2013).

and their galaxies are strongly correlated. They confirmed the result of West (1989) that groups tend to point to their nearest neighbours, in addition to showing that group central galaxies point to the nearest group, and that both have preferentially parallel major axes. These effects are strongest for early-type centrals in more massive groups and decline slowly with distance between the groups. Moreover, Paz et al. (2011) showed that this alignment extends to the surrounding large-scale structure, in the sense that groups with masses $M \gtrsim 6 \times 10^{13} M_{\odot}$ point towards galaxy overdensities in general, and that more massive groups do so more strongly.

In the most recent attempt, Smargon et al. (2012) measured alignments of galaxy cluster pairs out to 100 Mpc/h and $z < 0.44$ using two galaxy cluster catalogues extracted from SDSS data. The right-hand panels of Figure 12 show their measurements of radial alignment between cluster pairs. They compute these using the "pointing angle", $\theta_{\rm p}$, which is the angle on the sky between the projected cluster major axis and the line connecting one cluster to the other cluster in the pair. A positive correlation is detected out to $\sim$ 100 Mpc/h. The left-hand panels show a measurement of their common orientations, using the "correlation angle", $\theta_{\rm c}$, that is the angle between the projected major axes of the two clusters. This alignment is marginally detected for pairs separated by less than 20 Mpc/h. The top/bottom panels use different galaxy cluster catalogues, the Adaptive Matched Filament (AMF) (Dong et al. 2008) and maxBCG (Koester et al. 2007) catalogues respectively.

The observed signals, while significant, are weaker than the predictions from simulations. This discrepancy may be due to idealised assumptions that go into the simulations. Other possibile sources of difference are systematic effects

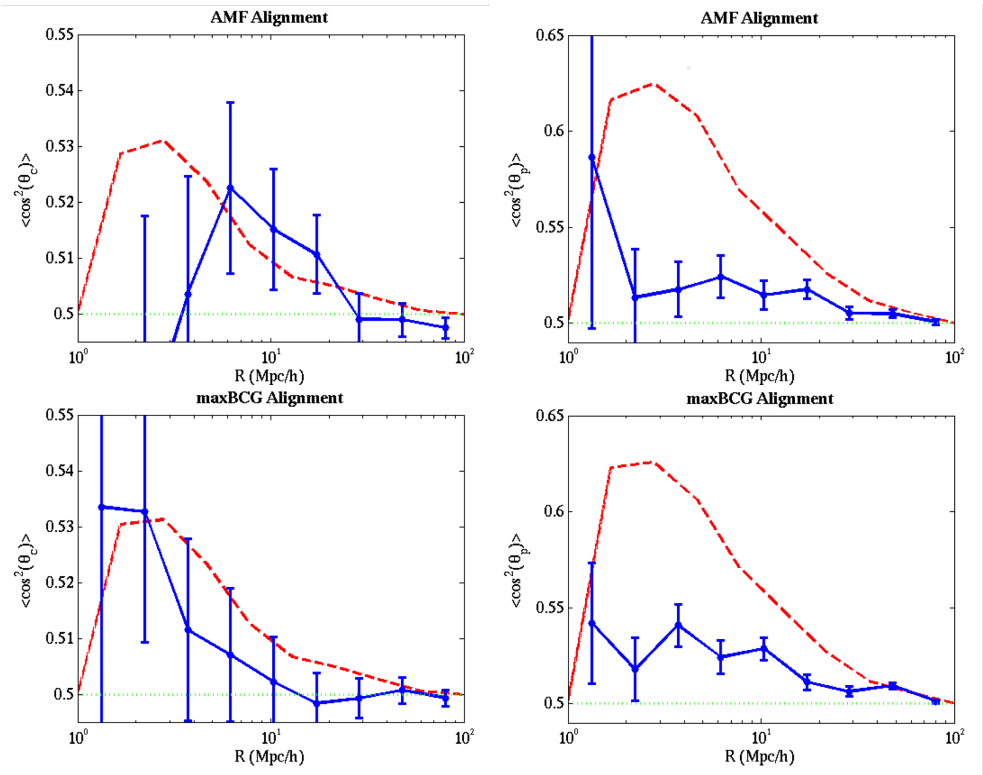


Fig. 12.— The cluster correlation angle alignment $\langle \cos^2 \theta_C \rangle$ (**left panels**) and the cluster pointing angle alignment $\langle \cos^2 \theta_p \rangle$ (**right panels**), as a function of comoving pair projected separation R in 2D. Note R in this plot is therefore equivalent to the 2D comoving separation that we elsewhere denote as $r_{\rm p}$. These angles are described in the text. The blue points with error bars are the observational results; the red dashed lines are theoretical predictions from N-body simulations assuming a ΛCDM cosmology (Hopkins et al. 2005), corrected for photometric redshift uncertainties; and the green dotted horizontal lines indicate purely random cluster orientations. The errors between the different bins in R are independent. **Top panels:** Uses the Adaptive Matched Filament (AMF) catalogue (Dong et al. 2008). **Bottom panels:** The maxBCG catalogue (Koester et al. 2007). *Reproduced with permission from* Smargon et al. (2012).

that weaken the observed signal, particularly errors in line-of-sight redshift selection due to the fact that photometric redshifts were used. The photometric redshift errors correspond to typical separations of $\sim 50 {\rm Mpc}/h$ along the line-of-sight, leading to contamination from clusters which are really unassociated, thus diluting the signal. Smargon et al. (2012) note that this effect alone cannot explain the full discrepancy; they discuss additional sources of error including centroiding and noise from both the small number of cluster members and clusters that are nearly round.

6. Impact on cosmology & Mitigation

Intrinsic alignments lead to additional contributions to the observed ellipticity correlation functions, thus compromising a simple cosmological interpretation of the results. The same is true for instrumental effects, such as contamination of the galaxy shapes by residual (uncorrected) PSF anisotropy. The impact of any systematic effect on a measurement of parameters of interest is to change the likelihood distribution for those parameters away from that which would have been observed if no systematic were present. If the systematic effect is sufficiently large, this can lead to parameter inferences that differ significantly, in a statistical sense, from the "true" values of those parameters (i.e. those that would have been found in a perfect experiment). Furthermore, the shape of the likelihood may change completely, for example from a surface with no curvature to something with significant curvature or even multi-modal

features. This scenario may possibly occur in the case of intrinsic alignments, where different galaxy populations may have different intrinsic alignment signal. A joint analysis of all galaxy types could result in a multi-peaked likelihood surface in the direction of the amplitude of the intrinsic alignment effect.

Systematics can both change the measured confidence levels for a particular parameter constraint (either increasing or decreasing them) and "bias" the measurement of a parameter, that is shift the maximum likelihood away from where it would be found in the absence of the systematic. The shift in the maximum likelihood, the biasing, is a general feature of any likelihood analysis in which the incorrect model is used – in the case of intrinsic alignments either because the effect was not included or mitigated at all, or because the assumed model is not correct. The change in confidence levels, or the errors on the parameters, is more complicated and can lead to an increased sensitivity (smaller error bars), or decreased sensitivity (larger error bars) on parameters depending on the nature of the assumptions made. For example, including a model for a systematic that depends also on the parameters of interest may increase sensitivity compared to a model that does not.

The observational evidence presented in Sections 4 and 5 suggests that the amplitude of the intrinsic alignment signal is such that it will lead to significant biases in ongoing and future cosmic shear surveys. In Section 6.1 we quantify this impact for a representative cosmic shear survey. The simplest way to deal with intrinsic alignment contamination would be to measure the cosmic shear signal and then subtract the intrinsic alignment contribution (both II and GI), leaving a "pure" signal. This would require perfect knowledge of the true intrinsic alignment signal as well as total confidence in the classification of galaxies and measurement of redshifts. It is therefore not considered feasible now or in the foreseeable future. This means that it is necessary to mitigate bias from intrinsic alignments in more imaginative ways. Most of these utilise the different redshift dependences of the GG, II and GI signals, as discussed in Section 6.2. The use of "nuisance parameters" to absorb the intrinsic alignment signal is discussed in Section 6.3 and the use of auxiliary data for "self-calibration" is summarised in Section 6.4. We discuss cosmic shear three-point statistics in Section 6.5 and novel probes of the unlensed galaxy shape in Section 6.6.

6.1. Quantifying Impact

The importance of intrinsic alignments for weak lensing studies was recognised early on and various studies have examined the expected impact. As early as Kamionkowski et al. (1998), novel mitigation schemes were being proposed at the same time as measurement of intrinsic alignments was being discussed.

Especially after the first detection of the cosmic shear signal (Bacon et al. 2000; Kaiser et al. 2000; Van Waerbeke et al. 2000; Wittman et al. 2000), much effort was spent on quantifying the impact of intrinsic alignments. Heavens et al. (2000) used N-body simulations to show that the impact of intrinsic alignments on cosmic shear correlation functions, as measured in their simulations, could be mitigated. They suggested that deep weak lensing surveys could be used to calibrate the level of intrinsic alignments because the broader source redshift distribution of sources in deeper surveys reduced the relative importance of intrinsic alignments. However, this suggestion neglected the importance of GI correlations and thus cannot be relied on. Croft & Metzler (2000) also studied intrinsic alignments in N-body simulations, and whilst coming to similar conclusions as Heavens et al. (2000), the magnitude of the effect appeared to be more problematic. They suggested that the signal could be measured (calibrated) using relatively small surveys of only a few thousand galaxies at low redshift, where intrinsic alignments dominate. This signal could then be applied to wider, deeper surveys, where the shear signal could be measured. The type of observations discussed in Section 4 might be suitable for such an approach but they should not be regarded as a sufficient substitute for measurements of intrinsic alignments over the redshift range representative of the full cosmic shear survey of interest (proper coverage of galaxy types is also very important). These, and other relevant results, are discussed in more detail in Kiessling et al. (2015).

Catelan et al. (2001) considered several ways to discriminate between weak gravitational lensing and the intrinsic alignment signal. The first method that they proposed was simple, based on their particular model for intrinsic alignments, which had a strong ellipticity dependence: the impact of intrinsic alignments could be reduced by using sources with smaller intrinsic ellipticities, but this would pose serious problems for ellipticity measurement. More practically, they also suggested the use of density correlations, such as the w_{g+} measurements presented in this review, around galaxy clusters and the use of morphological information to remove intrinsically aligned galaxies.

An attempt at total removal of intrinsic alignments is complicated, however, because, as we have already discussed, the observed ellipticity correlation is the sum of a gravitational lensing term, GG, an intrinsic alignment term, II, and a cross-term, GI,

$$C^{(ij)}_{\epsilon\epsilon}(\ell) = C^{(ij)}_{\rm GG}(\ell) + C^{(ij)}_{\rm II}(\ell) + C^{(ij)}_{\rm GI}(\ell), \tag{33}$$

where we have expressed each as a projected angular power spectrum $C^{(ij)}(\ell)$ in Fourier space for a pair of tomographic bins in spherical harmonic space and ℓ denotes the angular frequency, the Fourier variable on the sky. The superscripts i, j denote a redshift bin pair for the tomographic analysis. Note that, if galaxies are well separated in redshift, any IG term is expected to be zero. The importance of the GI correlation was not fully appreciated in the earliest literature discussing mitigation (Croft & Metzler 2000; Heavens et al. 2000; Catelan et al. 2001). This is a serious drawback as the GI term is not only more difficult to remove, it can also dominate over the II contribution for many tomographic bin pairs in realistic cosmic shear surveys. The details of the modelling of intrinsic alignments are given in our companion paper (Kiessling et al. 2015) but, for a linear alignment model, each of the 2D projected angular power spectra in Equation (33) can be constructed from the integration of the 3D power spectrum multiplied by the appropriate redshift distribution or lensing weight functions,

$$C^{(ij)}_{\rm GG}(\ell) = \int_0^{\chi_{\rm H}} d\chi \frac{q^{(i)}(\chi) q^{(j)}(\chi)}{f^2_{\rm K}(\chi)} P_{\delta\delta}\left(\frac{\ell}{f_{\rm K}(\chi)}, \chi\right), \tag{34}$$

$$C^{(ij)}_{\rm II}(\ell) = \int_0^{\chi_{\rm H}} d\chi \frac{p^{(i)}(\chi) p^{(j)}(\chi)}{f^2_{\rm K}(\chi)} P_{\rm II}\left(\frac{\ell}{f_{\rm K}(\chi)}, \chi\right), \tag{35}$$

$$C^{(ij)}_{\rm GI}(\ell) = \int_0^{\chi_{\rm H}} d\chi \frac{q^{(i)}(\chi) p^{(j)}(\chi)}{f^2_{\rm K}(\chi)} P_{\delta{\rm I}}\left(\frac{\ell}{f_{\rm K}(\chi)}, \chi\right). \tag{36}$$

Here $f_{\rm K}(\chi)$ is the comoving angular diameter distance, given by

$$f_{\rm K}(\chi) = \begin{cases} 1/\sqrt{K}\sin\left(\sqrt{K}\chi\right) & K > 0 \text{ (open)} \\ \chi & K = 0 \text{ (flat)} \\ 1/\sqrt{-K}\sinh\left(\sqrt{-K}\chi\right) & K < 0 \text{ (closed)}\,, \end{cases} \tag{37}$$

where $1/\sqrt{|K|}$ is interpreted as the curvature radius of the spatial part of spacetime.

$p^{(i)}(\chi) = p^{(i)}(z){\rm d}z/{\rm d}\chi$, where $p^{(i)}(z)$ is the galaxy redshift distribution of bin i, $q^{(i)}(\chi)$ is the lensing weight function of bin i (Joachimi & Bridle 2010),

$$q^{(i)}(\chi) = \frac{3H_0^2\,\Omega_{\rm m}}{2\,c^2}\frac{f_{\rm K}(\chi)}{a(\chi)}\int_\chi^{\chi_{\rm H}} {\rm d}\chi'\; p^{(i)}(\chi')\;\frac{f_{\rm K}(\chi'-\chi)}{f_{\rm K}(\chi')}, \tag{38}$$

and $\chi_{\rm H}$ is the comoving distance to the horizon. Ideally the tomographic bins do not overlap, which is possible in the case of spectroscopic redshifts. This is, however, not feasible in the case of cosmic shear surveys, which rely on photometric redshifts. Due to limitations in the precision with which photometric redshifts can be determined, as well as catastrophic outliers due to misidentification of features in the spectral energy distribution, the bins partially overlap in practice.

Examples of projected angular power spectra of the different GG, II, and GI terms for a projected spherical harmonic tomographic analysis of a fiducial wide-field survey are shown in Figure 13, alongside other terms related to number counts (see below). The figure shows forecasts originally made in Kirk et al. (2012). The II terms are positive (by definition), while the GI terms are negative in amplitude to match observations. Figure 13 illustrates how intrinsic alignment terms add (through the II term) and subtract (through the GI term) to the weak lensing GG power spectrum. Being a local effect, the II correlation is strongest for redshift bin auto-correlations, where the number of physically close pairs is largest. As this plot is for a photometric cosmic shear survey the redshift cross-terms do not have zero II contribution as there is usually some overlap in redshift between bins. In contrast the GI term is strongest for bins separated in redshift where the redshift distribution of the "I" bin overlaps with the lensing kernel of the "G" bin. In

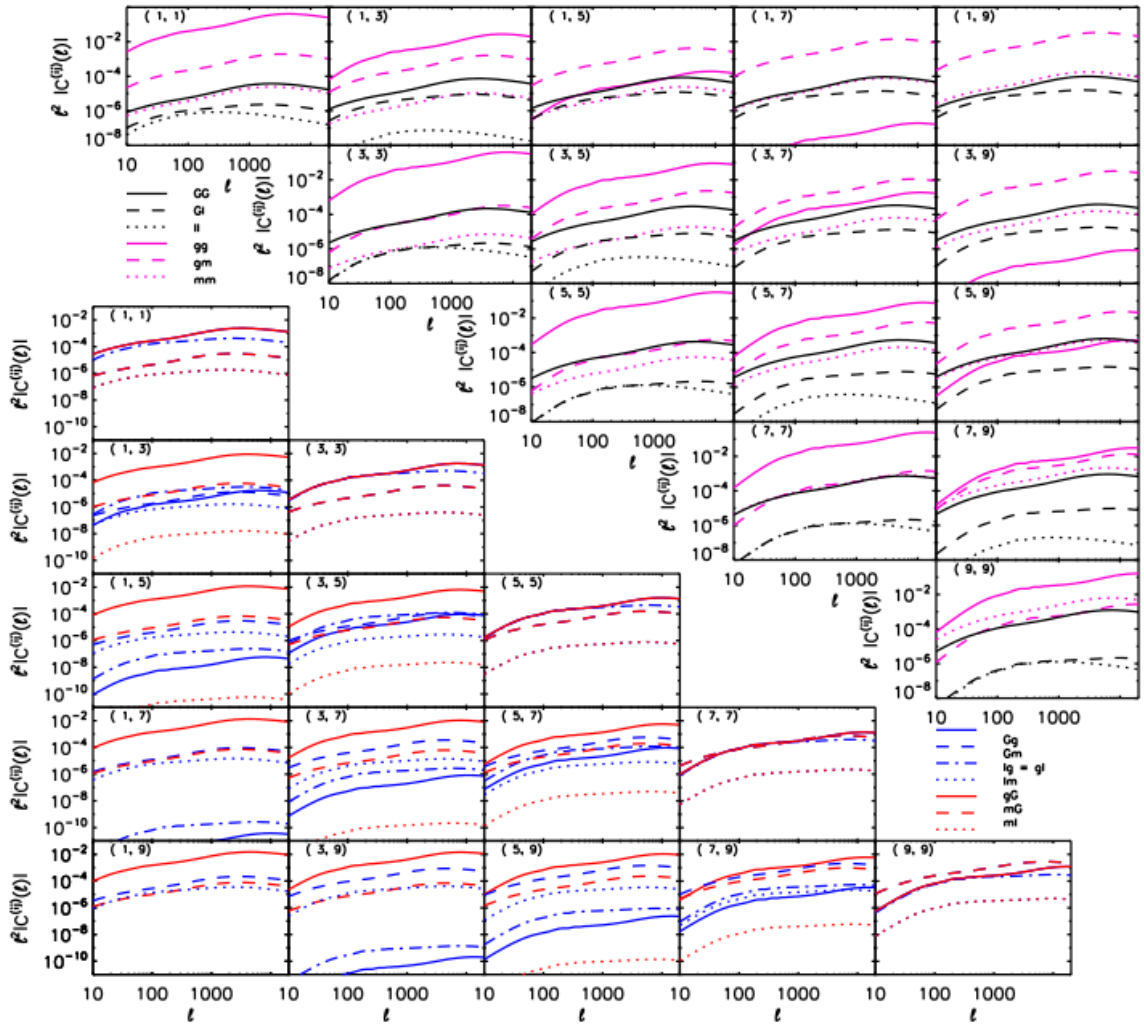


Fig. 13.— Forecast projected angular power spectra, $C^{(ij)}(\ell)$, for a tomographic analysis of a wide-field survey based on the Euclid mission design (Refregier et al. 2010). **Upper Right Panels:** Gravitational lensing and intrinsic alignment terms related to the observed ellipticity auto-correlation (GG, GI, II) and galaxy clustering and cosmic magnification terms related to the number count auto-correlation (gg, gm, mm). **Lower Left:** Terms related to the cross-correlation of ellipticity and number counts, including contributions from intrinsic alignment and magnification (gG, mG, gI, mI). The absolute value of these power spectra are shown but it should be remembered that the GI, gI and mI contributions are negative in amplitude. See Section 6.4 for more details on these power spectra. The numbers in the top right corner of each panel denote the tomographic bin pair being considered. There are 10 bins in total, split so each has roughly the same number density of source galaxies; bin 1 is the lowest redshift bin, while bin 10 is the highest redshift bin. See Sections 6.1 and 6.4 for detailed descriptions of each term. *Reproduced with permission from* Kirk et al. (2012).

general the relevant weight functions overlap differently for different combinations of tomographic bins, affecting both the amplitude and effective scale dependence of each contribution to the measured shear or galaxy position correlation.

Some features of the impact of intrinsic alignments on two-point statistics, as well as simple mitigation techniques,

are brought together in Figure 14. Here we forecast constraints on cosmology from a generic weak gravitational lensing survey, modelled on the European Space Agency Euclid mission[8] (Refregier et al. 2010; Laureijs et al. 2011). This generic survey covers 15,000 deg^2 with a galaxy density of 30 arcmin^{-2}, split into 10 tomographic redshift bins over the range $0 < z < 2.0$. A Gaussian total shape noise contribution of $\sigma_\epsilon = 0.35$ is assumed. Our results are shown as 95% confidence contours in the dark energy equation of state parameters w_0 and w_a. These describe the amplitude and time-evolution of the dark energy equation of state, $w_{\rm de}(z) = w_0 + w_a(1-a)$. All constraints are shown marginalised over the cosmological parameters: Ω_m, the dimensionless matter density, Ω_b, the dimensionless baryon density, σ_8, the amplitude of the density perturbations, h, the Hubble parameter, and n_s, the spectral index of the density perturbations. Euclid is an example of a Stage-IV survey as defined by the Dark Energy Task Force (Albrecht et al. 2006).

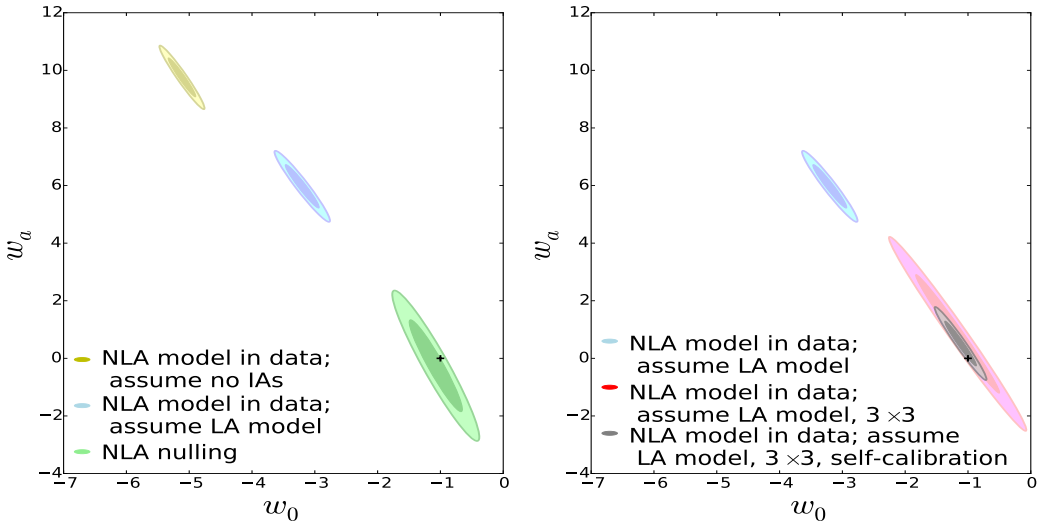


Fig. 14.— Forecast cosmological constraints for a generic Euclid-like survey, making different assumptions about intrinsic alignments. 95% confidence ellipses are shown for the dark energy equation of state parameters, w_0 and $w_{\rm a}$. Constraints shown have been marginalised over Ω_m, h, σ_8, $\Omega_{\rm b}$, n_s and nuisance parameters where appropriate, see Section 6.1 for more details. **Left Panel:** Impact of incorrect model choice. True model assumed is the non-linear alignment model (Hirata & Seljak 2004; Bridle & King 2007). The yellow contour shows constraints and bias on $w_0, w_{\rm a}$ when intrinsic alignments are ignored. The blue contour assumes the (incorrect) linear alignment model. The green contour shows the constraints from nulling, see Section 6.2 for more details. **Right Panel:** Impact of marginalising over a robust grid of nuisance parameters in redshift and angular scale and self-calibration with galaxy clustering information. Each contour uses the non-linear alignment model as the "truth". The blue contour is the same as in the left-hand panel i.e. it assumes the (incorrect) linear alignment model. The red contour also assumes the linear alignment model, marginalised over a 3×3 grid of nuisance parameters in redshift and angular scale. The grey contour shows the same scenario (assume linear alignment, 3×3 nuisance grid) with the inclusion of galaxy clustering information i.e. self-calibration, see Section 6.4 for more details. The black crosses show the fiducial values of $w_0, w_{\rm a}$.

The constraints are calculated by the Fisher matrix technique (Fisher 1935), assuming a Gaussian likelihood function and covariance matrix, independent of the fiducial cosmological parameter values. The Fisher matrix approach can be extended to make an estimate of the bias on cosmological parameters, Δp_α, when an incorrect cosmological

[8] http://www.euclid-ec.org/

model is assumed (Huterer et al. 2006; see also Amara & Réfrégier 2008 and Appendix A of Joachimi et al. 2011):

$$\Delta p_\alpha = \sum_\beta F^{-1}_{\alpha\beta} \sum_\ell \sum_{i\le j;m\le n} \Delta C^{(ij)}_{\epsilon\epsilon}(\ell) \left(\mathrm{Cov}\left[C^{(ij)}_{\epsilon\epsilon}(\ell), C^{(mn)}_{\epsilon\epsilon}(\ell)\right]\right)^{-1} \frac{\partial C^{(mn)}_{\epsilon\epsilon}(\ell)}{\partial p_\beta}, \tag{39}$$

where $\Delta C^{(ij)}_{\epsilon\epsilon}(\ell)$ is the difference between the power spectra for the true and assumed models; F is the Fisher matrix,

$$F_{\alpha\beta} = \sum_\ell \sum_{i\le j;m\le n} \frac{\partial C^{(ij)}_{\epsilon\epsilon}(\ell)}{\partial p_\alpha} \left(\mathrm{Cov}\left[C^{(ij)}_{\epsilon\epsilon}(\ell), C^{mn}_{\epsilon\epsilon}(\ell)\right]\right)^{-1} \frac{\partial C^{mn}_{\epsilon\epsilon}(\ell)}{\partial p_\beta}, \tag{40}$$

Cov is the covariance matrix (Takada & Jain 2004); i, j, m, n count over tomographic redshift bins and α, β count over some set of cosmological (and nuisance) parameters. p_α refers to a particular cosmological or nuisance parameter, hence Δp_α is the resulting bias on that parameter. The equations refer to the ellipticity-ellipticity auto-correlation, $C^{(ij)}_{\epsilon\epsilon}(\ell)$, and the bin pairs are restricted to $i \le j$ because the symmetry of the observable means that these pairs exhaust the available information. The formalism is easily extendable to the galaxy position-position correlation, $C^{(ij)}_{\mathrm{nn}}(\ell)$, and the position-ellipticity cross-term, $C^{(ij)}_{\mathrm{n}\epsilon}(\ell)$, see Section 6.4 below for more details.

We can use this to show the importance of a well-modelled intrinsic alignment contribution to the measured cosmic shear signal. We do not know the true intrinsic alignment model but the left-hand panel of Figure 14 shows the bias on cosmological parameters when we take the non-linear alignment model (with an amplitude of $C_1 = 5 \times 10^{-14} (h^2 \mathrm{M}_\odot \mathrm{Mpc}^{-3})^{-1}$ (Bridle & King 2007) and, for simplicity, no dependence on galaxy type or luminosity) as the (true) observed signal but use either no intrinsic alignments (yellow contour) or the linear alignment model (blue contour) in our analysis. The assumed intrinsic alignment amplitude is based on the SuperCOSMOS normalisation (Brown et al. 2002; Bridle & King 2007) and is consistent with the lower end of current observational constraints for early-type galaxies (Joachimi et al. 2011; Heymans et al. 2013), making the bias predictions realistic for current and future cosmic shear surveys. It is clear that the results are catastrophically biased. The true fiducial cosmology is indicated by a black cross and the forecast contours are off by several standard deviations. The contour that assumes the linear alignment model (blue) is less biased than that which ignores intrinsic alignments completely because the linear alignment model replicates the non-linear alignment phenomenology at linear scales.

Cosmic shear in tomographic redshift slices is an approximation of a more general formalism called 3D cosmic shear, the most notable being the Limber approximation, a binning in redshift. 3D cosmic shear uses the one-point shear transform coefficients that are calculated using a spherical-Bessel transform of the data (Heavens 2003). The impact and mitigation of intrinsic alignments in 3D cosmic shear analysis has been studied in Kitching et al. (2008); Merkel & Schäfer (2013); Kitching et al. (2014, 2015b). Results and strategies presented below are framed for tomographic analyses but can in principle also be applied to the 3D cosmic shear methodology.

6.2. Exploiting redshift dependence

Taking a conservative approach, one can assume a complete lack of knowledge about the physics underlying intrinsic alignments and thus the form of the II and GI spectra. In that case the only reliable information left to separate the weak lensing signal from intrinsic alignments is the redshift dependence of the signals, which is governed by the redshift distribution of the galaxy samples and their lensing weight functions (see Equations (34) to (35)). Here we describe some appraoches which exploit this information:

- **Downweighting:** King & Schneider (2002) proposed an algorithm to suppress the II term in non-tomographic weak lensing surveys with photometric redshift information. They demonstrated that incorporating a Gaussian kernel that downweights galaxy pairs close in redshift is effective at reducing the intrinsic alignment contamination while moderately reducing the effective number of galaxies in the analysis. In a similar analysis Heymans & Heavens (2003) derived statistically optimal weights for suppressing the II term if either photometric or spectroscopic redshift information is available. They concluded that high-quality photometric redshifts would be a necessity for the analysis of future weak lensing surveys.

Using redshifts to divide the galaxy sample into tomographic bins, King & Schneider (2003) fitted a linear combination of generic template functions to II and GG correlation functions. If the redshift overlap of neighbouring tomographic bins is small, it may well be sufficient to simply discard all redshift auto-correlations from analysis, which causes a 10 % increase in errors on cosmological parameters when at least five tomographic bins are used (Takada & White 2004). This approach was extended to include the GI term by King (2005), assuming independence of the II and GI terms, and demonstrated on toy models.

- **Nulling:** Joachimi & Schneider (2008, 2009) introduced a nulling technique for the GI term. For a given set of tomographic two-point statistics in N_z tomographic bins, one can construct new measures, the nulled power spectrum ζ, via linear combinations of the standard statistics, e.g. in the case of projected angular power spectra,

$$\zeta^{(i)}_{[q]}(\ell) = \sum_{j=i+1}^{N_z} T_{[q],j}\, C^{(ij)}(\ell)\ , \tag{41}$$

with weights $T_{[q],j}$, for every foreground redshift bin i. The weights are orthogonal to each other, and orthogonal to $1-\chi(z_i)/\chi(z_j)$, which is an approximation to the kernel of the GI term in the limit of redshift bins with narrow redshift distributions; compare to Equation (36). Depending on implementation, the redshifts z_i and z_j can correspond to the mean or median redshifts in each tomographic bin. In this way one can construct N_z-i-1 independent statistics $\zeta^{(i)}_{[q]}$ for every foreground bin, numbered by the index q in square brackets, in which the intrinsic alignment signal should be strongly suppressed.

Joachimi & Schneider (2009) showed that nulling, combined with a suppression of redshift auto-correlations, reduces the bias due to the combination of II and GI by at least an order of magnitude on well-constrained cosmological parameters. This was achieved robustly over a wide range of photometric redshift parameters, for random scatters up to $0.1(1+z)$ and catastrophic outlier (galaxies whose redshifts are comprehensively misidentified) fractions up to 10 %. However, due to the similar redshift scaling of the GI and GG signals, the robust removal of GI contamination comes at the price of substantially reducing the statistical power. Marginal errors on cosmological parameters increase by typically a factor of two, and by a factor of three in case of the dark energy equation of state parameters w_0 and w_a, whose constraints rely strongly on the redshift evolution of the lensing signal. While an order of magnitude loss in the dark energy figure of merit is intolerable for cosmological surveys, nulling techniques and their kin can still serve as a robust validation test for intrinsic alignment mitigation strategies that rely on more assumptions about the nature of these signals.

We show schematically the power of nulling in the left panel of Figure 14. The green contour shows the results of a nulling analysis of the same experimental scenario as for the other contours. Nulling succesfully reduces the bias to within the 1σ contour but at the cost of reducing usable information, hence the ellipse is broader i.e. less constraining.

- **Boosting:** As was already noted in the early works (e.g. King & Schneider 2002, 2003), any procedure to suppress the intrinsic alignment contribution can be reversed to boost these signals, which enables their study at scales and redshifts where the lensing signal would otherwise dominate. Joachimi & Schneider (2010) devised a GI boosting technique, again via linear combinations of tomographic two-point statistics and showed explicitly how it links to nulling. The method can turn a GI signal that is $10-30$ % of the GG term into being about one order of magnitude stronger than GG for good quality photometric redshifts and two orders of magnitude stronger for spectroscopic redshifts. Recently, Schneider (2014) refined this concept to boost the galaxy-magnification cross-correlation over the galaxy clustering signal, which de-biased and tightened cosmological constraints.

6.3. Parameterisation and marginalisation

The most common approach to dealing with intrinsic alignments in the literature is to introduce a number of free parameters that describe the amplitude, redshift/scale/colour dependence etc. of intrinsic alignments and allow these parameters to vary within some prior range as part of a cosmological likelihood analysis. These intrinsic alignment

"nuisance" parameters can be marginalised over when quoting constraints on cosmological parameters. This marginalisation will make cosmological parameter constraints weaker but, if the nuisance parameterisation is sufficiently flexible that it captures the full range of the intrinsic alignment signal, the resulting constraints will be unbiased. Note that the model being parameterised can be based on an assumed physical mechanism for intrinsic alignments and is therefore not distinct from the linear alignment or non-linear alignment models discussed above. For example Heymans et al. (2013) uses the non-linear alignment model with a single free amplitude parameter, which is marginalised over whenever constraints on cosmological parameters are discussed. See Section 4.3 for a more detailed discussion.

The benefit of the parameterisation/marginalisation approach is that it can be implemented simultaneously with the cosmological parameter estimation. This means that the same procedure produces constraints on cosmological parameters and the parameters of the intrinsic alignment model. The downside is that a higher dimensional parameter space must be explored, sometimes significantly higher, which is computationally expensive. There is also some ambiguity in the statement that cosmological constraints are unbiased "provided the parameterisation is sufficiently flexible." In the absence of very strong constraints on intrinsic alignments there is no definitive statement about either how many nuisance parameters are required or what their prior ranges should be. With this approach, it is easy to update the analysis as more precise measurements of intrinsic alignments become available, either through a joint likelihood analysis or by altering the priors of the initial analysis.

In the right-hand panel of Figure 14 we show an attempt to reduce bias through nuisance parameters and marginalisation for our toy survey. We also show the use of self-calibration to recover information through full exploitation of joint gravitational shear and galaxy position information, described in Section 6.4 below. Each contour takes the non-linear alignment model to be the true description of intrinsic alignments but models them (incorrectly) with the linear alignment model. The blue contour is the same as in the left hand panel, showing the bias this produces in the simple case.

The red contour is the result of the same analysis with additional nuisance parameters included. A grid of nuisance parameters which can vary in scale and redshift is employed: 3×3 parameters in $z \times k$, where k is the Fourier space wavenumber, are used for both the amplitude of the II and GI terms, as well as free amplitudes for each. This leads to a total of $2(3 \times 3) + 2 = 20$ nuisance parameters. Marginalising over these new parameters reduces the precision, as shown by the increased size of the contour, but it also reduces the bias in the inferred cosmological parameters to within the 1σ area. For a more detailed example of marginalisation using this parameterisation see Joachimi & Bridle (2010).

A goal of the parameterisation and marginalisation approach is to include information from intrinsic alignment measurements as physically motivated priors on the intrinsic alignment nuisance parameters. This inclusion of prior information from observations is not yet mature in the intrinsic alignment literature but, for example, Sifón et al. (2015) used measurements of intrinsic alignments in clusters to inform parameters for their implementation of the halo model. They aimed to test how strong a deviation from the non-linear alignment model at small scales was allowed by observations. They found an allowed deviation significantly lower than the fiducial model assumed in Schneider & Bridle (2010).

6.4. Self-calibration

All cosmic shear surveys contain information beyond the correlation of galaxy ellipticities. Even a survey with photometric-quality redshifts can be used to study galaxy clustering (i.e. position-position correlations), and additional information is contained in the cross-correlation between position and ellipticity. Exploitation of this additional information can regain some of the constraining power lost when marginalising over intrinsic alignment nuisance parameters. Bernstein (2009) outlined the formalism to treat a range of two-point correlations available with cosmic shear survey data. We summarise relevant aspects below and refer readers to that paper for more details.

Exploitation of this information is an example of "self-calibration" because the uncertainties due to intrinsic alignments are being calibrated by information contained in the cosmic shear survey itself. The effect of magnification is important in both galaxy position-galaxy position clustering and the galaxy position-ellipticity cross-correlation, so omitting it can bias results (Duncan et al. 2014). We can now write down a set of three observables, each made up of

multiple contributions, analogous to Equation (33),

$$C^{(ij)}_{\epsilon\epsilon}(\ell) = C^{(ij)}_{\rm GG}(\ell) + C^{(ij)}_{\rm II}(\ell) + C^{(ij)}_{\rm GI}(\ell) + C^{(ij)}_{\rm IG}(\ell), \tag{42}$$

$$C^{(ij)}_{{\rm n}\epsilon}(\ell) = C^{(ij)}_{\rm gG}(\ell) + C^{(ij)}_{\rm gI}(\ell) + C^{(ij)}_{\rm mG}(\ell) + C^{(ij)}_{\rm mI}(\ell), \tag{43}$$

$$C^{(ij)}_{\rm nn}(\ell) = C^{(ij)}_{\rm gg}(\ell) + C^{(ij)}_{\rm gm}(\ell) + C^{(ij)}_{\rm mg}(\ell) + C^{(ij)}_{\rm mm}(\ell). \tag{44}$$

These are the set of power spectra shown in Figure 13. As before "G" denotes gravitational lensing and "I" intrinsic alignment, we use "g" and "m" to refer to galaxy clustering and the change in number density due to magnification respectively (see below for more details). $\epsilon\epsilon$ is then the observed ellipticity correlation signal from both weak lensing and intrinsic alignment contributions while nn is the observed galaxy position correlation signal including the magnification contributions. nϵ is the observed cross-correlation.

The gG term is the cross-correlation of galaxy clustering and gravitational lensing. As galaxies are biased tracers of the underlying matter distribution, we would expect a foreground galaxy population to be correlated with the lensing of background source galaxies. This is often referred to as galaxy-galaxy lensing, especially on scales where the lensing is dominated by the haloes of the foreground galaxies (e.g. Mandelbaum et al. 2006b; van Uitert et al. 2011; Velander et al. 2014). It is clear that a galaxy-intrinsic alignment term, gI, appears in the galaxy-shear cross-correlation in an analogous way to the gravitational lensing-intrinsic alignment GI term. Consequently, intrinsic alignments are an important contamination in galaxy-galaxy lensing if the source and lens populations cannot be perfectly separated (Blazek et al. 2012; Chisari et al. 2014). We can write the projected angular power spectra of these terms as integrals over the three dimensional matter power spectrum and the appropriate window functions under the Limber approximation:

$$C^{(ij)}_{\rm gg}(\ell) = \int_0^{\chi_{\rm H}} d\chi \frac{p^{(i)}(\chi)p^{(j)}(\chi)}{f^2_{\rm K}(\chi)} b^2_{\rm g}\left(\frac{\ell}{f_{\rm K}(\chi)}, \chi\right) P_{\delta\delta}\left(\frac{\ell}{f_{\rm K}(\chi)}, \chi\right), \tag{45}$$

$$C^{(ij)}_{\rm gG}(\ell) = \int_0^{\chi_{\rm H}} d\chi \frac{p^{(i)}(\chi)q^{(j)}(\chi)}{f^2_{\rm K}(\chi)} b_{\rm g}\left(\frac{\ell}{f_{\rm K}(\chi)}, \chi\right) P_{\delta{\rm G}}\left(\frac{\ell}{f_{\rm K}(\chi)}, \chi\right), \tag{46}$$

$$C^{(ij)}_{\rm gI}(\ell) = \int_0^{\chi_{\rm H}} d\chi \frac{p^{(i)}(\chi)p^{(j)}(\chi)}{f^2_{\rm K}(\chi)} b_{\rm g}\left(\frac{\ell}{f_{\rm K}(\chi)}, \chi\right) P_{\delta{\rm I}}\left(\frac{\ell}{f_{\rm K}(\chi)}, \chi\right). \tag{47}$$

Weak gravitational lensing, as well as distorting the shape of galaxy images, changes their apparent sizes while the surface brightness is unchanged. This means that the flux of galaxies is changed and galaxy images can be either magnified or demagnified. This is the cosmic magnification contribution referred to by the subscript m. For a flux-limited survey this can mean galaxies are promoted or demoted across the detection threshold, changing the observed number density and the clustering statistics. Magnification also causes a change in effective area, which also modulates the observed number density. This is apparent in the mm term that contributes to the observed galaxy correlation, but there are also cross-correlations between magnification and galaxy counts, gm, mg, and cross-correlations between magnification and gravitational lensing, mG, and indeed, magnification-intrinsic alignment correlations, mI.

Magnification due to lensing arises due to the same gravitational potential responsible for the shear, therefore the magnification signal can be related to the correlation functions that involve the shear. The amplitude of the effect depends on $\alpha^{(i)}$, the power-law slope of the observed number counts for the galaxies in the ith tomographic bin. The form of the magnification terms is

$$C^{(ij)}_{\rm mm}(\ell) = 4(\alpha^{(i)} - 1)(\alpha^{(j)} - 1)C^{(ij)}_{\rm GG}(\ell), \tag{48}$$

$$C^{(ij)}_{\rm gm}(\ell) = 2(\alpha^{(i)} - 1)C^{(ij)}_{\rm gG}(\ell), \tag{49}$$

$$C^{(ij)}_{\rm mG}(\ell) = 2(\alpha^{(i)} - 1)C^{(ij)}_{\rm GG}(\ell), \tag{50}$$

$$C^{(ij)}_{\rm mI}(\ell) = 2(\alpha^{(i)} - 1)C^{(ij)}_{\rm GI}(\ell). \tag{51}$$

These magnification terms are important because results from an analysis that ignores them can be significantly biased (Duncan et al. 2014).

Exploitation of some of this set of observables has been proposed in different ways (Zhang 2010; Troxel & Ishak 2012b,a) and has been shown to be an effective self-calibration strategy in forecasts (Bernstein 2009; Joachimi & Bridle 2010; Laszlo et al. 2012; Kirk et al. 2013). Even if intrinsic alignment model ignorance is aggressively marginalised over, self-calibration can recover the bulk of the information present in a naive cosmic shear analysis that ignored intrinsic alignments, but without the bias on cosmology. This approach has yet to be attempted as part of a real data analysis because the statistical power of existing datasets does not warrant such a thorough treatment.

An example of the power of this self-calibration approach is shown in the forecasts of Figure 14. We have already shown how marginalisation over nuisance parameters can remove the cosmological bias due to intrinsic alignments, at the cost of constraining power. The grey contour in the right-hand panel uses the same approach but includes galaxy clustering information and galaxy + weak gravitational lensing cross-correlation, all from the same (photometric) survey as the cosmic shear signal. In the case where multiple probes are considered we replace the simple $C^{(ij)}(\ell)$ with a data vector, for example $\mathcal{D}^{(k)} = \{C^{(ij)}_{\epsilon\epsilon}(\ell), C^{(ij)}_{\mathrm{n}\epsilon}(\ell), C^{(ij)}_{\mathrm{nn}}(\ell)\}$, where k counts over bin pairs. Note that the inclusion of the $C^{(ij)}_{\mathrm{n}\epsilon}(\ell)$ cross-correlations breaks the bin pair symmetry and each bin pair i, j must be considered separately. The same grid parameterisation is extended to galaxy bias and the galaxy + weak gravitational lensing cross-correlation amplitude, giving an extra 20 nuisance parameters for a total of 40. Even with these new nuisance parameters, the self-calibration result is much tighter than that of weak gravitational lensing alone while remaining unbiased at 1σ. Indeed the self-calibration with 40 nuisance parameters is on a par with the naive weak gravitational lensing analysis without nuisance parameters in terms of constraining power.

Similarly, it has been shown that information contained in changes to the size of lensed galaxy images due to magnification can be exploited in parallel with that from image shape distortion (Heavens et al. 2013; Alsing et al. 2015). Using this magnification information mitigates the impact of intrinsic alignments by $\sim 20\%$, even in a pessimistic scenario. This information can also be included as part of a general self-calibration scheme, along with galaxy clustering information.

Self-calibration exploits information beyond shape measurements present in any cosmic shear survey. It is of course possible to calibrate uncertainty, from intrinsic alignments or other sources, by utilising additional data from beyond the optical weak lensing survey in question. This could mean assuming priors on cosmological parameters from cosmic microwave background (CMB) experiments, the use of spectroscopic redshift surveys to calibrate photometric redshift estimates or cross-correlation with a different dataset. The potential for measuring galaxy shapes in radio surveys has been noted (Brown et al. 2015). This could be used to make a weak lensing measurement in the radio or to calibrate shape measurement systematics or the intrinsic alignment signal in an optical weak lensing survey (Kitching et al. 2015a; Kirk et al. 2015; Patel et al. 2015). A note of caution should be drawn from Patel et al. (2010) however, who found no evidence of correlation between shapes measured in optical and radio surveys. Further work is required to determine the true relationship between galaxy shapes in optical and radio wavelengths. If they were truly uncorrelated, they could not be used for mutual calibration but the effective number density of the combined surveys would be increased by a factor of two. We discuss novel approaches to intrinsic alignment mitigation using radio surveys in Section 6.6 below.

Another interesting cross-correlation is between weak lensing of galaxy images and weak lensing of the CMB (Hand et al. 2015; Troxel & Ishak 2014; Hall & Taylor 2014). Light from the CMB is lensed on its way to the observer, just like light from galaxies. In the case of the CMB there is a single source plane, the surface of last scattering, and the light pattern contains the imprinted signal of all the structure formation from last scattering until today. There is no equivalent to intrinsic alignments in the source of the CMB. However, when one cross-correlates the weak gravitational lensing signal from galaxies with that from the CMB, which we indicate by $\epsilon\mathrm{G}^{\mathrm{CMB}}$, there will also be a cross-term from galaxy intrinsic alignments and the CMB lensing:

$$C^{(i)}_{\epsilon\mathrm{G}^{\mathrm{CMB}}}(\ell) = C^{(i)}_{\mathrm{GG}^{\mathrm{CMB}}}(\ell) + C^{(i)}_{\mathrm{IG}^{\mathrm{CMB}}}(\ell), \tag{52}$$

where i labels a weak gravitational lensing tomographic bin (the CMB lensing has only one source plane). The contribution of this term to the observed cross-correlation signal has been estimated to be $\sim 15\%$ (Hall & Taylor 2014) in a survey combination such as the ACTPol/CFHT (Atacama Cosmology Telescope-polarisation/Canada France Hawaii Telescope) Stripe 82 cross-correlation of Hand et al. (2015). Troxel & Ishak (2014) suggested a self-calibration technique for the CMB-intrinsic alignment correlation using a scaling relation between the intrinsic alignment information

in the weak gravitational lensing and the combined weak gravitational lensing and CMB observables. They claim that this self-calibration allows one to reduce the impact of intrinsic alignments in the cross-correlation by a factor of 20 or more in all redshift bins.

6.5. Higher-order cosmic shear statistics

The three-point statistics of the shear field can in principle be used to mitigate the intrinsic alignment systematics in the two-point analysis, because the dependencies of the three-point intrinsic alignment terms on cosmological parameters is different from those in the two-point measurement (Vafaei et al. 2010; Troxel & Ishak 2012b,a). In the three-point case, the correlation terms that arise have the form GGG, IGG, GII and III (and combinatorial variations thereof). The origin is analogous to that of two-point intrinsic alignments; here GGG is the pure gravitational lensing three-point, IGG contains one intrinsic alignment term, GII contains two and III is the three-point intrinsic alignment auto-correlation.

The most recent observations of three-point cosmic shear were presented in Fu et al. (2014). They inferred constraints on three-point intrinsic alignments by including it in their model and found a slight improvement in cosmological parameter measurements when intrinsic alignments were included. The amplitude of the three-point intrinsic alignment signal was tested using simulations in Semboloni et al. (2011), who found that third-order weak lensing statistics are typically more strongly contaminated by intrinsic alignments than second-order shear measurements, which leads to the possibility of using three-point statistics to measure the intrinsic alignment amplitude and constrain intrinsic alignment models. This knowledge of intrinsic alignments could then be used to improve the accuracy of two-point cosmic shear measurements. Shi et al. (2010) applied the nulling method to three-point statistics and showed that a factor of ten suppression can be achieved in the GGI/GGG ratio. Valageas (2014) found that source-lens clustering can affect both two- and three-point statistics, and that the intrinsic alignment bias is typically about 10% of the signal for both two-point and three-point statistics.

Higher than second-order statistics are essential to studies of non-Gaussianity in the weak lensing signal. One way to access the full information encoded in weak lensing is to produce reconstructed maps of convergence or mass (Kaiser & Squires 1993) from cosmic shear surveys. These maps can then be analysed statistically, for example the counting of peaks in the convergence distribution is a source of cosmological information (e.g. Bacon & Taylor 2003; Van Waerbeke et al. 2013). Pires et al. (2012) showed that these peak counts capture rich non-Gaussian information beyond the skewness and kurtosis of the distribution, while Dietrich & Hartlap (2010) showed significant statistical improvement when peak counts were combined with two-point statistics. Alternatively, topological features can be exploited by decomposing the map into Minkowksi functionals (Kratochvil et al. 2012; Petri et al. 2013; Shirasaki & Yoshida 2014). The impact of intrinsic alignments on mass reconstruction, peak counts and Minkowski functionals is a subject of current study. Simon et al. (2009) included intrinsic alignments in their mass reconstruction estimator, based on 3D cosmic shear, while a new peak counts model has been proposed by Lin & Kilbinger (2015) which can be adapted to include intrinsic alignments.

6.6. Probes of the unlensed galaxy shape

One potentially very useful avenue for the control of intrinsic alignments is the use of observables that can access information about the intrinsic (or "unlensed") galaxy shapes and/or orientations. Here we discuss two possible observables of this type: the polarised emission from background galaxies observed in the radio (Section 6.6.1) and estimates of the rotation velocity axis of disc galaxies (Section 6.6.2).

6.6.1. Radio polarisation as a tracer of intrinsic orientation

Several authors have demonstrated from a theoretical perspective that, for observations using radio telescopy, the local plane of polarisation is not altered by gravitational light deflection effects (Kronberg et al. 1991; Dyer & Shaver 1992; Faraoni 1993; Surpi & Harari 1999). This property was first exploited by Kronberg et al. (1991), who developed and applied a technique for measuring gravitational lensing using polarisation observations of the resolved radio jets of distant quasars.

Audit & Simmons (1999) demonstrated how the integrated polarisation emission from "normal" star-forming galaxies could in principle be included in weak lensing estimators of the parameters describing intervening lenses. The fundamental assumption underlying the technique is that the orientation of the integrated polarised emission from a background galaxy is a noisy tracer of the intrinsic structural position angle of the galaxy. Kronberg et al. (1991) and Audit & Simmons (1999) focused on the reduction in uncertainty on estimates of the lensing shear signal that is afforded by including the polarisation information.

It was further shown in Brown & Battye (2011) that the use of polarisation may potentially be a powerful tool to help separate intrinsic alignments from weak lensing distortions of galaxy shapes. The idea is that optical surveys provide a measure of the intrinsic ellipticity plus the shear from weak lensing, while the radio polarisation provides information about the unlensed galaxy orientation. In combination, these estimators effectively provide a measure of the difference between the intrinsic and observed orientations of individual galaxies. They are by construction insensitive to contamination by intrinsic alignments in the limit of a perfect relationship between the orientation of the polarised emission and the structural position angle. The weak lensing analysis could be conducted using radio images alone (Brown et al. 2015) but this type of measurement has been limited to date by the low source counts available (Chang et al. 2004).

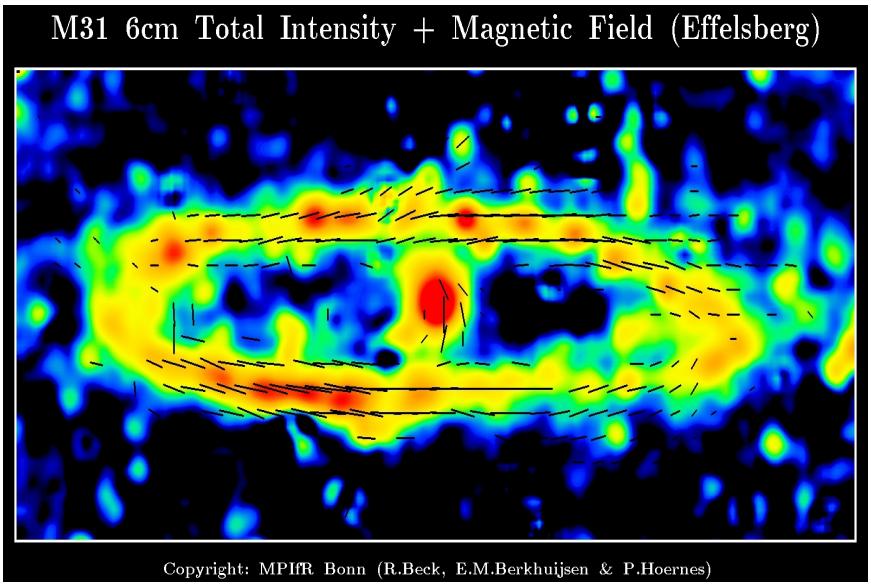


Fig. 15.— Total emission (colour scale) and polarised emission (black vectors) from M31 at λ =6.2 cm, smoothed to an angular resolution of 5 arcmin. Contour levels are 5, 10, 15, 20, 30, 40 and 60 mJy/beam area. *Reproduced with permission from* Berkhuijsen et al. (2003) © *ESO.*

Figure 15 shows an apparent alignment between polarisation pseudo-vectors and total intensity from radio wavelengths (Berkhuijsen et al. 2003) for the galaxy M31. Stil et al. (2009) further suggested alignment between the polarisation orientation and the emission at optical wavelengths. If this relationship was found to generally hold, one could potentially use the radio polarisation orientation as a proxy for the optical intrinsic position angle in order to mitigate intrinsic alignments in overlapping optical and radio surveys. However in order to fully exploit this potential, in addition to understanding the relationship between polarisation and structural position angles, one would also require a much deeper understanding of the correlation between the shapes of galaxies as measured in optical data and their shapes as measured from radio observations. At the current time, the situation with respect to this issue is not clear and more work is required in advance of results from the SKA, Euclid and LSST (Patel et al. 2010; Brown et al. 2015; Patel et al. 2015). One benefit of shape measurements from both radio and optical surveys is that shape measurement systematics are expected to be very different for each, so cross-correlation of measured shapes should

reduce the impact of these measurement systematics (Bacon et al. 2015). See Whittaker et al. (2015) for a recent overview of the potential uses of radio observations for intrinsic aligment purposes.

6.6.2. Rotational velocities as a tracer of intrinsic orientation

A second novel approach is to use rotational velocity measurements to provide information about the intrinsic shapes of galaxies. The idea, first suggested by Blain (2002) and Morales (2006), is to measure the axis of rotation of a disc galaxy and to compare this to the orientation of the major axis of the galaxy disc image. In the absence of lensing, these two orientations should be perpendicular, so measuring the departure from perpendicularity directly estimates the shear field at the galaxy's position. The basic technique is illustrated in Figure 16.

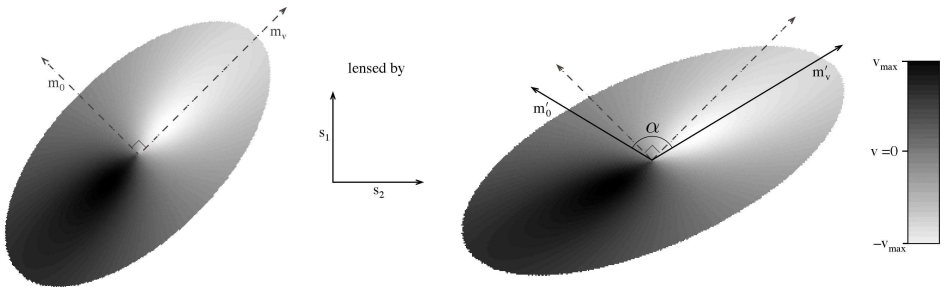


Fig. 16.— An illustration of the rotational velocity lensing technique. The grey scale indicates the observed radial velocity. A model galaxy in the absence of lensing is shown in the left-hand panel, where the zero velocity axis (m_0) and the axis defined by the maximum radial velocity (m_v) are perpendicular. The application of a shear (here applied along the s_1 and s_2 axes) breaks this perpendicularity. The observed angle α directly measures the shear component. © *AAS. Reproduced with permission from* Morales (2006).

We note that this technique can in principle be applied in both the radio and optical bands, making use of spectral line observations in the former and spectroscopic observations in the latter. It is worth pointing out that many future radio surveys plan to conduct HI line observations alongside continuum-mode observations (which can be done at no extra cost in terms of telescope time).

The rotation velocity technique shares many of the characteristics of the polarisation approach described above – in the limit of perfectly well-behaved, infinitely thin disc galaxies, it is also free of shape noise and it can also be used to remove the contaminating effect of intrinsic galaxy alignments. In practice, the degree to which the rotational velocity technique improves on standard methods will be dependent on observational parameters. First, one would need to account for the fact that the HI line emission of galaxies is much fainter than the broad-band continuum emission and so the number of galaxies will be reduced. Secondly, for a population of real disc galaxies, there will again be some scatter in the relationship between the rotation axis and the major axis of the galaxy disc. Recently Huff et al. (2013) proposed to extend this technique using the Tully-Fisher relation to calibrate the rotational velocity shear measurements and thus reduce the residual shape noise even further. This approach would require overlapping photometric and spectroscopic survey data.

7. Summary & Outlook

Historically, studies of galaxy shape alignments have focused on the role of the environment on the formation and evolution of galaxies. However, the diversity of results in the literature also highlight the difficulty of measuring the observational signatures. Closer examination shows that the findings are expected to depend on the methods used to quantify galaxy shapes. The importance of intrinsic alignments for the interpretation of weak lensing measurements has renewed interest in this field of research, with larger data sets expected to become available soon.

Shape estimation itself continues to be an area of active development because improvements on current shear measurement pipelines (e.g. Mandelbaum et al. 2015) are necessary to cope with the statistical accuracy of next-generation surveys. The determination of the intrinsic alignment signal depends critically on the adopted algorithm for shape measurement. Consequently, results from early measurements of galaxy shape alignment cannot be readily applied to current studies. On the other hand, it is also not clear that the algorithms used in lensing studies are optimal for the study of environment-dependent galaxy shape alignments. Regardless, a careful accounting for a range of observational biases is essential, and progress in either field will benefit from advances in the other. The last decade has also seen the development of a sophisticated set of statistics and estimators that allow for the measurement of ellipticity-density correlation on large scales and the development of a theory which matches the data at linear scales. Results have so far largely been limited to two-point statistics, but with the advent of larger data sets, which can probe smaller physical scales, we expect that the study of higher-order statistics will gain further interest.

The existence of intrinsic galaxy alignments is now well established, to a large extent thanks to modern wide area surveys, such as the SDSS, where we need to distinguish between galaxy type and the physical scales involved. For early-type galaxies significant detections have been reported: they show a clear intrinsic alignment signal, in good agreement with the linear alignment model at scales > 10 Mpc/h. At intermediate scales the non-linear alignment model, which uses the non-linear power spectrum to boost the amplitude of the predicted signal, provides a good fit to data. We stress, however, that there is currently no theoretical justification for this phenomenology and more work on these quasi-linear scales is required. At smaller scales, $< 2-6$ Mpc/h, these models fail to explain the strength of the observed correlation and attempts to model local alignments through, for example, the halo model are required. The halo model tends to match the observations well, though the number of free parameters provides a good deal of freedom in the fit. There is no significant evidence for redshift-dependence of the signal beyond that which is already included in the linear alignment model, but there exists strong evidence for a dependence of intrinsic alignment on luminosity, with the brightest galaxies exhibiting stronger alignments.

In contrast, for late-type galaxies the situation is less clear. Observational constraints are more limited because of the limited spectroscopic coverages for large samples, and no statistically significant evidence for shape alignment has been detected from such surveys. This null signal is consistent with the quadratic alignment model at linear scales, though a higher number density in observations would be desirable to reduce the statistical errors of current measurements. Some papers that studied the alignment of disc galaxy spin vectors, as an alternative to direct measurement of the ellipticity correlation of spirals, did see evidence, albeit at low significance, of correlation at small scales $\lesssim 1$ Mpc/h.

Hence, the picture at large scales, where correlations between large, diverse galaxy samples of galaxies are considered, is starting to become clear as powerful datasets become available. The results at scales where the morphology of the local large-scale structure becomes important are more ambiguous. This is not surprising as the intricacies of astrophysics, galaxy formation physics and galaxy evolution history are complicated and far from perfectly understood. The existing literature tends to classify the alignment of galaxy shapes on small scales by reference to the local morphology of the large-scale structure: galaxies located in voids, sheets, filaments or knots (groups and clusters) are expected to exhibit different shape alignment properties. In addition, the influence of galaxy type and history remains relevant at small scales.

These complications hamper a clear interpretation and comparison of the results. For instance the study of alignments for galaxies on the surfaces of voids has produced measurements that are consistent with no alignment, a significant alignment parallel to the void surface and the opposite, alignment perpendicular to the void surface. This highlights a need for more observations aimed at determining environment-dependent alignment. Even for well-defined structures such as groups and clusters of galaxies contradictory results have been reported, while we note that all the most recent studies in galaxy clusters find no evidence for shape alignments, neither from studies using spectroscopic redshifts (Sifón et al. 2015) nor those using photometric redshifts (Chisari et al. 2014). In such high-density environments the presence of nearby galaxies can affect shape measurements, especially those based on the shapes of isophotes, which may have biased earlier measurements.

A main driver of current research into galaxy alignments is the promise of cosmic shear as a powerful probe of cosmology. For this applications, the intrinsic alignments compromise a straightforward interpretation of the measure-

ments and thus represent a dominant astrophysical source of bias. If ignored, the biases in the resulting cosmological parameter estimates are much larger than the statistical uncertainties afforded by future wide-field cosmic shear surveys using photometric redshifts such as Euclid, LSST and WFIRST (Laureijs et al. 2011; LSST Science Collaboration et al. 2009; Spergel et al. 2015). Consequently, the desire to constrain the nature of dark energy will drive much development in this field in terms of observations and the development of shape measurement and analysis pipelines.

These data will not be optimal for the study of environment-dependent alignments because of the relatively crude redshift precision. To clear up the uncertainties about the relation of alignment to morphology, and hence learn about galaxy formation and evolution, we need surveys with (near-)spectroscopic redshifts that have high galaxy density down to relatively faint magnitudes. Such data will allow a good determination of the local morphology required for unambiguous measurements of shape alignments. Many of the future spectroscopic surveys plan to survey the brightest, easiest target galaxies, which may not provide the type of data we need for environment-dependent intrinsic alignment studies but there is some reason to expect progress in the right direction. For instance, the Dark Energy Spectroscopic Instrument (DESI) bright survey (Levi et al. 2013) or Subaru Prime Focus Spectrograph (PFS) (Takada et al. 2014) may extend the sample to fainter magnitudes and higher redshifts. Wide-area observations using a large number of narrow-band filters, such as PAUCam (Martí et al. 2014), provide another avenue. These yield photometric redshifts that are much more precise than those obtained using broad-band observations, and do so for a wide range of galaxy types.

Despite the expected progress in measuring alignments, the much smaller uncertainties from future surveys with larger area will require significantly improved strategies for mitigation if we are to produce unbiased measurements of cosmology. To this end, much effort is spent on exploring general approaches that seek to exploit the different redshift dependencies of the GG, II and GI contributions. The most promising alternative involves the use of a flexible model of the intrinsic alignment contribution that includes a number of variable "nuisance parameters" which can be explored in tandem with the cosmological parameter space under consideration. The nuisance parameters are then marginalised over. If the model is sufficiently flexible, then the resulting cosmological constraints will be unbiased, albeit with a loss in overall constraining power. It has been demonstrated that, even after marginalising aggressively over uncertainties in intrinsic alignments, useful cosmological information can be gained from a photometric cosmic shear survey (Joachimi & Bridle 2010). In this context, the goal of observational studies of intrinsic alignments, as they relate to cosmic shear systematics, can be thought of as applying more rigorous priors to the intrinsic alignment nuisance parameters. The large- and small-scale observations quoted in this review are an excellent start to this process, though it is worth noting that no paper seeking to marginalise over intrinsic alignments in the pursuit of cosmic shear has, thus far, explicitly employed priors derived from dedicated observations of intrinsic alignments.

For this reason it is also worthwhile to examine the value of complementary data to reduce or calibrate the intrinsic alignment signal. An interesting application in the near term is the cross-correlation between galaxy cosmic shear surveys and weak lensing of the CMB. Further ahead, the large density of sources at radio wavelengths that will arrive with the forthcoming SKA survey offers a number of exciting possibilities for the study of intrinsic alignments. In this case information from radio polarisation or rotational velocity measurements could allow the intrinsic alignment and weak lensing information to be separated cleanly. These constitute extremely powerful datasets, complementary to those from optical weak lensing surveys, and, if the many practical difficulties of radio weak lensing can be surmounted, they will provide important advances in our understanding of intrinsic alignments across all galaxy types, particularly much improved statistical uncertainties for late-type galaxies.

In the meantime a number of important open questions remain, including: are late-type galaxies really free of intrinsic alignment? How do intrinsic alignments evolve with redshift? Can we predict the alignments for a mix of morphological type? Addressing these questions requires additional measurements with larger number densities, covering higher redshifts. They should be a priority, as answering these questions also sheds light on the relative importance of the physical mechanisms that give rise to the alignments. The greater uncertainty at small scales is somewhat offset by the presence of competing systematics like non-linear clustering and the influence of baryon physics on the matter power spectrum. On the one hand, this means that the pressure to fully understand intrinsic alignments at these scales is reduced, as the other sources of uncertainty may make these scales less useful regardless of our intrinsic alignment knowledge. Nevertheless, future weak gravitational lensing surveys such as Euclid or LSST aim to exploit cosmic shear down to scales of 1.5 Mpc/h (Kitching et al. 2015b), so a dedicated programme of intrinsic

alignment measurements at small scales would be beneficial and may require auxiliary datasets in addition to those planned for standard cosmic shear analysis. For example, good spectroscopic redshifts for reasonably well-sampled galaxies representative of cosmic shear survey galaxies would be invaluable in making accurate measurements of the relevant intrinsic alignment contamination signal.

In this review we have provided an overview of the current status of observations of intrinsic alignments, perhaps with a bias towards the impact on cosmic shear. It is clear, however, that the data that are due to become available over the next decade offer exciting opportunities to test methods for intrinsic alignment measurement and mitigation much more rigorously. The larger number density will allow us to measure intrinsic alignments in large shear catalogues with more precision, particularly for late-type galaxies, while deeper surveys will push our baseline for intrinsic alignment measurements to higher redshift. Despite all the progress, the most unclear part of the current intrinsic alignment observational landscape is certainly still the dependence on environment of the alignments on quasi- and non-linear scales. Although planned surveys may help in this regard, dedicated efforts to resolve this situation will be needed.

Acknowledgements

We acknowledge the support of the International Space Science Institute Bern for two workshops at which this work was conceived. We thank S. Bridle and J. Blazek for stimulating discussions.

MLB is supported by the European Research Council (EC FP7 grant number 280127) and by a STFC Advanced/Halliday fellowship (grant number ST/I005129/1).

HH, MC and CS acknowledge support from the European Research Council under FP7 grant number 279396.

BJ acknowledges support by an STFC Ernest Rutherford Fellowship, grant reference ST/J004421/1.

TDK is supported by a Royal Society URF.

RM acknowledges the support of NASA ROSES 12-EUCLID12-0004.

MC was supported by the Netherlands organisation for Scientific Research (NWO) Vidi grant 639.042.814.

AC acknowledges support from the European Research Council under the EC FP7 grant number 240185.

AK was supported in part by JPL, run under a contract by Caltech for NASA. AK was also supported in part by NASA ROSES 13-ATP13-0019 and NASA ROSES 12-EUCLID12-0004.

AL acknowledges the support of the European Union Seventh Framework Programme (FP7/2007-2013) under grant agreement number 624151.

REFERENCES

Adami, C., Durret, F., Guennou, L., & Da Rocha, C. 2013, Diffuse light in the young cluster of galaxies CL J1449+0856 at z = 2.07, A&A, 551, A20 [10]

Agustsson, I., & Brainerd, T. G. 2006, The Orientation of Satellite Galaxies: Evidence of Elongation in the Direction of the Host, ApJ, 644, L25 [6, 10, 31]

Alam, S., Albareti, F. D., Allende Prieto, C., et al. 2015, The Eleventh and Twelfth Data Releases of the Sloan Digital Sky Survey: Final Data from SDSS-III, ArXiv e-prints, arXiv:1501.00963 [23]

Albrecht, A., Bernstein, G., Cahn, R., et al. 2006, Report of the Dark Energy Task Force, ArXiv Astrophysics e-prints, astro-ph/0609591 [41]

Alsing, J., Kirk, D., Heavens, A., & Jaffe, A. H. 2015, Weak lensing with sizes, magnitudes and shapes, MNRAS, 452, 1202 [46]

Amara, A., & Réfrégier, A. 2008, Systematic bias in cosmic shear: extending the Fisher matrix, MNRAS, 391, 228 [11, 42]

Andrae, R., & Jahnke, K. 2011, Only marginal alignment of disc galaxies, MNRAS, 418, 2014 [19]

Annis, J., Soares-Santos, M., Strauss, M. A., et al. 2014, The Sloan Digital Sky Survey Coadd: 275 deg^2 of Deep Sloan Digital Sky Survey Imaging on Stripe 82, ApJ, 794, 120 [27]

Antilogus, P., Astier, P., Doherty, P., Guyonnet, A., & Regnault, N. 2014, The brighter-fatter effect and pixel correlations in CCD sensors, Journal of Instrumentation, 9, C3048 [10]

Appenzeller, I. 2013, Introduction to Astronomical Spectroscopy [15]

Applegate, D. E., von der Linden, A., Kelly, P. L., et al. 2014, Weighing the Giants - III. Methods and measurements of accurate galaxy cluster weak-lensing masses, MNRAS, 439, 48 [11]

Audit, E., & Simmons, J. F. L. 1999, The use of light polarization in weak-lensing inversions, MNRAS, 303, 87 [47, 48]

Austin, T. B., & Peach, J. V. 1974, Studies of rich clusters of galaxies - II. The structure and luminosity function of the cluster A 1413., MNRAS, 168, 591 [30]

Azzaro, M., Patiri, S. G., Prada, F., & Zentner, A. R. 2007, Angular distribution of satellite galaxies from the Sloan Digital Sky Survey Data Release 4, MNRAS, 376, L43 [29, 30]

Bacon, D., Bridle, S., Abdalla, F. B., et al. 2015, Synergy between the Large Synoptic Survey Telescope and the Square Kilometre Array, Advancing Astrophysics with the Square Kilometre Array (AASKA14), 145 [49]

Bacon, D. J., Refregier, A. R., & Ellis, R. S. 2000, Detection of weak gravitational lensing by large-scale structure, MNRAS, 318, 625 [4, 38]

Bacon, D. J., & Taylor, A. N. 2003, Mapping the 3D dark matter potential with weak shear, MNRAS, 344, 1307 [47]

Bailin, J., Power, C., Norberg, P., Zaritsky, D., & Gibson, B. K. 2008, The anisotropic distribution of satellite galaxies, MNRAS, 390, 1133 [29]

Barnes, J. E., & Hernquist, L. 1992, Dynamics of interacting galaxies, ARA&A, 30, 705 [2]

Bartelmann, M. 2010, TOPICAL REVIEW Gravitational lensing, Classical and Quantum Gravity, 27, 233001 [4]

Bartelmann, M., & Schneider, P. 2001, Weak gravitational lensing, Phys. Rep., 340, 291 [4]

Berkhuijsen, E. M., Beck, R., & Hoernes, P. 2003, The polarized disk in M 31 at lambda 6 cm, A&A, 398, 937 [48]

Bernstein, G. M. 2009, Comprehensive Two-Point Analyses of Weak Gravitational Lensing Surveys, ApJ, 695, 652 [5, 44, 46]

Bernstein, G. M., & Jarvis, M. 2002, Shapes and Shears, Stars and Smears: Optimal Measurements for Weak Lensing, AJ, 123, 583 [9]

Binggeli, B. 1982, The shape and orientation of clusters of galaxies, A&A, 107, 338 [30, 35]

Blain, A. W. 2002, Detecting Gravitational Lensing Cosmic Shear from Samples of Several Galaxies Using Two-dimensional Spectral Imaging, ApJ, 570, L51 [49]

Blanton, M. R., Schlegel, D. J., Strauss, M. A., et al. 2005, New York University Value-Added Galaxy Catalog: A Galaxy Catalog Based on New Public Surveys, AJ, 129, 2562 [26]

Blazek, J., Mandelbaum, R., Seljak, U., & Nakajima, R. 2012, Separating intrinsic alignment and galaxy-galaxy lensing, J. Cosmology Astropart. Phys., 5, 41 [26, 27, 31, 45]

Blazek, J., McQuinn, M., & Seljak, U. 2011, Testing the tidal alignment model of galaxy intrinsic alignment, J. Cosmology Astropart. Phys., 5, 10 [25, 26]

Blazek, J., Vlah, Z., & Seljak, U. 2015, Tidal alignment of galaxies, J. Cosmology Astropart. Phys., 8, 015 [23]

Brainerd, T. G. 2005, Anisotropic Distribution of SDSS Satellite Galaxies: Planar (Not Polar) Alignment, ApJ, 628, L101 [29]

Bridle, S., & King, L. 2007, Dark energy constraints from cosmic shear power spectra: impact of intrinsic alignments on photometric redshift requirements, New Journal of Physics, 9, 444 [18, 20, 41, 42]

Bridle, S., Balan, S. T., Bethge, M., et al. 2010, Results of the GREAT08 Challenge: an image analysis competition for cosmological lensing, MNRAS, 405, 2044 [8, 9]

Brown, M., Bacon, D., Camera, S., et al. 2015, Weak gravitational lensing with the Square Kilometre Array, Advancing Astrophysics with the Square Kilometre Array (AASKA14), 23 [46, 48]

Brown, M. L., & Battye, R. A. 2011, Polarization as an indicator of intrinsic alignment in radio weak lensing, MNRAS, 410, 2057 [48]

Brown, M. L., Taylor, A. N., Hambly, N. C., & Dye, S. 2002, Measurement of intrinsic alignments in galaxy ellipticities, MNRAS, 333, 501 [18, 42]

Burke, C., Collins, C. A., Stott, J. P., & Hilton, M. 2012, Measurement of the intracluster light at z 1, MNRAS, 425, 2058 [10]

Carter, D., & Metcalfe, N. 1980, The morphology of clusters of galaxies, MNRAS, 191, 325 [30]

Catelan, P., Kamionkowski, M., & Blandford, R. D. 2001, Intrinsic and extrinsic galaxy alignment, MNRAS, 320, L7 [18, 38, 39]

Cervantes-Sodi, B., Hernandez, X., & Park, C. 2010, Clues on the origin of galactic angular momentum from looking at galaxy pairs, MNRAS, 402, 1807 [18, 19]

Chang, T.-C., Refregier, A., & Helfand, D. J. 2004, Weak Lensing by Large-Scale Structure with the FIRST Radio Survey, ApJ, 617, 794 [48]

Chisari, N. E., Mandelbaum, R., Strauss, M. A., Huff, E. M., & Bahcall, N. A. 2014, Intrinsic alignments of group and cluster galaxies in photometric surveys, MNRAS, 445, 726 [10, 27, 31, 45, 50]

Colina, L., & Wada, K. 2000, Nuclear Bar, Star Formation, and Gas Fueling in the Active Galaxy NGC 4303, ApJ, 529, 845 [8]

Colless, M., Dalton, G., Maddox, S., et al. 2001, The 2dF Galaxy Redshift Survey: spectra and redshifts, MNRAS, 328, 1039 [32]

Conn, A. R., Lewis, G. F., Ibata, R. A., et al. 2013, The Three-dimensional Structure of the M31 Satellite System; Strong Evidence for an Inhomogeneous Distribution of Satellites, ApJ, 766, 120 [29]

Crittenden, R. G., Natarajan, P., Pen, U.-L., & Theuns, T. 2001, Spin-induced Galaxy Alignments and Their Implications for Weak-Lensing Measurements, ApJ, 559, 552 [13]

—. 2002, Discriminating Weak Lensing from Intrinsic Spin Correlations Using the Curl-Gradient Decomposition, ApJ, 568, 20 [13]

Croft, R. A. C., & Metzler, C. A. 2000, Weak-Lensing Surveys and the Intrinsic Correlation of Galaxy Ellipticities, ApJ, 545, 561 [18, 38, 39]

Csabai, I., Budavári, T., Connolly, A. J., et al. 2003, The Application of Photometric Redshifts to the SDSS Early Data Release, AJ, 125, 580 [21]

Cuesta, A. J., Prada, F., Klypin, A., & Moles, M. 2008, The virialized mass of dark matter haloes, MNRAS, 389, 385 [33]

Dawson, K. S., Schlegel, D. J., Ahn, C. P., et al. 2013, The Baryon Oscillation Spectroscopic Survey of SDSS-III, AJ, 145, 10 [23]

Dawson, W. A., Schneider, M. D., Tyson, J. A., & Jee, M. J. 2014, The Ellipticity Distribution of Ambiguously Blended Objects, ArXiv e-prints, arXiv:1406.1506 [10]

Dietrich, J. P., & Hartlap, J. 2010, Cosmology with the shear-peak statistics, MNRAS, 402, 1049 [47]

Dong, F., Pierpaoli, E., Gunn, J. E., & Wechsler, R. H. 2008, Optical Cluster Finding with an Adaptive Matched-Filter Technique: Algorithm and Comparison with Simulations, ApJ, 676, 868 [36, 37]

Doroshkevich, A. G. 1970, The space structure of perturbations and the origin of rotation of galaxies in the theory of fluctuation., Astrofizika, 6, 581 [18]

Dossett, J. N., Ishak, M., Parkinson, D., & Davis, T. M. 2015, Constraints and tensions in testing general relativity from Planck and CFHTLenS data including intrinsic alignment systematics, Phys. Rev. D, 92, 023003 [28]

Dressler, A. 1978, A comprehensive study of 12 very rich clusters of galaxies. II - Dynamics, ApJ, 226, 55 [30]

—. 1980, Galaxy morphology in rich clusters - Implications for the formation and evolution of galaxies, ApJ, 236, 351 [2]

Drinkwater, M. J., Jurek, R. J., Blake, C., et al. 2010, The WiggleZ Dark Energy Survey: survey design and first data release, MNRAS, 401, 1429 [19]

Driver, S. P., GAMA Team, Baldry, I. K., et al. 2009, in IAU Symposium, Vol. 254, IAU Symposium, ed. J. Andersen, Nordströara, B. m, & J. Bland-Hawthorn, 469–474 [31]

Duncan, C. A. J., Joachimi, B., Heavens, A. F., Heymans, C., & Hildebrandt, H. 2014, On the complementarity of galaxy clustering with cosmic shear and flux magnification, MNRAS, 437, 2471 [44, 45]

Dyer, C. C., & Shaver, E. G. 1992, On the rotation of polarization by a gravitational lens, ApJ, 390, L5 [47]

Faltenbacher, A., Li, C., Mao, S., et al. 2007, Three Different Types of Galaxy Alignment within Dark Matter Halos, ApJ, 662, L71 [6, 10, 30, 31]

Faltenbacher, A., Li, C., White, S. D. M., et al. 2009, Alignment between galaxies and large-scale structure, Research in Astronomy and Astrophysics, 9, 41 [6, 26]

Faraoni, V. 1993, On the rotation of polarization by a gravitational lens, A&A, 272, 385 [47]

Fisher, R. A. 1935, The Logic of Inductive Inference, Journal of the Royal Statistical Society, 98, 39 [41]

Fu, L., Kilbinger, M., Erben, T., et al. 2014, CFHTLenS: cosmological constraints from a combination of cosmic shear two-point and three-point correlations, MNRAS, 441, 2725 [47]

Gonzalez, A. H., Zaritsky, D., & Zabludoff, A. I. 2007, A Census of Baryons in Galaxy Clusters and Groups, ApJ, 666, 147 [10]

Gruen, D., Bernstein, G. M., Jarvis, M., et al. 2015, Characterization and correction of charge-induced pixel shifts in DECam, Journal of Instrumentation, 10, C05032 [10]

Guennou, L., Adami, C., Da Rocha, C., et al. 2012, Intracluster light in clusters of galaxies at redshifts 0.4 z 0.8, A&A, 537, A64 [10]

Hahn, O., Carollo, C. M., Porciani, C., & Dekel, A. 2007, The evolution of dark matter halo properties in clusters, filaments, sheets and voids, MNRAS, 381, 41 [28]

Hall, A., & Taylor, A. 2014, Intrinsic alignments in the cross-correlation of cosmic shear and cosmic microwave background weak lensing, MNRAS, 443, L119 [46]

Hambly, N. C., MacGillivray, H. T., Read, M. A., et al. 2001, The SuperCOSMOS Sky Survey - I. Introduction and description, MNRAS, 326, 1279 [18]

Hand, N., Leauthaud, A., Das, S., et al. 2015, First measurement of the cross-correlation of CMB lensing and galaxy lensing, Phys. Rev. D, 91, 062001 [46]

Hao, J., Kubo, J. M., Feldmann, R., et al. 2011, Intrinsic Alignment of Cluster Galaxies: The Redshift Evolution, ApJ, 740, 39 [10, 26, 30, 31]

Hao, J., McKay, T. A., Koester, B. P., et al. 2010, A GMBCG Galaxy Cluster Catalog of 55,424 Rich Clusters from SDSS DR7, ApJS, 191, 254 [30]

Hashimoto, Y., Henry, J. P., & Boehringer, H. 2008, Alignment of galaxies and clusters, MNRAS, 390, 1562 [30]

Hawley, D. L., & Peebles, P. J. E. 1975, Distribution of observed orientations of galaxies, AJ, 80, 477 [29]

Haynes, M. P., & Giovanelli, R. 1984, Neutral hydrogen in isolated galaxies. IV - Results for the Arecibo sample, AJ, 89, 758 [8]

Heavens, A. 2003, 3D weak lensing, MNRAS, 343, 1327 [42]

Heavens, A., Alsing, J., & Jaffe, A. H. 2013, Combining size and shape in weak lensing, MNRAS, 433, L6 [46]

Heavens, A., Refregier, A., & Heymans, C. 2000, Intrinsic correlation of galaxy shapes: implications for weak lensing measurements, MNRAS, 319, 649 [18, 38, 39]

Heymans, C., & Heavens, A. 2003, Weak gravitational lensing: reducing the contamination by intrinsic alignments, MNRAS, 339, 711 [12, 42]

Heymans, C., Rowe, B., Hoekstra, H., et al. 2012a, The impact of high spatial frequency atmospheric distortions on weak-lensing measurements, MNRAS, 421, 381 [10]

Heymans, C., Van Waerbeke, L., Bacon, D., et al. 2006, The Shear Testing Programme - I. Weak lensing analysis of simulated ground-based observations, MNRAS, 368, 1323 [8, 9]

Heymans, C., Van Waerbeke, L., Miller, L., et al. 2012b, CFHTLenS: the Canada-France-Hawaii Telescope Lensing Survey, MNRAS, 427, 146 [8, 10]

Heymans, C., Grocutt, E., Heavens, A., et al. 2013, CFHTLenS tomographic weak lensing cosmological parameter constraints: Mitigating the impact of intrinsic galaxy alignments, MNRAS, 432, 2433 [5, 27, 28, 42, 44]

Hildebrandt, H., Erben, T., Kuijken, K., et al. 2012, CFHTLenS: improving the quality of photometric redshifts with precision photometry, MNRAS, 421, 2355 [15]

Hirata, C. M., Mandelbaum, R., Ishak, M., et al. 2007, Intrinsic galaxy alignments from the 2SLAQ and SDSS surveys: luminosity and redshift scalings and implications for weak lensing surveys, MNRAS, 381, 1197 [5, 17, 18, 19, 21, 23, 26]

Hirata, C. M., & Seljak, U. 2004, Intrinsic alignment-lensing interference as a contaminant of cosmic shear, Phys. Rev. D, 70, 063526 [5, 13, 15, 18, 20, 41]

Hoekstra, H. 2004, The effect of imperfect models of point spread function anisotropy on cosmic shear measurements, MNRAS, 347, 1337 [10]

Hoekstra, H., Bartelmann, M., Dahle, H., et al. 2013, Masses of Galaxy Clusters from Gravitational Lensing, Space Sci. Rev., 177, 75 [11]

Hoekstra, H., Herbonnet, R., Muzzin, A., et al. 2015, The Canadian Cluster Comparison Project: detailed study of systematics and updated weak lensing masses, MNRAS, 449, 685 [9, 10, 11]

Hoekstra, H., & Jain, B. 2008, Weak Gravitational Lensing and Its Cosmological Applications, Annual Review of Nuclear and Particle Science, 58, 99 [4]

Holmberg, E. 1969, A study of physical groups of galaxies, Arkiv for Astronomi, 5, 305 [29]

Hopkins, P. F., Bahcall, N. A., & Bode, P. 2005, Cluster Alignments and Ellipticities in ΛCDM Cosmology, ApJ, 618, 1 [37]

Hoshino, H., Leauthaud, A., Lackner, C., et al. 2015, Luminous red galaxies in clusters: central occupation, spatial distributions and miscentring, MNRAS, 452, 998 [30]

Hu, F. X., Wu, G. X., Song, G. X., Yuan, Q. R., & Okamura, S. 2006, Orientation of Galaxies in the Local Supercluster: A Review, Astrophysics and Space Science, 302, 43 [34]

Hubble, E. P. 1926, Extragalactic nebulae., ApJ, 64, 321 [2]

Huff, E. M., Hirata, C. M., Mandelbaum, R., et al. 2014, Seeing in the dark - I. Multi-epoch alchemy, MNRAS, 440, 1296 [27]

Huff, E. M., Krause, E., Eifler, T., George, M. R., & Schlegel, D. 2013, Cosmic shear without shape noise, ArXiv e-prints, arXiv:1311.1489 [49]

Hung, C.-L., & Ebeling, H. 2012, Galaxy alignments in very X-ray luminous clusters at z ¿ 0.5, MNRAS, 421, 3229 [10, 31]

Huterer, D., Takada, M., Bernstein, G., & Jain, B. 2006, Systematic errors in future weak-lensing surveys: requirements and prospects for self-calibration, MNRAS, 366, 101 [42]

Hutsemékers, D. 1998, Evidence for very large-scale coherent orientations of quasar polarization vectors, A&A, 332, 410 [29]

Hutsemékers, D., Braibant, L., Pelgrims, V., & Sluse, D. 2014, Alignment of quasar polarizations with large-scale structures, A&A, 572, A18 [29]

Hutsemékers, D., Cabanac, R., Lamy, H., & Sluse, D. 2005, Mapping extreme-scale alignments of quasar polarization vectors, A&A, 441, 915 [29]

Hutsemékers, D., & Lamy, H. 2001, Confirmation of the existence of coherent orientations of quasar polarization vectors on cosmological scales, A&A, 367, 381 [29]

Ibata, R. A., Lewis, G. F., Conn, A. R., et al. 2013, A vast, thin plane of corotating dwarf galaxies orbiting the Andromeda galaxy, Nature, 493, 62 [29]

Jain, B., Jarvis, M., & Bernstein, G. 2006, PSF anisotropy and systematic errors in weak lensing surveys, J. Cosmology Astropart. Phys., 2, 1 [10]

Joachimi, B., & Bridle, S. L. 2010, Simultaneous measurement of cosmology and intrinsic alignments using joint cosmic shear and galaxy number density correlations, A&A, 523, A1 [5, 11, 39, 44, 46, 51]

Joachimi, B., Mandelbaum, R., Abdalla, F. B., & Bridle, S. L. 2011, Constraints on intrinsic alignment contamination of weak lensing surveys using the MegaZ-LRG sample, A&A, 527, A26 [5, 15, 16, 17, 21, 22, 23, 24, 26, 27, 42]

Joachimi, B., & Schneider, P. 2008, The removal of shear-ellipticity correlations from the cosmic shear signal via nulling techniques, A&A, 488, 829 [43]

—. 2009, The removal of shear-ellipticity correlations from the cosmic shear signal. Influence of photometric redshift errors on the nulling technique, A&A, 507, 105 [43]

—. 2010, Intrinsic alignment boosting. Direct measurement of intrinsic alignments in cosmic shear data, A&A, 517, A4 [43]

Joachimi, B., Cacciato, M., Kitching, T. D., et al. 2015, Galaxy Alignments: An Overview, Space Sci. Rev., 193, 1 [2, 4, 5, 6, 17, 28, 29, 31]

Jones, B. J. T., van de Weygaert, R., & Aragón-Calvo, M. A. 2010, Fossil evidence for spin alignment of Sloan Digital Sky Survey galaxies in filaments, MNRAS, 408, 897 [34]

Kacprzak, T., Zuntz, J., Rowe, B., et al. 2012, Measurement and calibration of noise bias in weak lensing galaxy shape estimation, MNRAS, 427, 2711 [8]

Kaiser, N., & Squires, G. 1993, Mapping the dark matter with weak gravitational lensing, ApJ, 404, 441 [47]

Kaiser, N., Squires, G., & Broadhurst, T. 1995, A Method for Weak Lensing Observations, ApJ, 449, 460 [9, 30, 31]

Kaiser, N., Wilson, G., & Luppino, G. A. 2000, Large-Scale Cosmic Shear Measurements, ArXiv Astrophysics e-prints, astro-ph/0003338 [4, 38]

Kamionkowski, M., Babul, A., Cress, C. M., & Refregier, A. 1998, Theory and statistics of weak lensing from large-scale mass inhomogeneities, MNRAS, 301, 1064 [38]

Kashikawa, N., & Okamura, S. 1992, Spatial orientation of spin vectors of galaxies in the Local Supercluster, PASJ, 44, 493 [8]

Kauffmann, G., Heckman, T. M., White, S. D. M., et al. 2003, The dependence of star formation history and internal structure on stellar mass for 10^5 low-redshift galaxies, MNRAS, 341, 54 [20]

Kiessling, A., Cacciato, M., Joachimi, B., et al. 2015, Galaxy Alignments: Theory, Modelling and Simulations, Space Sci. Rev., 193, 67 [5, 6, 7, 15, 17, 18, 20, 21, 24, 26, 27, 29, 34, 38, 39]

King, L., & Schneider, P. 2002, Suppressing the contribution of intrinsic galaxy alignments to the shear two-point correlation function, A&A, 396, 411 [42, 43]

King, L. J. 2005, Cosmic shear as a tool for precision cosmology: minimising intrinsic galaxy alignment-lensing interference, A&A, 441, 47 [43]

King, L. J., & Schneider, P. 2003, Separating cosmic shear from intrinsic galaxy alignments: Correlation function tomography, A&A, 398, 23 [43]

Kirk, D., Abdalla, F. B., Benoit-Lévy, A., Bull, P., & Joachimi, B. 2015, Cross correlation surveys with the Square Kilometre Array, Advancing Astrophysics with the Square Kilometre Array (AASKA14), 20 [46]

Kirk, D., Laszlo, I., Bridle, S., & Bean, R. 2013, Optimizing cosmic shear surveys to measure modifications to gravity on cosmic scales, MNRAS, 430, 197 [5, 46]

Kirk, D., Rassat, A., Host, O., & Bridle, S. 2012, The cosmological impact of intrinsic alignment model choice for cosmic shear, MNRAS, 424, 1647 [5, 39, 40]

Kitching, T., Bacon, D., Brown, M., et al. 2015a, Euclid & SKA Synergies, Advancing Astrophysics with the Square Kilometre Array (AASKA14), 146 [46]

Kitching, T. D., Heavens, A. F., & Das, S. 2015b, 3D weak gravitational lensing of the CMB and galaxies, MNRAS, 449, 2205 [42, 51]

Kitching, T. D., Taylor, A. N., & Heavens, A. F. 2008, Systematic effects on dark energy from 3D weak shear, MNRAS, 389, 173 [42]

Kitching, T. D., Balan, S. T., Bridle, S., et al. 2012, Image analysis for cosmology: results from the GREAT10 Galaxy Challenge, MNRAS, 423, 3163 [8, 9]

Kitching, T. D., Heavens, A. F., Alsing, J., et al. 2014, 3D cosmic shear: cosmology from CFHTLenS, MNRAS, 442, 1326 [42]

Koch, A., & Grebel, E. K. 2006, The Anisotropic Distribution of M31 Satellite Galaxies: A Polar Great Plane of Early-type Companions, AJ, 131, 1405 [29]

Koester, B. P., McKay, T. A., Annis, J., et al. 2007, A MaxBCG Catalog of 13,823 Galaxy Clusters from the Sloan Digital Sky Survey, ApJ, 660, 239 [30, 36, 37]

Kratochvil, J. M., Lim, E. A., Wang, S., et al. 2012, Probing cosmology with weak lensing Minkowski functionals, Phys. Rev. D, 85, 103513 [47]

Kronberg, P. P., Dyer, C. C., Burbidge, E. M., & Junkkarinen, V. T. 1991, A technique for using radio jets as extended gravitational lensing probes, ApJ, 367, L1 [47, 48]

Kroupa, P., Theis, C., & Boily, C. M. 2005, The great disk of Milky-Way satellites and cosmological sub-structures, A&A, 431, 517 [29]

Kunkel, W. E., & Demers, S. 1976, in Royal Greenwich Observatory Bulletins, Vol. 182, The Galaxy and the Local Group, ed. R. J. Dickens, J. E. Perry, F. G. Smith, & I. R. King, 241 [29]

Landy, S. D., & Szalay, A. S. 1993, Bias and variance of angular correlation functions, ApJ, 412, 64 [13]

Laszlo, I., Bean, R., Kirk, D., & Bridle, S. 2012, Disentangling dark energy and cosmic tests of gravity from weak lensing systematics, MNRAS, 423, 1750 [5, 11, 46]

Laureijs, R., Amiaux, J., Arduini, S., et al. 2011, Euclid Definition Study Report, ArXiv e-prints, arXiv:1110.3193 [31, 41, 51]

Lee, J. 2004, The Intrinsic Inclination of Galaxies Embedded in Cosmic Sheets and Its Cosmological Implications: An Analytic Calculation, ApJ, 614, L1 [32]

—. 2011, On the Intrinsic Alignments of the Late-type Spiral Galaxies from the Sloan Digital Sky Survey Data Release 7, ApJ, 732, 99 [7, 19]

Lee, J., & Erdogdu, P. 2007, The Alignments of the Galaxy Spins with the Real-Space Tidal Field Reconstructed from the 2MASS Redshift Survey, ApJ, 671, 1248 [8, 19, 34]

Lee, J., & Pen, U.-L. 2000, Cosmic Shear from Galaxy Spins, ApJ, 532, L5 [7, 32]

—. 2001, Galaxy Spin Statistics and Spin-Density Correlation, ApJ, 555, 106 [34]

—. 2002, Detection of Galaxy Spin Alignments in the Point Source Catalog Redshift Survey Shear Field, ApJ, 567, L111 [34]

Levi, M., Bebek, C., Beers, T., et al. 2013, The DESI Experiment, a whitepaper for Snowmass 2013, ArXiv e-prints, arXiv:1308.0847 [51]

Li, C., Jing, Y. P., Faltenbacher, A., & Wang, J. 2013a, The Detection of the Large-scale Alignment of Massive Galaxies at z ˜ 0.6, ApJ, 770, L12 [6]

Li, Z., Wang, Y., Yang, X., et al. 2013b, Brightest Satellite Galaxy Alignment of Sloan Digital Sky Survey Galaxy Groups, ApJ, 768, 20 [30, 31]

Lin, C.-A., & Kilbinger, M. 2015, A new model to predict weak-lensing peak counts. I. Comparison with N-body simulations, A&A, 576, A24 [47]

LSST Science Collaboration, Abell, P. A., Allison, J., et al. 2009, LSST Science Book, Version 2.0, ArXiv e-prints, arXiv:0912.0201 [31, 51]

Lynden-Bell, D. 1976, Dwarf galaxies and globular clusters in high velocity hydrogen streams, MNRAS, 174, 695 [29]

Mandelbaum, R., Hirata, C. M., Ishak, M., Seljak, U., & Brinkmann, J. 2006a, Detection of large-scale intrinsic ellipticity-density correlation from the Sloan Digital Sky Survey and implications for weak lensing surveys, MNRAS, 367, 611 [5, 20]

Mandelbaum, R., Seljak, U., Kauffmann, G., Hirata, C. M., & Brinkmann, J. 2006b, Galaxy halo masses and satellite fractions from galaxy-galaxy lensing in the Sloan Digital Sky Survey: stellar mass, luminosity, morphology and environment dependencies, MNRAS, 368, 715 [45]

Mandelbaum, R., Blake, C., Bridle, S., et al. 2011, The WiggleZ Dark Energy Survey: direct constraints on blue galaxy intrinsic alignments at intermediate redshifts, MNRAS, 410, 844 [13, 14, 15, 17, 18, 19, 20, 21, 27]

Mandelbaum, R., Rowe, B., Armstrong, R., et al. 2015, GREAT3 results - I. Systematic errors in shear estimation and the impact of real galaxy morphology, MNRAS, 450, 2963 [8, 9, 50]

Martí, P., Miquel, R., Castander, F. J., et al. 2014, Precise photometric redshifts with a narrow-band filter set: the PAU survey at the William Herschel Telescope, MNRAS, 442, 92 [21, 51]

Massey, R., Heymans, C., Bergé, J., et al. 2007, The Shear Testing Programme 2: Factors affecting high-precision weak-lensing analyses, MNRAS, 376, 13 [8]

Massey, R., Hoekstra, H., Kitching, T., et al. 2013, Origins of weak lensing systematics, and requirements on future instrumentation (or knowledge of instrumentation), MNRAS, 429, 661 [9, 10]

Massey, R., Schrabback, T., Cordes, O., et al. 2014, An improved model of charge transfer inefficiency and correction algorithm for the Hubble Space Telescope, MNRAS, 439, 887 [10]

Melchior, P., Böhnert, A., Lombardi, M., & Bartelmann, M. 2010, Limitations on shapelet-based weak-lensing measurements, A&A, 510, A75 [8]

Melchior, P., & Viola, M. 2012, Means of confusion: how pixel noise affects shear estimates for weak gravitational lensing, MNRAS, 424, 2757 [8]

Merkel, P. M., & Schäfer, B. M. 2013, Intrinsic alignments and 3d weak gravitational lensing, MNRAS, 434, 1808 [42]

Miller, L., Heymans, C., Kitching, T. D., et al. 2013, Bayesian galaxy shape measurement for weak lensing surveys - III. Application to the Canada-France-Hawaii Telescope Lensing Survey, MNRAS, 429, 2858 [8, 9]

Morales, M. F. 2006, A Technique for Weak Lensing with Velocity Maps: Eliminating Ellipticity Noise in H I Radio Observations, ApJ, 650, L21 [49]

Munshi, D., Valageas, P., van Waerbeke, L., & Heavens, A. 2008, Cosmology with weak lensing surveys, Phys. Rep., 462, 67 [4]

Niederste-Ostholt, M., Strauss, M. A., Dong, F., Koester, B. P., & McKay, T. A. 2010, Alignment of brightest cluster galaxies with their host clusters, MNRAS, 405, 2023 [7, 30]

Nierenberg, A. M., Auger, M. W., Treu, T., Marshall, P. J., & Fassnacht, C. D. 2011, Luminous Satellites of Early-type Galaxies. I. Spatial Distribution, ApJ, 731, 44 [29]

Nilson, P. 1973, Uppsala general catalogue of galaxies [34]

Obreschkow, D., & Glazebrook, K. 2014, Fundamental Mass-Spin-Morphology Relation Of Spiral Galaxies, ApJ, 784, 26 [8]

Obreschkow, D., Meyer, M., Popping, A., et al. 2015, The SKA as a Doorway to Angular Momentum, Advancing Astrophysics with the Square Kilometre Array (AASKA14), 138 [8]

Okabe, N., Takada, M., Umetsu, K., Futamase, T., & Smith, G. P. 2010, LoCuSS: Subaru Weak Lensing Study of 30 Galaxy Clusters, PASJ, 62, 811 [11]

Okumura, T., Jing, Y. P., & Li, C. 2009, Intrinsic Ellipticity Correlation of SDSS Luminous Red Galaxies and Misalignment with Their Host Dark Matter Halos, ApJ, 694, 214 [5, 6, 25, 26]

Patel, P., Bacon, D. J., Beswick, R. J., Muxlow, T. W. B., & Hoyle, B. 2010, Radio weak gravitational lensing with VLA and MERLIN, MNRAS, 401, 2572 [46, 48]

Patel, P., Harrison, I., Makhathini, S., et al. 2015, Weak Lensing Simulations for the SKA, Advancing Astrophysics with the Square Kilometre Array (AASKA14), 30 [46, 48]

Patiri, S. G., Betancort-Rijo, J. E., Prada, F., Klypin, A., & Gottlöber, S. 2006, Statistics of voids in the two-degree Field Galaxy Redshift Survey, MNRAS, 369, 335 [32]

Pawlowski, M. S., & Kroupa, P. 2013, The rotationally stabilized VPOS and predicted proper motions of the Milky Way satellite galaxies, MNRAS, 435, 2116 [29]

Pawlowski, M. S., Kroupa, P., & Jerjen, H. 2013, Dwarf galaxy planes: the discovery of symmetric structures in the Local Group, MNRAS, 435, 1928 [29]

Paz, D. J., Sgró, M. A., Merchán, M., & Padilla, N. 2011, Alignments of galaxy group shapes with large-scale structure, MNRAS, 414, 2029 [36]

Peebles, P. J. E. 1969, Origin of the Angular Momentum of Galaxies, ApJ, 155, 393 [18, 19]

Pelgrims, V., & Hutsemékers, D. 2015, Polarization alignments of quasars from the JVAS/CLASS 8.4-GHz surveys, MNRAS, 450, 4161 [29]

Peng, C. Y., Ho, L. C., Impey, C. D., & Rix, H.-W. 2002, Detailed Structural Decomposition of Galaxy Images, AJ, 124, 266 [30, 31]

Pereira, M. J., & Kuhn, J. R. 2005, Radial Alignment of Cluster Galaxies, ApJ, 627, L21 [6, 10, 31]

Petri, A., Haiman, Z., Hui, L., May, M., & Kratochvil, J. M. 2013, Cosmology with Minkowski functionals and moments of the weak lensing convergence field, Phys. Rev. D, 88, 123002 [47]

Pires, S., Leonard, A., & Starck, J.-L. 2012, Cosmological constraints from the capture of non-Gaussianity in weak lensing data, MNRAS, 423, 983 [47]

Plionis, M. 1994, Position angles and alignments of clusters of galaxies, ApJS, 95, 401 [35]

Presotto, V., Girardi, M., Nonino, M., et al. 2014, Intracluster light properties in the CLASH-VLT cluster MACS J1206.2-0847, A&A, 565, A126 [10]

Refregier, A., Amara, A., Kitching, T. D., et al. 2010, Euclid Imaging Consortium Science Book, ArXiv e-prints, arXiv:1001.0061 [40, 41]

Refregier, A., Kacprzak, T., Amara, A., Bridle, S., & Rowe, B. 2012, Noise bias in weak lensing shape measurements, MNRAS, 425, 1951 [8]

Reynolds, J. H. 1920, Nebulæ, The galactic distribution of the large spiral, MNRAS, 81, 129 [34]

Rhodes, J., Leauthaud, A., Stoughton, C., et al. 2010, The Effects of Charge Transfer Inefficiency (CTI) on Galaxy Shape Measurements, PASP, 122, 439 [10]

Riess, A. G., Macri, L., Casertano, S., et al. 2011, A 3% Solution: Determination of the Hubble Constant with the Hubble Space Telescope and Wide Field Camera 3, ApJ, 730, 119 [28]

Rood, H. J., & Sastry, G. N. 1972, Static properties of galaxies in the cluster Abell 2199., AJ, 77, 451 [30]

Rykoff, E. S., Rozo, E., Busha, M. T., et al. 2014, redMaPPer. I. Algorithm and SDSS DR8 Catalog, ApJ, 785, 104 [30]

Sales, L., & Lambas, D. G. 2009, Erratum: Anisotropy in the distribution of satellites around primary galaxies in the 2dF Galaxy Redshift Survey: the Holmberg effect, MNRAS, 395, 1184 [29]

Sastry, G. N. 1968, Clusters Associated with Supergiant Galaxies, PASP, 80, 252 [30]

Schäfer, B. M. 2009, Galactic Angular Momenta and Angular Momentum Correlations in the Cosmological Large-Scale Structure, International Journal of Modern Physics D, 18, 173 [6]

Schneider, M. D. 2014, Probing Dark Energy with Lensing Magnification in Photometric Surveys, Physical Review Letters, 112, 061301 [43]

Schneider, M. D., & Bridle, S. 2010, A halo model for intrinsic alignments of galaxy ellipticities, MNRAS, 402, 2127 [23, 44]

Schneider, M. D., Cole, S., Frenk, C. S., et al. 2013, Galaxy And Mass Assembly (GAMA): galaxy radial alignments in GAMA groups, MNRAS, 433, 2727 [10, 31]

Schneider, P., & Seitz, C. 1995, Steps towards nonlinear cluster inversion through gravitational distortions. 1: Basic considerations and circular clusters, A&A, 294, 411 [4]

Schneider, P., van Waerbeke, L., Kilbinger, M., & Mellier, Y. 2002a, Analysis of two-point statistics of cosmic shear. I. Estimators and covariances, A&A, 396, 1 [12]

Schneider, P., van Waerbeke, L., & Mellier, Y. 2002b, B-modes in cosmic shear from source redshift clustering, A&A, 389, 729 [13]

Schweizer, F. 1986, Colliding and merging galaxies, Science, 231, 227 [2]

Scoville, N., Aussel, H., Brusa, M., et al. 2007, The Cosmic Evolution Survey (COSMOS): Overview, ApJS, 172, 1 [3]

Semboloni, E., Hoekstra, H., Schaye, J., van Daalen, M. P., & McCarthy, I. G. 2011, Quantifying the effect of baryon physics on weak lensing tomography, MNRAS, 417, 2020 [18, 47]

Sersic, J. L. 1968, Atlas de galaxias australes [3]

Sharp, N. A., Lin, D. N. C., & White, S. D. M. 1979, A test of the tidal hypothesis for the origin of galactic angular momentum, MNRAS, 187, 287 [29]

Sheth, R. K., & van de Weygaert, R. 2004, A hierarchy of voids: much ado about nothing, MNRAS, 350, 517 [32]

Shi, X., Joachimi, B., & Schneider, P. 2010, Controlling intrinsic-shear alignment in three-point weak lensing statistics, A&A, 523, A60 [47]

Shirasaki, M., & Yoshida, N. 2014, Statistical and Systematic Errors in the Measurement of Weak-Lensing Minkowski Functionals: Application to the Canada-France-Hawaii Lensing Survey, ApJ, 786, 43 [47]

Sifón, C., Hoekstra, H., Cacciato, M., et al. 2015, Constraints on the alignment of galaxies in galaxy clusters from ˜14 000 spectroscopic members, A&A, 575, A48 [10, 17, 30, 31, 44, 50]

Simon, P., Taylor, A. N., & Hartlap, J. 2009, Unfolding the matter distribution using three-dimensional weak gravitational lensing, MNRAS, 399, 48 [47]

Singh, S., Mandelbaum, R., & More, S. 2015, Intrinsic alignments of SDSS-III BOSS LOWZ sample galaxies, MNRAS, 450, 2195 [5, 17, 23, 24, 25, 26, 30, 31]

Siverd, R. J., Ryden, B. S., & Gaudi, B. S. 2009, Galaxy Orientation and Alignment Effects in the SDSS DR6, ArXiv e-prints, arXiv:0903.2264 [30]

Skibba, R. A., Coil, A. L., Mendez, A. J., et al. 2015, Dark Matter Halo Models of Stellar Mass-dependent Galaxy Clustering in PRIMUS+DEEP2 at 0.2>z>1.2, ApJ, 807, 152 [30]

Skrutskie, M. F., Cutri, R. M., Stiening, R., et al. 2006, The Two Micron All Sky Survey (2MASS), AJ, 131, 1163 [34]

Slosar, A., & White, M. 2009, Alignment of galaxy spins in the vicinity of voids, J. Cosmology Astropart. Phys., 6, 9 [8, 32, 33]

Slosar, A., Land, K., Bamford, S., et al. 2009, Galaxy Zoo: chiral correlation function of galaxy spins, MNRAS, 392, 1225 [18, 19]

Smargon, A., Mandelbaum, R., Bahcall, N., & Niederste-Ostholt, M. 2012, Detection of intrinsic cluster alignments to 100 h^{-1} Mpc in the Sloan Digital Sky Survey, MNRAS, 423, 856 [7, 36, 37]

Smith, J. E., Robinson, A., Alexander, D. M., et al. 2004, Seyferts on the edge: polar scattering and orientation-dependent polarization in Seyfert 1 nuclei, MNRAS, 350, 140 [29]

Spergel, D., Gehrels, N., Baltay, C., et al. 2015, Wide-Field InfrarRed Survey Telescope-Astrophysics Focused Telescope Assets WFIRST-AFTA 2015 Report, ArXiv e-prints, arXiv:1503.03757 [51]

Springel, V., White, S. D. M., Jenkins, A., et al. 2005, Simulations of the formation, evolution and clustering of galaxies and quasars, Nature, 435, 629 [29]

Stil, J. M., Krause, M., Beck, R., & Taylor, A. R. 2009, The Integrated Polarization of Spiral Galaxy Disks, ApJ, 693, 1392 [48]

Struble, M. F. 1987, Alignment statistics of clusters with their brightest members at bright and faint isophotes, ApJ, 317, 668 [30]

—. 1988, Position-angle statistics of the brightest binary galaxies in Abell clusters, AJ, 96, 1534 [30]

Surpi, G. C., & Harari, D. D. 1999, Weak Lensing by Large-Scale Structure and the Polarization Properties of Distant Radio Sources, ApJ, 515, 455 [47]

Takada, M., & Jain, B. 2004, Cosmological parameters from lensing power spectrum and bispectrum tomography, MNRAS, 348, 897 [4, 42]

Takada, M., & White, M. 2004, Tomography of Lensing Cross-Power Spectra, ApJ, 601, L1 [43]

Takada, M., Ellis, R. S., Chiba, M., et al. 2014, Extragalactic science, cosmology, and Galactic archaeology with the Subaru Prime Focus Spectrograph, PASJ, 66, 1 [51]

Tempel, E., & Libeskind, N. I. 2013, Galaxy Spin Alignment in Filaments and Sheets: Observational Evidence, ApJ, 775, L42 [34]

Tempel, E., Stoica, R. S., & Saar, E. 2013, Evidence for spin alignment of spiral and elliptical/S0 galaxies in filaments, MNRAS, 428, 1827 [34]

Toomre, A., & Toomre, J. 1972, Galactic Bridges and Tails, ApJ, 178, 623 [2]

Trowland, H. E., Lewis, G. F., & Bland-Hawthorn, J. 2013, The Cosmic History of the Spin of Dark Matter Halos within the Large-scale Structure, ApJ, 762, 72 [34]

Troxel, M. A., & Ishak, M. 2012a, Self-calibration for three-point intrinsic alignment autocorrelations in weak lensing surveys, MNRAS, 423, 1663 [46, 47]

—. 2012b, Self-calibration technique for three-point intrinsic alignment correlations in weak lensing surveys, MNRAS, 419, 1804 [46, 47]

—. 2014, Cross-correlation between cosmic microwave background lensing and galaxy intrinsic alignment as a contaminant to gravitational lensing cross-correlated probes of the Universe, Phys. Rev. D, 89, 063528 [46]

—. 2015, The intrinsic alignment of galaxies and its impact on weak gravitational lensing in an era of precision cosmology, Phys. Rep., 558, 1 [6]

Trujillo, I., Carretero, C., & Patiri, S. G. 2006, Detection of the Effect of Cosmological Large-Scale Structure on the Orientation of Galaxies, ApJ, 640, L111 [8, 32, 33]

Vafaei, S., Lu, T., van Waerbeke, L., et al. 2010, Breaking the degeneracy: Optimal use of three-point weak lensing statistics, Astroparticle Physics, 32, 340 [47]

Valageas, P. 2014, Source-lens clustering and intrinsic-alignment bias of weak-lensing estimators, A&A, 561, A53 [47]

van den Bosch, F. C., Abel, T., & Hernquist, L. 2003, The angular momentum of gas in protogalaxies - II. The impact of pre-heating, MNRAS, 346, 177 [7]

van Uitert, E., Hoekstra, H., Velander, M., et al. 2011, Galaxy-galaxy lensing constraints on the relation between baryons and dark matter in galaxies in the Red Sequence Cluster Survey 2, A&A, 534, A14 [45]

Van Waerbeke, L., Mellier, Y., Erben, T., et al. 2000, Detection of correlated galaxy ellipticities from CFHT data: first evidence for gravitational lensing by large-scale structures, A&A, 358, 30 [4, 38]

Van Waerbeke, L., Benjamin, J., Erben, T., et al. 2013, CFHTLenS: mapping the large-scale structure with gravitational lensing, MNRAS, 433, 3373 [47]

Varela, J., Betancort-Rijo, J., Trujillo, I., & Ricciardelli, E. 2012, The Orientation of Disk Galaxies around Large Cosmic Voids, ApJ, 744, 82 [8, 32, 33, 35]

Velander, M., van Uitert, E., Hoekstra, H., et al. 2014, CFHTLenS: the relation between galaxy dark matter haloes and baryons from weak gravitational lensing, MNRAS, 437, 2111 [45]

Viola, M., Kitching, T. D., & Joachimi, B. 2014, On the probability distributions of ellipticity, MNRAS, 439, 1909 [9]

Voigt, L. M., & Bridle, S. L. 2010, Limitations of model-fitting methods for lensing shear estimation, MNRAS, 404, 458 [8]

Wang, H., Mo, H. J., Jing, Y. P., Yang, X., & Wang, Y. 2011, Internal properties and environments of dark matter haloes, MNRAS, 413, 1973 [35]

Wang, H., Mo, H. J., Yang, X., & van den Bosch, F. C. 2012, Reconstructing the cosmic velocity and tidal fields with galaxy groups selected from the Sloan Digital Sky Survey, MNRAS, 420, 1809 [35]

Wang, Y., Park, C., Hwang, H. S., & Chen, X. 2010, Distribution of Satellite Galaxies in High-redshift Groups, ApJ, 718, 762 [30]

Wang, Y., Park, C., Yang, X., Choi, Y.-Y., & Chen, X. 2009, Alignments of Group Galaxies with Neighboring Groups, ApJ, 703, 951 [35]

Wang, Y., Yang, X., Mo, H. J., et al. 2008, Probing the intrinsic shape and alignment of dark matter haloes using SDSS galaxy groups, MNRAS, 385, 1511 [30]

Wen, Z. L., Han, J. L., & Liu, F. S. 2012, A Catalog of 132,684 Clusters of Galaxies Identified from Sloan Digital Sky Survey III, ApJS, 199, 34 [30]

West, M. J. 1989, Groups of galaxies and large-scale structure, ApJ, 344, 535 [35, 36]

White, S. D. M. 1984, Angular momentum growth in protogalaxies, ApJ, 286, 38 [18]

Whittaker, L., Brown, M. L., & Battye, R. A. 2015, Separating weak lensing and intrinsic alignments using radio observations, MNRAS, 451, 383 [49]

Wittman, D. M., Tyson, J. A., Kirkman, D., Dell'Antonio, I., & Bernstein, G. 2000, Detection of weak gravitational lensing distortions of distant galaxies by cosmic dark matter at large scales, Nature, 405, 143 [4, 38]

Wyder, T. K., Martin, D. C., Schiminovich, D., et al. 2007, The UV-Optical Galaxy Color-Magnitude Diagram. I. Basic Properties, ApJS, 173, 293 [20]

Yang, X., Mo, H. J., van den Bosch, F. C., et al. 2007, Galaxy Groups in the SDSS DR4. I. The Catalog and Basic Properties, ApJ, 671, 153 [35]

—. 2005, The cross-correlation between galaxies and groups: probing the galaxy distribution in and around dark matter haloes, MNRAS, 362, 711 [35]

Yang, X., van den Bosch, F. C., Mo, H. J., et al. 2006, The alignment between the distribution of satellites and the orientation of their central galaxy, MNRAS, 369, 1293 [10, 30, 31]

Zaritsky, D., Smith, R., Frenk, C. S., & White, S. D. M. 1997, Anisotropies in the Distribution of Satellite Galaxies, ApJ, 478, L53 [29]

Zhang, P. 2010, Self-calibration of Gravitational Shear-Galaxy Intrinsic Ellipticity Correlation in Weak Lensing Surveys, ApJ, 720, 1090 [46]

Zhang, Y., Yang, X., Wang, H., et al. 2015, Spin Alignments of Spiral Galaxies within the Large-scale Structure from SDSS DR7, ApJ, 798, 17 [35]

—. 2013, Alignments of Galaxies within Cosmic Filaments from SDSS DR7, ApJ, 779, 160 [35, 36]

Zuntz, J., Kacprzak, T., Voigt, L., et al. 2013, IM3SHAPE: a maximum likelihood galaxy shear measurement code for cosmic gravitational lensing, MNRAS, 434, 1604 [8]

Zwicky, F. 1933, Die Rotverschiebung von extragalaktischen Nebeln, Helvetica Physica Acta, 6, 110 [29]

—. 1937, On the Masses of Nebulae and of Clusters of Nebulae, ApJ, 86, 217 [29]

—. 1951, The Coma Cluster of Galaxies, PASP, 63, 61 [10]

This 2-column preprint was prepared with the AAS LaTeX macros v5.2.